



**INSTITUTO POTOSINO DE INVESTIGACIÓN  
CIENTÍFICA Y TECNOLÓGICA, A.C.**

**DOCTORADO EN CIENCIAS AMBIENTALES**

**Electroadsorción de fluoruros por electrodos de  
carbón activado modificados con Lantano(III)**

Tesis que presenta

**David Ricardo Martínez Vargas**

Para obtener el grado de

**Doctor en Ciencias Ambientales**

**Codirectores de la Tesis:**

**Dr. José René Rangel Méndez**

**Dr. Luis Felipe Cházaro Ruiz**

San Luis Potosí, S.L.P., 03 de junio de 2022



## **Constancia de aprobación de la tesis**

La tesis “**Electroadsorción de fluoruros por electrodos de carbón activado modificados con Lantano(III)**” presentada para obtener el Grado de Doctor(a) en Ciencias Ambientales fue elaborada por **David Ricardo Martínez Vargas** y aprobada el **17 de junio de 2022** por los suscritos, designados por el Colegio de Profesores de la División de Ciencias Ambientales del Instituto Potosino de Investigación Científica y Tecnológica, A.C.

---

**Dr. José René Rangel Méndez**  
Codirector de la tesis

---

**Dr. Luis Felipe Cházaro Ruiz**  
Codirector de la tesis

---

**Dr. María Isabel Lázaro Báez**  
Miembro del Comité Tutora

---

**Dr. Érika Roxana Larios Durán**  
Miembro del Comité Tutora

---

**Dr. Fátima Pérez Rodríguez**  
Miembro del Comité Tutora

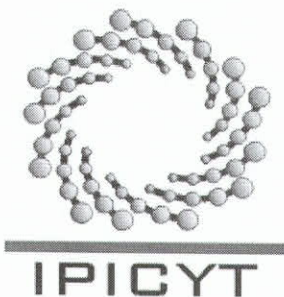


## **Institutional support**

The research described in this thesis was financially supported by grants from the “Consejo Nacional de Ciencia y Tecnología de México,” (CONACyT), through the project Atención a problemas nacionales, PDCPN-2015-789. In addition, there was also financial support from Fomento Regional para el Desarrollo Científico, Tecnológico y de Innovación (FORDECYT-2018-8-297525).

The experimental work was performed at the laboratories of the Environmental Science Division of Instituto Potosino de Investigación Científica y Tecnológica A. C. (IPICYT), under the supervision of Prof. Luis Felipe Cházaro Ruiz and Prof. José René Rangel Méndez.

The author of this thesis was financially supported by CONACyT through the scholarship with register number 478185. The participation in most national and international conferences was financially supported by the Environmental Science Division of IPICYT.



# Instituto Potosino de Investigación Científica y Tecnológica, A.C.

## Acta de Examen de Grado

La Secretaria Académica del Instituto Potosino de Investigación Científica y Tecnológica, A.C., certifica que en el Acta 032 del Libro Primero de Actas de Exámenes de Grado del Programa de Doctorado en Ciencias Ambientales está asentado lo siguiente:

En la ciudad de San Luis Potosí a los 17 días del mes de junio del año 2022, se reunió a las 09:00 horas en las instalaciones del Instituto Potosino de Investigación Científica y Tecnológica, A.C., el Jurado integrado por:

<b>Dra. María Isabel Lázaro Báez</b>	<b>Presidenta</b>	<b>UASLP</b>
<b>Dra. Erika Roxana Larios Durán</b>	<b>Secretaria</b>	<b>UdeG</b>
<b>Dr. César Nieto Delgado</b>	<b>Sinodal</b>	<b>IPICYT</b>
<b>Dra. Fátima Pérez Rodríguez</b>	<b>Sinodal externo</b>	<b>Xignux</b>
<b>Dr. José René Rangel Méndez</b>	<b>Sinodal</b>	<b>IPICYT</b>
<b>Dr. Luis Felipe Cházaro Ruiz</b>	<b>Sinodal</b>	<b>IPICYT</b>

a fin de efectuar el examen, que para obtener el Grado de:

**DOCTOR EN CIENCIAS AMBIENTALES**

sustentó el C.

**David Ricardo Martínez Vargas**

sobre la Tesis intitulada:

***Electroadsorción de fluoruros por electrodos de carbón activado modificados con La(III)***

que se desarrolló bajo la codirección de

**Dr. José René Rangel Méndez**  
**Dr. Luis Felipe Cházaro Ruiz**


El Jurado, después de deliberar, determinó

**APROBARLO**

Dándose por terminado el acto a las 12:15 horas, procediendo a la firma del Acta los integrantes del Jurado. Dando fe la Secretaria Académica del Instituto.

A petición del interesado y para los fines que al mismo convengan, se extiende el presente documento en la ciudad de San Luis Potosí, S.L.P., México, a los 17 días del mes de junio de 2022.

  
**Mtra. Ivonne Lizette Cuevas Vélez**  
Jefa del Departamento del Posgrado

  
**Dra. Lina Raquel Riego Ruiz**  
Secretaria Académica



**IPICYT**  
SECRETARÍA ACADÉMICA  
INSTITUTO POTOSINO DE  
INVESTIGACIÓN CIENTÍFICA  
Y TECNOLÓGICA, A.C.

## Dedicatory

Quisiera dedicar esta tesis a todas las personas con las que tuve la oportunidad de interactuar durante estos cuatro años. Ahora todos ustedes son parte de mí, y los integro en mi vida, en mis sentires y sensaciones que correspondan a esta época. Al final, fueron cuatro años de mi vida, cuatro largos y tortuosos años llenos de pláticas, reuniones, anécdotas, risas, abrazos, lamentos, lágrimas, comidas, alcohol (mucho), cariño y demás. Todos esos recuerdos quedarán desperdigados en mi memoria y seguro no podré acceder a ellos de forma recurrente. Pero espero que un día en el futuro, antes de que Mefistófeles extienda su mano para atraparme y llevarme a mi lugar final, todos esos recuerdos atraviesen mi pensamiento de forma esporádica y se liberen esos sentimientos comprimidos en el ayer, del mismo modo que un costal de granos que fue perforado desde el fondo y resulta imposible detener la salida de su contenido.

Me gustaría comenzar agradeciendo a Diana Cecilia Rodríguez Ugalde, una gran y encantadora compañera, alguien muy cercana a la definición de espíritu libre, según Nietzsche, y a quien tuve la dicha de conocer hace muchos años atrás. Ella fue la razón real de que yo llegara a San Luis Potosí y quien fomentó mi deseo de inscribirme al doctorado en IPICYT. Además, ella catalizó muchos aspectos positivos en mí, por lo que no me queda más que estarle eternamente agradecido por su tiempo y sus infinitos deseos de compartir. Diana, desde que te conocí, las pocas veces en que equivocaste, fueron sólo aquellas veces en que me diste la razón. Espero que te encuentres excelente en donde quiera que estés y no me queda más que desearte el más sincero éxito en todo lo que realices.

Sería el turno de todos mis mentores científicos, donde entrarían mi comité evaluador, incluyendo a mis directores de tesis. Sé que no soy la persona más agradable con quien trabajar de forma constante y les agradezco la paciencia que tuvieron conmigo, en todos los aspectos posibles. Aquí también me gustaría incluir a todas las personas de los grupos de investigación de adsorción y de electroquímica en sus diferentes etapas y generaciones, haciendo mención honorífica de Joel, quien fue prácticamente el único que no me dio descanso durante los seminarios y me realizaba preguntas muy complejas e interesantes que sacaban lo mejor y lo peor de mí y de mi experticia en el tema. A quienes les agradezco aún más enérgicamente son todas aquellas personas con quienes tuve la oportunidad de establecer una muy buena y altamente productiva amistad. Lo anterior se refiere a aquellas personas con quienes compartí físicamente mucho tiempo en el laboratorio o en la labor científica, aquellas personas que fomentaban que llegara muy temprano y que me fuera muy tarde del instituto y con quienes pude platicar ampliamente en ese largo intervalo de tiempo. De esta forma, logramos acompañarnos en nuestro aburrimiento ocasional, nos apoyamos a reducir el estrés y, por supuesto, avanzamos mucho en nuestros experimentos. Aquí quisiera destacar a mis grandes y muy queridas amigas Jaqueline y Kristell, quienes asistían diariamente, de lunes a lunes y de sol a sol. En este conjunto de personas también están Alan, Yecenia y Anai, de forma no simultánea. Desde que partieron todos ustedes, la labor experimental se volvió cada vez más pesada y frustrante. Además de que perdí personas con quienes disfrutaba convivir.

También agradezco a otro conjunto de personas, aquellas totalmente ajenas y parcialmente ajenas a mi formación científica. Aquellas personas que me acompañaron desde otras trincheras, como mis excelentes roomies Mario, Chava, Óscar y sobre todo a Diego, con sus exquisitas recomendaciones de películas, de música y de alcohol. Y mis compañeros académicos de grupos ajenos a la tesis, donde entrarían, entre otros más, Ricardo, Sandra, Gerardo, Karen, Itzel, Abraham, Federico, Verónica y Olga. Ese CONIP que organizamos es lo mejor que le ha sucedido a IPICYT, sólo que está demasiado adelantado a su época y nadie lo puede ver aún. Y por supuesto, también entraría mi familia cercana y adoptada, mis padres y mis hermanos. Aquí puntualmente agradezco a Voltinea por salvarme la vida e impedir que perdiera otro poco de cordura durante la pandemia.

Una persona que merece una mención especial y se integra a todos los grupos anteriores sin ningún problema es Virginia Montiel Corona. Podría extenderme tanto en redactar agradecimientos particularmente para ti, que mi tesis doctoral pasaría a formar sólo un anexo, una fracción mínima de todo lo globalmente escrito. No me queda una sola duda de que fuiste lo mejor que me pudo ocurrir en todos estos cuatro años doctorales o, incluso, en un nivel extra. Te quedas con una gran parte de mí. No es la mejor, ni la más agradable, ni la más racional, ni siquiera la más madura o la más congruente, pero sí una muy cariñosa. Mi mayor deseo es que sigas siendo la increíble mujer que siempre fuiste. Ansío el día en que pueda verte nuevamente y platicar tendido de todo y de nada, tal como en el pasado. Tendré la tetera lista y una bandeja de brownies recién horneados.

Ahora, en este momento que por fin terminé la tesis y estoy a unos días del examen de grado, siento mucha incertidumbre por todo lo que dejo atrás. Sé que es normal, pero sí voy a extrañar mucho estos días tan gratos que pasé al lado de todos ustedes. Como dije al principio, fueron importantes. Se convirtieron en una luz muy agradable que le dio mucha claridad a mi existir y a mi camino, permitiéndome avanzar con mucha certeza y determinación, pero también alumbraron partes de mí que se encontraban en penumbras. Lamentablemente, nada en nuestro universo es eterno ni atemporal, y cualquier luz puede agotarse o extinguirse. Lo importante será hacernos a la idea de que estos periodos de oscuridad al que me toca incursionar son facetas tanto positivas como necesarias. Aún cuando la claridad, su claridad, no se encuentre directamente conmigo o cercana a mí, esta serie de recuerdos los almaceno en partes muy profundas de mi ser y sé que alumbrarán de formas distantes pero continua mis años siguientes, del mismo modo que podemos observar estrellas en el cielo cuando oscurece. Justamente las estrellas nos recuerdan que, incluso una luz tan lejana (con énfasis en temporalidad y no en distancia), es suficiente para poder iluminar, para poder ver, para guiarnos cuando estamos perdidos, para poder seguir o simplemente para voltear y disfrutar al observarlas por un rato. En realidad, nunca estuve a oscuras. Y, después del doctorado y de conocerlos, difícilmente estaré a oscuras nuevamente. Aún en las noches más oscuras, en donde no exista el más mínimo fulgor, no requiero más que mirar hacia arriba, cerrar los ojos y acordarme de ustedes.

# Table of Contents

Institutional support.....	iii
Structure of the thesis .....	xvii
Abstract.....	xviii
Resumen .....	xix
Research products derived from the thesis .....	xx
Contributions to conferences and symposia .....	xxi
Outline .....	1
Chapter One: Background .....	3
1.1 Stress on water quality and quantity.....	3
1.2 Fluoride pollution .....	5
1.2.1 Hydrogeochemistry and over-exploitation of groundwater.....	5
1.2 Fluoride pollution .....	5
1.2.2 Health implications.....	6
1.2.3 Fluoride treatment in waters .....	7
1.3 Electrosorption .....	8
1.3.1 The working electrode: activated carbon.....	9
1.3.1.1 Physical properties.....	9
1.3.1.2 Chemical properties .....	12
1.3.1.3 Electrical properties .....	13
1.3.2 Surface charges and the electrosorption performance.....	16
1.3.2.1 The point and potential of zero charge .....	16

1.3.2.2 The amphoteric Donnan model .....	20
1.3.3 Performance in electrosorption.....	23
1.3.3.1 Charge efficiency.....	23
1.3.3.2 Faradaic reactions .....	25
1.3.3.3 Regeneration and cyclic performance .....	27
1.3.4 Fluoride removal by electrosorption processes .....	27
1.4 Lanthanum(III) as a modifying agent.....	29
1.4.1 Adsorption performance .....	29
1.4.2 Capacitive performance.....	30
Motivation of this research.....	32
Hypothesis .....	33
General objective.....	34
Specific objectives.....	34
Chapter two: Exploring the polarization window during fluoride electrosorption in activated carbons with differences in their pore-size distribution .....	35
2.1. Introduction .....	35
2.2. Materials and methods.....	36
2.2.1 Material standardization and characterization.....	36
2.2.2 Kinetics.....	38
2.3. Results and discussion.....	39
2.3.1 Characterization.....	39
2.3.2 Kinetics and the overlapping of the electrical layers.....	43
2.3.3 Polarization limits and parasitic reactions .....	50
2.3.4 Cyclic performance.....	51



2.4. Conclusions .....	52
Chapter three: Fluoride Electrosorption by Hybrid Lanthanum-Carbon Electrodes.....	54
3.1 Introduction .....	54
3.2 Materials and methods.....	55
3.2.1 Material standardization and physicochemical characterization .....	55
3.2.2 Cell arrangement and electrochemical characterization .....	56
3.2.3 Kinetics.....	57
3.3 Results and discussion .....	58
3.3.1 Characterization.....	58
3.3.1.1 Textural properties.....	58
3.3.1.2 Surface chemistry and surface charge	60
3.3.1.3 Cyclic voltammetry .....	61
3.3.2 Kinetics.....	63
3.3.2.1 Conventional adsorption vs electrosorption .....	63
3.3.2.2 The polarization profile and interfacial changes after adsorption .....	65
3.3.2.2.1 The electrical pore blockage of the micropores.....	67
3.3.2.2.2 Polarization and charging processes.....	68
3.3.2.2.3 Comparison to other works .....	71
3.3.3 Electrosorption at other polarization potentials.....	72
3.3.4 Electrosorption cycles by depolarization.....	75
3.3.4.1 Depolarization at the OCP .....	75
3.3.4.2 By reversing the polarization at negative potentials.....	78
3.4 Conclusions .....	79

Chapter four: Fluoride electrosorption in the presence of competing anions of environmental relevance.....	81
4.1 Introduction .....	81
4.2 Materials and methods.....	82
4.2.1 Material standardization and modification.....	82
4.2.2 Cell configuration and electrochemical characterization .....	82
4.2.3 Analytical determinations.....	83
4.3 Results and discussion.....	84
4.3.1 Characterization.....	84
4.3.2 Electrosorption kinetics .....	91
4.3.2.1 Binary solutions.....	91
Table 4.4. Thermodynamic values of interest of the studied anions and of sodium cation.	94
4.3.2.2 Complex mixt involving all anions .....	95
4.3.2.3 pH and conductivity .....	96
4.4 Conclusions .....	98
Chapter five: Global discussion.....	100
Final conclusions .....	103
Perspectives .....	105
References .....	106

# List of figures

Figure 1.1. A schematic representation of a section of an electrosorption cell [48]. ..... 8

Figure 1.2. Representation of a graphitic lattice. Each lattice comprises a graphene layer, in which a displacement of the subsequent graphene sheet can be identified [65]. ..... 10

Figure 1.3. Energy peaks and distribution of the pores according to their size [65]. ..... 11

Figure 1.4. Conventional acid (left) and basic (right) groups comprising oxygen atoms on a graphenecomprisehe delocalized electrons of the aromatic honey-combs are also illustrated [66]. ..... 12

Figure 1.5. [LEFT] a) Difference between the surface area and the geometric area of an electrode [84]. b) The roughness promotes changes in the energy distribution [85,90], but also c) in the diffusion profiles to the electrode surface [84]. [RIGHT] Schematic representation of electrical layers at positively charged surfaces [84–86,88–90]. ..... 15

Figure 1.6. Normalized differential capacitance curves obtained from electrochemical impedance spectroscopy for two carbons with positive  $E_{PZC}$  values (red and green) and one carbon (blue) with a negative  $E_{PZC}$  [101]. ..... 17

Figure 1.7. (a) Proton binding curve or released ions as a function of pH. .... 19

Figure 1.8. Schematic representation of a charged solid-liquid interface to highlight different electric potentials, i.e., the inner, surface and outer potentials. .... 20

Figure 1.9. Practical application of the amphoteric Donnan model. I) The properties and allocation of the electrode influence their performance [104]. II) The correct allocation of an electrode could increase the polarization limits of the electrosorption cell by distancing the  $E_{PZC}$  from the applied potential [62]. ..... 23

Figure 1.10. Different effects of the electrical polarization of porous adsorbents during the electrosorption process: a) counter-ion adsorption, b) ion-swapping and c) co-ion expulsion [43]. ..... 24

Figure 1.11 a) Pourbaix diagram of water. b) Three possible cases related to water electrolysis at pH 7 according to the open-circuit potential of the counter electrode. .... 26

Figure 2.1. a) Schematic representation of the electrosorption cell. b) Photo of the assembled electrode pair (working electrode (WE) and counter electrode (CE) separated by a Teflon membrane). ..... 38

Figure 2.2. a) Adsorption-desorption isotherms of N <sub>2</sub> at 77 K. b) Cumulative pore volume obtained by non-linear density functional theory (Mic = micropores, Mes = mesopores, Mac = macropores, “X” axis in logarithmic scale). .....	40
Figure 2.3. a) Surface charge distribution and b) pK <sub>a</sub> distribution (in 0.1 M NaCl, M = 100 mg, V = 50 mL, T = 25 °C, deaerated with N <sub>2</sub> ). .....	41
Figure 2.4. a) Cyclic voltammetry at 1 mV s <sup>-1</sup> in the anodic direction and b) gravimetric capacitances at different sweep rates (‘x’ axis in log-scale). The reported voltammograms and the computed capacitances correspond to the 3rd cycle (in 0.1 M K <sub>2</sub> SO <sub>4</sub> , M = 50 mg, V = 25 mL, T = 25 °C, Ag/AgCl/3M NaCl as the reference electrode and SSM as the counter electrode, undeaerated solution). .....	42
Figure 2.5. Adsorption and electrosorption kinetics of fluoride for a) bituminous and b) coconut-shell carbon at different potentials (y-axis in different scale). c) Comparison of the capacities between both carbons at each of the applied potentials for the bituminous (gray) and coconut-shell (orange) carbon (C <sub>0</sub> = 5 ppm F <sup>-</sup> , M = 50 mg, V = 25 mL, pH <sub>0</sub> = 7, T = 25 °C and 120-130 rpm, SSM as counter electrode). .....	44
Figure 2.6. Fluoride removal ratio (q <sub>bit</sub> / q <sub>coconut</sub> ) during fluoride kinetics (C <sub>0</sub> = 5 ppm F <sup>-</sup> , M = 50 g, V = 25 mL, T = 25 °C, 120-130 rpm, SSM as the counter electrode). .....	45
Figure 2.7. Recorded a) current and b) charge, both normalized per carbon mass during the electrosorption kinetics. c) Charge efficiency (M = 50 mg, V = 25 mL, C <sub>0</sub> = 5 ppm F <sup>-</sup> , pH <sub>0</sub> = 7, rpm = 120-130, T = 25 °C). .....	46
Figure 2.8. Linear sweep voltammetry for the studied electrodes in 5 ppm F <sup>-</sup> with constant agitation (v = 0.1 mV s <sup>-1</sup> , M = 50 g, V = 25 mL, T = 25 °C, 120-130 rpm, SSM as the counter electrode). .....	47
Figure 2.9. a) EDL overlapping in a slit-shaped pore (Ψ <sub>s</sub> = surface potential). b) Decrease of the EDL overlapping as a function of increasing the potential (Ψ <sub>s</sub> ). c) Allocation of the fluoride anions at the Stern layer in a microporous carbon. ....	48
Figure 2.10. Electrosorption and desorption (a) and (b) and current profiles (c) and (d) during five electrosorption cycles for the bituminous and the coconut-shell carbon, respectively (C <sub>0</sub> = 5 ppm F, M = 50 mg, V = 25 mL, pH <sub>0</sub> = 7, T = 25 °C and 120-130 rpm, SSM as counter electrode). .....	52
Figure 3.1. Cumulative pore volume by N <sub>2</sub> adsorption-desorption isotherms at 77 K, obtained by non-linear density functional theory (x-axis in logarithmic scale, Mic = micropores, Mes = mesopores and Mac = macropores). .....	59

Figure 3.2. a) SEM-EDS mapping of Lanthanum (in blue color) for the modified carbon La-0.5% at 250x. b) Diffractograms of the adsorbents (Cu K $\alpha$  radiation  $\lambda = 1.546 \text{ \AA}$ , step time =  $0.02^\circ$  every 10 s). ..... 60

Figure 3.3. Cyclic voltammetry in 0.1 M NaF, from -0.5 to 0.5 V a) at  $1 \text{ mV s}^{-1}$  for all the carbons ( $M = 0.025 \text{ g}$ ,  $V = 0.050 \text{ L}$ , rpm = 120-130,  $T = 25 \text{ }^\circ\text{C}$ ). The measurements correspond to the 3rd cycle..... 62

Figure 3.4. Gravimetric capacitances obtained from cyclic voltammetry in 0.1 M NaF, from -0.5 to 0.5 V at several sweep rates for La-0.5% ( $M = 0.025 \text{ g}$ ,  $V = 0.050 \text{ L}$ , rpm = 120-130,  $T = 25 \text{ }^\circ\text{C}$ ). The measurements correspond to the 3rd cycle. .... 63

Figure 3.5. Adsorption kinetics for the adsorbents a) without polarization and b) polarizing at 0.8 V. c) Comparison of the obtained capacities by both adsorption and electrosorption kinetics ( $M = 0.25 \text{ g}$ ,  $V = 0.5 \text{ L}$ ,  $C_0 = 20 \text{ ppm F}$ ,  $\text{pH}_0 = 7$ , rpm = 120-130,  $T = 25 \text{ }^\circ\text{C}$ )..... 64

Figure 3.6. a) Comparison of conventional adsorption kinetics and stepped electrosorption kinetics for La-0.5% and La-1.5% ( $E_{\text{pol}} = 0.8 \text{ V}$ ,  $M = 0.25 \text{ g}$ ,  $V = 0.5 \text{ L}$ ,  $C_0 = 20 \text{ ppm F}$ ,  $\text{pH}_0 = 7$ , rpm = 120-130,  $T = 25 \text{ }^\circ\text{C}$ ). Shift in the b)  $\text{pH}_{\text{PZC}}$  and c)  $E_{\text{PZC}}$  due to fluoride adsorption. The filled figures correspond to the initial determination, before fluoride adsorption; the unfilled figures to the determination after fluoride adsorption ( $M = 0.025 \text{ g}$ ,  $V = 0.05 \text{ L}$ ,  $\text{pH}_0 = 7$ , rpm = 120-130,  $T = 25 \text{ }^\circ\text{C}$ ,  $E_{\text{amp}} = 10 \text{ mV}$ ). ..... 66

Figure 3.7. Schematic differentiation between a physical (left) and electrical (right) pore blockage..... 68

Figure 3.8. a) Current and b) charge profiles for La-0.5% and La-1.5% during the electrosorption kinetics. The arrows indicate the difference between both polarization profiles by the same electrode. .... 69

Figure 3.9. Recording of the open-circuit potential (OCP) values for the electrodes during a kinetics..... 70

Figure 3.10. Schematic representation of useful and non-useful polarization using the values of the electrode La-1.5% I) before and II) after reaching the adsorption equilibrium, based on the electrochemical values of the potential of zero charge ( $E_{\text{PZC}}$ ), the open-circuit potentials (OCP) and the polarization potential ( $E_{\text{POL}}$ ). ..... 71

Figure 3.11. a) Stepped-potential kinetics for fluoride; b) capacities from OCP adsorption (gray) and electrosorption (orange) for the stepped-potential sequence; c) comparison of the capacities between both sequences for each of the applied potentials: stepped-potential (gray) and single-potential (orange) ( $C_0 = 20 \text{ ppm F}$ ,  $M = 0.3 \text{ g}$ ,  $V = 0.5 \text{ L}$ ,  $\text{pH}_0 = 7$ ,  $T = 25 \text{ }^\circ\text{C}$  and 120-130 rpm). ..... 73

Figure 3.12. a) Linear sweep voltammetry at  $\nu = 0.2 \text{ mV s}^{-1}$ . b) Current profiles from stepped-potential and single potential kinetics for the b) pristine carbon and c) La-0.5%. The black lines represent the current measured during the kinetics by stepped-potential increases. ( $C_0 = 20 \text{ ppm F}$ ,  $M = 0.3 \text{ g}$ ,  $V = 0.5 \text{ L}$ ,  $\text{pH}_0 = 7$ ,  $T = 25 \text{ }^\circ\text{C}$  and 120-130 rpm, SSM as the counter electrode.)..... 74

Figure 3.13. a) Electrosorption-desorption cycles ( $C_0 = 20 \text{ ppm fluoride}$ ,  $M = 0.3 \text{ g}$ ,  $V = 0.5 \text{ L}$ ,  $\text{pH}_0 = 7$ ,  $T = 298 \text{ K}$  and 120-130 rpm, Ag/AgCl/3M NaCl as reference electrode, SSM as counter electrode, POL = polarization, OCP = open circuit potential). b) Point of zero charge values determined before polarizing or basal determination, after the 1st polarization and after the 6th polarization. c) Open circuit potential recorded before each polarization step..... 76

Figure 3.14. Electrosorption-desorption cycle of fluoride by reversing the polarization of the working electrode ( $M = 0.3 \text{ g}$ ,  $C_0 = 20 \text{ ppm F}$ ,  $V = 0.5 \text{ L}$ ,  $\text{pH}_0 = 7$ ,  $T = 298 \text{ K}$  and 120-130 rpm, Ag/AgCl/3M NaCl as reference electrode, SSM as counter electrode)..... 78

Figure 4.1. Speciation diagrams of a) phosphate and b) arsenate. .... 83

Figure 4.2. Electrochemical impedance spectroscopy at the open circuit potential of the studied activated carbons: a) Nyquist plots and b) Bode plots in 0.1 M NaF ( $f_0 = 10 \text{ kHz}$ ,  $f_f = 10 \text{ mHz}$ ,  $M = 50 \text{ mg}$ ,  $V = 50 \text{ mL}$ ,  $E_{\text{amp}} = 10 \text{ mV}$ , Ag/AgCl/3M NaCl as reference electrode, SSM as counter electrode). For the Nyquist plots, the fitting model is represented by the continuous lines over the experimental data points..... 85

Figure 4.3. Equivalent circuits used to fit the electrodes in a 0.1 M NaF solution for a) the pristine carbon and La-0.5% and b) La-1.5%.  $R_s$ : resistance of the electrolyte, CPE are capacitances of the electrical double-layer and  $R_{ct}$  correspond to charge-transfer resistances..... 86

Figure 4.4. Electrochemical impedance spectroscopy at the open circuit potential of the studied activated carbons: a) Nyquist plots and b) Bode plots in 5 ppm  $\text{F}^-$  or 0.263 mM NaF ( $f_0 = 10 \text{ kHz}$ ,  $f_f = 10 \text{ mHz}$ ,  $M = 50 \text{ mg}$ ,  $V = 50 \text{ mL}$ ,  $E_{\text{amp}} = 10 \text{ mV}$ , Ag/AgCl/3M NaCl as reference electrode, SSM as counter electrode). For the Nyquist plots, the fitting model is represented by the continuous lines over the experimental data points. .... 88

Figure 4.5. Equivalent circuits used to fit the electrodes in a 5 ppm  $\text{F}^-$  solution.  $R_s$ : resistance of the electrolyte, CPE are capacitances of the electrical double-layer and  $R_{ct}$  correspond to charge-transfer resistances..... 89

Figure 4.6. Potentials of zero charge in 5 ppm or 0.263 mM  $\text{F}^-$  ( $f = 100 \text{ mHz}$ ,  $M = 50 \text{ mg}$ ,  $V = 50 \text{ mL}$ ,  $E_{\text{amp}} = 10 \text{ mV}$ , Ag/AgCl/3M NaCl as reference electrode, SSM as counter electrode). The asterisks denote the potential of zero charge for each electrode. .... 90

Figure 4.7. Electrosorption kinetics of fluoride and of binary solutions comprising fluoride in the presence of several competing anions of environmental relevance (fluoride vs. anion) for a) La-0.5% and b) La-1.5%. c) Obtained capacities of fluoride electrosorption kinetics for each competing anion and for each carbon at  $t = 60$  min. d) Obtained capacities for each competing anion for each carbon at  $t = 60$  min ( $C_0 = 0.263$  mM of each anion,  $M = 50$  mg,  $V = 50$  mL,  $E_{\text{cell}} = 1.2$  V,  $\text{pH}_0 = \sim 7$ ,  $T = 25$  °C and 120-130 rpm, SSM as counter electrode). ..... 92

Figure 4.8. Electrosorption removal of each anion in the complex mixture (at  $t = 60$  min) in equimolar initial concentrations by La-0.5% and La-1.5% ( $C_0 = 0.263$  mM of each anion,  $M = 50$  mg,  $V = 50$  mL,  $E_{\text{cell}} = 1.2$  V,  $\text{pH}_0 = \sim 7$ ,  $T = 25$  °C and 120-130 rpm, SSM as counter electrode). ..... 96

Figure 4.9. Measured changes in the pH (y-axis in different scale) during the electrosorption kinetics of binary solutions for a) La-0.5% and b) La-1.5%. ( $C_0 = 0.263$  mM of each anion,  $M = 50$  mg,  $V = 50$  mL,  $E_{\text{cell}} = 1.2$  V,  $\text{pH}_0 = \sim 7$ ,  $T = 25$  °C and 120-130 rpm, SSM as counter electrode). ..... 97

Figure 4.10. Measured changes in the conductivity during the electrosorption kinetics of binary solutions for a) La-0.5% and b) La-1.5% ( $C_0 = 0.263$  mM of each anion,  $M = 50$  mg,  $V = 50$  mL,  $E_{\text{cell}} = 1.2$  V,  $\text{pH}_0 = \sim 7$ ,  $T = 25$  °C and 120-130 rpm, SSM as counter electrode). Due to space, phosphate and arsenate species are represented as  $\text{PO}_4^{x-}$  and  $\text{AsO}_4^{x-}$  ..... 98

## List of tables

Table 2.1. Textural properties.....	40
Table 2.2. Removal velocities by adsorption and electrosorption in $\text{mg g}^{-1} \text{hr}^{-1}$ (obtained at $t = 25 \text{ min}$ , $M = 50 \text{ mg}$ , $V = 25 \text{ mL}$ , $C_0 = 5 \text{ ppm F}^-$ , $\text{pH}_0 = 7$ , $\text{rpm} = 120\text{-}130$ , $T = 25 \text{ }^\circ\text{C}$ )....	45
Table 3.1. Textural, physicochemical and electrochemical properties of the studied carbons. .....	59
Table 3.2. Removal velocities by adsorption and electrosorption in $\text{mg g}^{-1} \text{h}^{-1}$ ( $M = 0.25 \text{ g}$ , $V = 0.5 \text{ L}$ , $C_0 = 20 \text{ ppm F}^-$ , $\text{pH}_0 = 7$ , $\text{rpm} = 120\text{-}130$ , $T = 25 \text{ }^\circ\text{C}$ ).....	64
Table 4.1. Electrical parameters obtained from the fitting of the equivalent circuits for each electrode in $0.1 \text{ M NaF}$ .....	86
Table 4.2. Values of resistance and capacitances obtained from the equivalent circuits for each electrode in a $5 \text{ ppm F}$ solution. ....	89
Table 3. Electrosorption velocities of fluoride and of fluoride in the presence of competing anions of environmental relevance (binary solutions) for both carbons (at $t = 10 \text{ min}$ , in $\mu\text{mol g}^{-1} \text{min}^{-1}$ ).....	92
Table 4.4. Thermodynamic values of interest of the studied anions and of sodium cation.	94



## **Structure of the thesis**

The thesis was structured according to the specifications of Instituto Potosino de Investigación Científica y Tecnológica. Chapters 2, 3 and 4 correspond to, at least, one research product (research article) and each of these chapters must be able to stand alone. For this reason, all these chapters present the same structure and some similar information, especially related to the subsections of Introduction and Methodology. Nevertheless, some adjustments were indeed performed, as for the case of the equation numbering and the cited references, among others.

## Abstract

Chronic and excessive fluoride consumption in drinking waters above the international standards has implications for human health. Electrosorption is an interesting option for water treatment and consists in the electrical polarization of a conductive adsorbent with high surface area and pore volume. This work first reports the effect of the pore-size distribution of two commercial activated carbons, a coconut-shell carbon (95% microporous) and a bituminous carbon (25% of mesopores). Electrosorption was evaluated at several potentials ( $E_{\text{cell}} = 1.2, 1.6, 2$  and  $2.4$  V). The fluoride removal capacity and rate without polarizing was really low and increased at different degrees as a function of increasing the applied potential for both carbons. At  $2$  V<sub>cell</sub>, the removal capacity of the carbons increased ~6 times, compared to that of conventional adsorption, while the removal rate of the bituminous carbon was ~4 times faster than that of the coconut-shell carbon at short times (<30 minutes) and at all potentials. Then, the bituminous carbon performed better as an electrode, which was attributed to the presence of mesopores, as they enhance the mass-transport and allow a better allocation of the electrical double-layer.

Then, the bituminous activated carbon was impregnated with 3 La(III) percentages (w/w): La-0.5%, La-1.5% and La-2.0%. The formed La(III) clusters decreased the surface area and pore volume of the adsorbents, which also decreased their polarizable surface. In addition, the deprotonation of the hydroxyls provided by the La(III) clusters increased the input of negative charges on the carbon surface. Electrosorption was evaluated by applying  $0.8$  V (vs. Ag/AgCl/3M NaCl) in two profiles: (i) polarizing from the beginning and (ii) polarizing after the adsorption equilibrium. *In situ* information helped to explain and corroborate the processes taking place during both profiles. Further studies comprised the evaluation of fluoride desorption by depolarizing at the open circuit potential and by reversing the polarization at negative potentials, in which the surface of the carbons oxidized after each polarization.

The last step comprised the evaluation of fluoride electrosorption in the presence of competing anions of environmental relevance (chloride, nitrate, sulfate, phosphate and arsenate) by La-0.5% and La-1.5% (w/w%) using equimolar initial concentrations ( $0.263$  mM of each studied anion) in both binary solutions ( $F^-$  vs. competing anion) and in a complex mixture comprising all anions. For La-0.5%, the presence of nitrate and chloride did not significantly modify its fluoride removal, while these same anions decreased the fluoride removal of La-1.5% by half. In general, the divalent anions competed the most during the kinetics. The discussion of the results was not only centered in the charge and hydrated radius of the anions, but is was expanded to other thermodynamic parameters that also denote selectivity, as the hydration energies and mass-transport parameters.

## Resumen

El consumo crónico de fluoruro en agua por encima de estándares internacionales implica degeneración de la salud. La electroadsorción es un acercamiento interesante para el tratamiento de agua con bajas concentraciones de iones orgánicos e inorgánicos, tales como el fluoruro, y consiste en la polarización eléctrica de un adsorbente conductor con alta área específica y volumen de poro.

Este trabajo reporta primeramente el efecto de la distribución del tamaño de poro de dos carbones activados comerciales, concha de coco (95% microporoso y 5% mesoporoso) y carbón bituminoso (25% de mesoporos). La electroadsorción se evaluó a diferentes potenciales ( $E_{\text{celda}} = 1.2, 1.6, 2 \text{ and } 2.4 \text{ V}$ ). La remoción de fluoruro sin polarizar fue realmente baja e incrementó en diferentes grados en función de incrementar el potencial aplicado. Al polarizar a  $2 \text{ V}_{\text{celda}}$ , la capacidad de los carbones incrementó ~6 veces, comparado con la adsorción convencional, mientras que la velocidad del carbón bituminoso fue ~4 veces más rápida que la de concha de coco a tiempos cortos y a todos los potenciales. Entonces, el carbón bituminoso se desempeñó mejor como electrodo, lo cual se atribuyó a la presencia de mesoporos, ya que mejoran el transporte de masa y permiten un mejor acomodo de la doble capa eléctrica.

Posteriormente, el carbón activado bituminoso se impregnó con 3 porcentajes de La(III): La-0.5%, La-1.5% and La-2.0%. Los clústers formados disminuyeron el área superficial y el volumen de poro de los adsorbentes, lo cual también disminuyó su superficie polarizable. Además, la desprotonación de los hidroxilos proporcionados por los clústers de La(III) incrementaron las cargas negativas en la superficie del electrodo. La electroadsorción se evaluó aplicando  $0.8 \text{ V}$  (vs. Ag/AgCl/NaCl 3M) en dos perfiles: (i) polarizando desde el inicio y (ii) polarizando después del equilibrio de adsorción. Información obtenida *in situ* ayudó a explicar y corroborar los procesos que tuvieron lugar durante ambos perfiles. También se evaluó la desorción de fluoruro por despolarización y por inversión de la polarización a potenciales negativos.

En último apartado se estudió la electroadsorción de fluoruro en presencia de aniones de relevancia ambiental (cloruro, nitrato, sulfato, fosfato y arseniato) con los electrodos La-0.5% y La-1.5% (p/p%). Esto se realizó utilizando concentraciones equimolares iniciales (0.263 mM de cada anión estudiado) en soluciones binarias ( $\text{F}^-$  vs. anión de competencia) y en una mezcla compleja que contenía a todos los aniones de forma simultánea. Para La-0.5%, la presencia de nitrato y cloruro no modificó de forma significativa su remoción de fluoruro, mientras que sí disminuyeron el desempeño de La-1.5% a la mitad. En general, los aniones divalentes compitieron mucho más durante las cinéticas. La discusión de los resultados no sólo se centró en la carga y el radio hidratado de los aniones, sino que la discusión se basó en otros parámetros termodinámicos que también denotan selectividad, como las energías de hidratación y parámetros de transporte de masa.

## Research products derived from the thesis

**D.R. Martinez-Vargas**, E.R. Larios-Durán, L.F. Cházaro-Ruiz, J.R. Rangel-Méndez, Correlation between physicochemical and electrochemical properties of an activated carbon doped with lanthanum for fluoride electrosorption, *Sep. Purif. Technol.* 268 (2021). <https://doi.org/10.1016/j.seppur.2021.118702>.

**D.R. Martinez-Vargas**, J.R. Rangel-Méndez, L.F. Cházaro-Ruiz, Fluoride electrosorption by hybrid La(III)-activated carbon electrodes under the influence of the La(III) content and the polarization profile, *J. Environ. Chem. Eng.* 10 (2021) 106926. <https://doi.org/10.1016/j.jece.2021.106926>.

**D.R. Martinez-vargas**, L.F. Chazaro-ruiz, J.R. Rangel-mendez, Exploring the polarization window during fluoride electrosorption in two activated carbons with significant differences in their pore-size distribution, *Sep. Purif. Technol.* 295 (2022) 121360. <https://doi.org/10.1016/j.seppur.2022.121360>.

**D.R. Martinez-Vargas**, E.R. Larios-Durán, J.R. Rangel-Méndez, L.F. Cházaro-Ruiz, Fluoride electrosorption in the presence of competing anions of environmental relevance. Sent to *Electrochimica Acta*.

## Contributions to conferences and symposia

\***Martinez-Vargas, D.R.**, Rangel-Méndez, J.R., Cházaro-Ruiz, L.F. Electroadsorción de fluoruro sobre carbón activado modificado con La(III). Oral presentation. Taller Latinoamericano de Materiales de Carbono 2018. Bogotá, Colombia.

\***Martinez-Vargas, D.R.**, Rangel-Méndez, J.R., Cházaro-Ruiz, L.F. Electroadsorción de fluoruro sobre electrodos de carbón activado dopados con La(III). Oral presentation. Congreso Nacional de la Sociedad Mexicana de Electroquímica 2019. Querétaro, México.

\***Martinez-Vargas, D.R.**, Rangel-Méndez, J.R., Cházaro-Ruiz, L.F. Remoción de fluoruros mediante electrodos híbridos La(III)-carbón activado con propiedades supercapacitivas. Oral presentation. Congreso Amexcarb 2019. SLP, México.

\***Martinez-Vargas, D.R.**, Rangel-Méndez, J.R., Cházaro-Ruiz, L.F. Fluoride electrosorption by an activated carbon doped with lanthanum. Poster presentation. Pacific Rim Meeting on Electrochemical and solid state science 2020 a joint international meeting of the Electrochemical Society - VIRTUAL.

\***Martinez-Vargas, D.R.**, Rangel-Méndez, J.R., Cházaro-Ruiz, L.F. Fluoride electrosorption on activated carbon electrodes doped with La(III). Poster presentation. Congreso LatinXChem 2020 - VIRTUAL.

\***Martinez-Vargas, D.R.**, Rangel-Méndez, J.R., Cházaro-Ruiz, L.F. The effect of the Potential Profile on the Electrosorption of Fluoride by Hybrid Lanthanum-carbon Electrodes. Poster presentation. Congreso LatinXChem 2021 - VIRTUAL.

\***Martinez-Vargas, D.R.**, Rangel-Méndez, J.R., Cházaro-Ruiz, L.F. Electroadsorción de fluoruros por electrodos de carbón activado con diferentes propiedades texturales. Oral presentation. Taller Latinoamericano de Materiales de Carbono 2021. SLP - VIRTUAL (Híbrido), México.

\*J.R., Cházaro-Ruiz, L.F, **Martinez-Vargas, D.R.**, Larios-Duran, E.R., Rangel-Méndez. Activated Carbon Electrode Modified with Lanthanum(III) for Fluoride Electrosorption. Oral presentation. 72nd Annual Meeting of the International Society of Electrochemistry 2021. Jeju Island, Korea/Online (Hybrid).

\***Martinez-Vargas, D.R.** Electroadsorción de fluoruros en electrodos de carbón activado modificados con La(III). Oral presentation. Ciclo de conferencias sobre manejo, gestión y tratamiento de agua 2022. SLP - VIRTUAL (Híbrido), México.

## Outline

**Chapter One** provides an theoretical background on several relevant topics on fluoride electrosorption, which comprise water pollution processes, water pollution with fluoride by overexploitation of groundwaters, although mostly centered in San Luis Potosí, México. Afterwards, topics involve electrosorption for water treatment, with special interest in the structure and (physical, chemical and electrical) properties of the electrode, carbon-based materials. Some practical aspects of the electrosorption cell are also discussed, especially those related to the surface charges of activated carbons and how their understanding provides an insight of the electrosorption performance. Afterwards, fluoride electrosorption is revised, the State-of-the-Art of activated carbons modified with metals and finalizing with the importance to consider lanthanum as a promising modifying agent even for electrosorption.

In **Chapter Two**, fluoride electrosorption was evaluated by two commercial activated carbons (bituminous F-400 and coconut-shell) with a similar surface area (SBET), surface chemistry (pHPZC) and charging processes (current and charge profiles), but with significant differences in their pore-size distributions. Fluoride electrosorption was evaluated in sacrifice cells by polarizing at several potentials beyond that of water electrolysis ( $E_{cell} = 0, 1.2, 1.6, 2.0$  and  $2.4$  V) to additionally address the effect of parasitic faradaic reactions during the electrosorption kinetics. **Chapter Three** centers in the fluoride electrosorption results of the bituminous activated carbon F400 impregnated with three La(III) percentages: La-0.5%, La-1.5% and La-2.0%. The textural, physicochemical and electrochemical properties of the materials were completely characterized and their electrosorption performances were extensively evaluated under different conditions. In addition, desorption and electrosorption cycles were studied with particular interest in the analysis of the stability of the electrode.

**Chapter Four** described the fluoride electrosorption performance in the presence of competing anions for La-0.5% and La-1.5%. The studied competing anions were those of environmental relevance: chloride, nitrate, arsenate, sulfate and phosphate and the kinetics were performed using equimolar initial concentrations in both binary solutions (fluoride vs. anion) and in a complex mixture comprising all anions. The last sections of the thesis comprise **Chapter Five**, which provides a global discussion on the most relevant findings of the thesis, followed by the sections **Final conclusions and Perspectives**.

## Introduction

Pollution processes decrease the quality and finite quantity of water available for human consumption. For the specific case of areas located in arid and semi-arid zones, i.e., zones with important levels of hydric stress, over-exploitation of groundwaters is one of the main processes that simultaneously affects water quantity and quality. In groundwaters, water quality is a function of the depth, as depth will modify the temperature and thus, most chemical equilibria, such as the solubility of gases and of minerals, among others. Then, water quality could decrease when these minerals comprise hazardous components or ions in its structure, in which their higher solubility will increase their concentration in the water reservoir. In San Luis Potosí, our research area, fluoride highlights among these primary inorganic pollutants, as there is an abundance of minerals that contain fluoride. Fluoride, on the other hand, promotes important and undesired health implications, such as skeletal and odontological deformations. For this, international guidelines established that fluoride concentration in drinking waters should not exceed 1.5 ppm, while in Mexico, the guideline established a limit of only 1 ppm. Nevertheless, its concentration has been reported several times higher (~5 ppm) in the metropolitan area of San Luis Potosí and its suburbs than those previous recommended values, while farther regions could present even 20 ppm. Then, it becomes crucial to remove fluoride from these water sources for human consumption, although conventional water treatment processes lack selectivity and/or performance (removal capacity and velocity) towards this specific anion, especially in such low concentrations. Several processes and technologies have already evaluated fluoride removal in different conditions. Among them, electrosorption highlights as one excellent option, in which the performance of adsorbents with good electrical conductivity is enhanced by the imposition of an electrical stimulus by an external power source. In this sense, the State-of-the-Art is focusing on studying commercial activated carbon electrodes modified with metals, which not only increase the polarity of the surface and promote stronger interactions towards fluoride anions, but some metallic compounds can also increase the electrical conductivity of the new hybrid electrode. The main goal of this work was to impregnate a commercial activated carbon with lanthanum, as the physicochemical properties of lanthanum have been reported to increase the fluoride removal by a chemisorption mechanism, while lanthanum compounds have also shown important capacitive properties during a several hundredths of cycles, which could also retain fluoride by electrostatic interactions and directly correlates to the possible reusability of the hybrid lanthanum-carbon electrode for several cycles.

# Chapter one: Background

## *1.1 Stress on water quality and quantity*

Water is one of the most abundant substances in our planet. The first organisms appeared in an aqueous environment and the unique properties of this molecule had its implications in the development of life and its evolution through history. Even when water can be found naturally in three states of matter and it is an ubiquitous resource, organisms rely on drinkable water sources, i.e., water that can be consumed without any health implications. Then, the absence and limitations of drinking water will hinder the proper development of life in the planet. For this reason, the main (biotic) interest is to have access to this resource with a sufficient quantity and proper quality standards that do not limit the development of organisms nor its quality of life. Nevertheless, drinkable water sources are far more limited than other water sources and its quantity (and quality) is reduced every year due to several processes. For the aim of this manuscript, the discussion will be centered in environmental pollution, overpopulation and overexploitation, especially centered in groundwaters, to finally address groundwater pollution by the modification of the chemical equilibria due to groundwater exploitation.

Pollution processes and the subsequent alteration of the ecosystems and ecological relationships is a problem associated to technological and industrial human development. This is of relevance as the physical, chemical and biological parameters to evaluate water quality have significantly increased over time, in conjunction with the increasing demand on their detection and quantification limits by analytical instruments. Regarding human health, one of the most severe impacts is the lack of sanitation and disinfection. This limits the access to drinkable water and affects directly to more than one third of the total population of the planet [1]. Biological hazards, such as cholera and typhoid, have killed millions of people in the past, promoting states of emergency in developing countries even nowadays [2].

Concerning non biological hazards, a common report on water quality for drinking water must provide information on 161 chemical agents [3]. This list comprises common species already present in natural waters, such as nitrate, phosphate and fluoride, heavy metals, pesticides and emerging pollutants. It is worth to highlight that these 161 agents do not include common derivatives and other isoforms of the chemical entities listed, for which the number is much higher. For example, some pollutants are reported as a comprehensive set, such as chlorophenols, chlorobenzenes, synthetic detergents, oils, products obtained from oil and polynuclear aromatic hydrocarbons, among others [3]. On the other hand, the hydrosphere is not a hermetic nor an isolated compartment from the other environmental



compartments (soil, air, organisms), but it is highly interconnected and presents a high degree of matter and energy exchanges [2]. Then, pollution processes should not be identified and studied only in water, as those occurring in air and soil and even in organisms could impact water quality. It is worth reiterating that hazardous entities could also be present naturally without any human intervention, although human intervention could increase their content and concentration, as will be addressed below.

Over exploitation is another factor that has modified the ratio or balance between the density of organisms (per unit of area) and the quantity and quality of water in their environment. The decrease in water availability is related to overpopulation, in which higher population implies a higher consumption of the resource over shorter periods of time, which leads to over exploitation. Over exploitation reduces the time to recover the aquifer storage capacity above the annual average recharge [4], decreasing the access to the resource as a function of time, possibly reaching to its depletion. One third of the global population lives in high water stress situations [5], which promotes new problems and inconveniences related to water transport and storage from, most times, distant regions [6,7]. Over exploitation is not only related to a higher consumption due to overpopulation, as several industrial processes are highly dependent on significant amounts of the resource. Then, non-overpopulated industrial zones can present a high degree of hydric stress due to water overexploitation.

It is also worth to highlight that the composition of groundwaters change as a function of its depth. As an example, the temperature of water and oxygen solubility decreases as a function of increasing the depth of the water reservoir, which modifies several chemical reactions and equilibria and thus, the presence and concentration of species [2,8,9,10]. Then, overexploitation of depth water reservoirs promotes that the water quality of the extracted liquid also changes as a function of time (i.e, as a function of the depth), which could increase the concentration of toxic species that were not present at more surface levels. In this regard, the presence of trace elements of natural origin derived from dissolution processes can be substantial in several regions, and their presence and impact are not always considered in the design and implementation of groundwater treatment processes [11]. This is of great interest as it reflects a correlation and interrelationship between overexploitation and pollution processes, which is totally unrelated to the anthropogenic input of toxic species reviewed above. This previous, the pollution of groundwaters as a function of over exploitation, event will be further addressed upon next for the specific case of fluoride.

## ***1.2 Fluoride pollution***

### ***1.2.1 Hydrogeochemistry and over exploitation of groundwater***

Arid and semi-arid zones present a high hydric stress due to the low or null margin of recharge or quantity of the resource [12,13]. Arid and semi-arid zones cover about 41% of the surface of the planet and more than 38% of the total global population is settled there [4]. Some particularities of these zones are a low productivity of vegetation, due to the low and erratic availability of rainwater, temperature fluctuations and an intense solar radiation [14]. Then, water is the most limiting resource for organisms in such regions, in general, and more than 250 million people are affected by water scarcity in arid and semi-arid zones located in developing countries [15,16].

Groundwaters represent an abundant resource for drinking water supply in arid and semiarid zones and their availability can be affected by the processes explained above. In addition, the rocks that hold water in these spaces strongly affect its quality, but also groundwater itself is responsible for the formation of several secondary minerals [2]. The geological framework, i.e., the lithology, hydrology and hydrogeochemistry, determines the specific conditions that controls and differentiates the aquifer [17]. Then, the contact of groundwater with nearby rocks, gases and biological metabolites determines the chemical, physical and biological processes occurring during water infiltration and thus, the final composition of this complex aquifer system [8]. For this same reason, research on groundwater quality represents a problem due to the heterogeneity and anisotropy of the media where water runs and deposits. In this regard, the presence of trace elements of natural origin derived from dissolution processes can be substantial in several regions, but their presence and impact are not considered in the design and implementation of groundwater treatment processes [11]. In Mexico, a great amount of groundwaters changed the chemical composition and quality of such waters mainly due to an inadequate exploitation policy, but also due to filtration of polluted water [9,11,18].

## ***1.2 Fluoride pollution***

San Luis Potosí (SLP) is a State at the center of Mexico located in a semi-arid zone. The rain average is of 400 mm per year, which occurs primarily in the summer (from June to September), and with a mean temperature between 17 and 21 °C [19]. The capital city of SLP and its suburbs have presented a considerable urban and industrial growth in the last decades, which has promoted an intensive exploitation of groundwaters: 92% of the water used for urban development comes from groundwater sources. Exploitation of groundwaters has occurred between 180 m and 350 m, but the defection of phreatic levels has promoted deeper perforation up to 700 and 1000 m [10].

This specific urban and geologic scenario of SLP combined with the specific hydrogeological precarious conditions due to the imbalance between charge and extraction

has caused many inconveniences of subsidence, failure and cracking in some zones in the suburbs [20]. Over exploitation in this region has mainly occurred due to an inadequate management and distribution of the liquid, as the concentration of wells in small areas produces their dejection, which promotes the ascension of regional fluxes of thermal water. Pollution is induced when non-controlled extraction of groundwater does not allow its recharge and thus, promotes the incorporation of fluorine [10].

Fluorine is one of the elements that enrich the groundwater in the volcanic zones where it is present in silicic minerals and hydrothermal solutions. In these volcanic zones, the concentration of fluoride is correlated with the temperature of groundwaters [17,19,21]. Its origin is linked to a natural source from the dissolution and lixiviation of rhyolitic rocks, such as fluorite and topaz, especially in thermal zones to the south and southwest of the city. Fluorite ( $pK_s = 10.51$ ),  $\text{CaF}_2$ , is the most abundant mineral that contains fluoride in the region and it is usually found in hydrothermal reservoirs. In fact, the whole basin and the surroundings, are located in the fluorite belt. In addition, fluoride is also found in minerals from igneous or rhyolitic rocks, such as topaz and fluoroapatite. Topaz ( $pK_s = 24.99$ ),  $\text{Al}_2\text{SiO}_4(\text{F},\text{OH})_2$ , and fluoroapatite ( $pK_s = 59.6$ ),  $\text{Ca}_5(\text{PO}_4)_3\text{F}$ , also present a high percentage of fluoride in its chemical composition and represents another viable and strong source of fluoride to groundwaters [22,23]. For all previous reasons, high fluoride concentrations have been found in several water samples of the city of San Luis Potosí and its suburbs [11,21,24,25].

### ***1.2.2 Health implications***

Fluorine absorbs mainly in the intestine, although it can also absorb significantly in the lungs and skin, according to the exposition. The degree of absorption of a compound with fluorine is correlated to its solubility. Relatively soluble compounds, as sodium fluoride, absorbs practically by depletion, while relatively insoluble compounds as cryolite ( $\text{Na}_3\text{AlF}_6$ ) and fluorapatite ( $\text{Ca}_5(\text{PO}_4)_3\text{F}$ ) are absorbed to a much lesser degree [26]. Fluoride has been detected in all organs and tissues and is concentrated by deposition in the bones and teeth, as this element is a mitogen for osteoblasts and stimulates the formation of the bones [26]. The level of esquelital fluoride is related with ingestion and age. The storage in a developing bone (growing) shows higher fluoride deposit than for mature mammals. Fluorine intake at low doses during the formation period of the teeth protects them against posterior teeth caries or cavities and the subsequent decay of the teeth. Fluorine does not fortifies the teeth, but rather suppresses dental caries, probably due to its deposition in hydroxyapatite crystals located in the teeth enamel. This hinders the action of different oligoelements that are necessary to activate the bacterial enzymes that produce dental caries [27].

Excessive fluorine consumption produces fluorosis, which manifests by mottled teeth, in its very mild condition, and can increase the size of the teeth and even of the bones [28,29]. As

mottled teeth are very resistant to dental caries, the structural force of the teeth is weakened considerably [27]. In human beings, the main manifestations of chronic fluorine ingestion are osteosclerosis and mottled enamel. Osteosclerosis is a phenomenon that increases the bone density due to a high osteoblastic activity and by the replacement of hydroxyapatite ( $\text{Ca}_{10}(\text{PO}_4)_6(\text{OH})_2$ ) by fluorapatite, which is denser. In its most severe form, it becomes a disabling condition. Mottled enamel is characterized by opaque areas scattered irregularly over the tooth. In more severe cases, brown stains resemble a corroded-looking appearance [26]. For all previous reasons, the World Health Organization [30,31] established a maximum concentration limit of 1.5 ppm in waters for human consumption. On the other hand, the USEPA's enforceable standard in public water supplies is 4.0 ppm, with a secondary maximum contaminant level of 2.0 ppm in areas that have high levels of naturally occurring fluoride [32], while the Department of Health and Human Services recommends an optimal level of only 0.7 ppm. In Mexico, the limit of fluoride is of 1.5 ppm, although a new regulation project states that the limit will be of 1 ppm [33].

### ***1.2.3 Fluoride treatment in waters***

To date, several approaches have been developed and implemented to decrease the concentration of fluoride in drinking water to the acceptable limits [34,35], such as adsorption [36], coagulation [37], filtration [38], ion-exchange [39], electro flocculation [40], electrocoagulation [41], electrodialysis [42], among other processes. Of course, each approach presents a diverse set of advantages and disadvantages, according to several parameters. For example, it is always desired that the process presents a fast removal and with a high capacity, which mainly depends on the initial concentration of fluoride, the pH and temperature of the water, among other properties. Due to the discussion presented above, it can be inferred that the interval of concentrations to treat the desired water reservoir should be useful to discard processes. Several treatment processes are evaluated in much higher initial concentrations than those regularly found in water reservoirs. Of course, the water will also present other anions that could compete with fluoride removal. For this, the selective removal of specific pollutants is always desired in several processes, although it usually increases the costs. The viability of implementation comprise several aspects of the treatment process, such as if the water treatment plant was designed to, for example, add another adsorption column or an electrocoagulation step, to even acquire and transfer the reagents and/or materials to the plant.

Regarding the previous discussion, the author of this work considers that it is not optimal to redesign water treatment plants to adjust to these “emergent pollutants” from natural sources and that new water treatment technologies that tackle such pollutants, as fluoride, should be easy to implement, comprising materials, equipment and reagents of easy access or even already acquired by the water treatment plant. As an example, water technologies based on nanotechnology present high, fast and efficient fluoride removal with high regeneration and even using low-cost materials, but very few water treatment plants around

the world are designed to implement such technology, especially regarding the impossibility to retain the nanomaterials inside the water treatment plant and the long-term effects of their possible liberation to the water stream.

In summary: i) fluoride is a harmful ion in specific concentrations, above which removal is needed; ii) fluoride pollution can occur due to groundwater overexploitation processes, for which a specific water treatment plant could not be initially designed for its removal to the acceptable levels of consumption and; iii) as the reader notices, not all water treatment processes can be adapted to a water treatment plant that has been already designed and has been running for a certain amount of time, for which the treatment technologies should be easy to implement or should be based on already acquired materials. The next section will focus on describing a specific water treatment process that can comply as one excellent option for fluoride pollution and that could fully cover the third (iii) issue.

### 1.3 Electrosorption

Capacitive processes, such as electrosorption or capacitive deionization, provide a treatment option for waters with even low amounts of either organic or inorganic ions or in water with a low ionic strength. This process involves in the electrical polarization of porous conductive solids (working electrode) with high surface area and good electrical conductivity [43–47]. Even when the process has been mainly implemented to deionize water, several efforts have been made to understand and attain the selective removal of specific charged species from complex solutions, which is known as electrosorption [43–47].

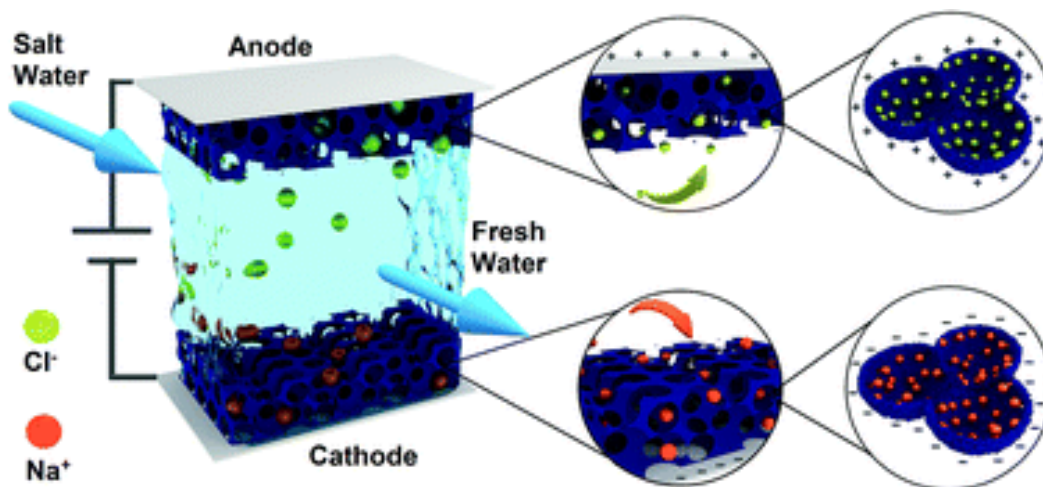


Figure 1.1. A schematic representation of a section of an electrosorption cell [48].

Recently, capacitive processes have gained attention due to several advantages over more conventional water treatment processes. For example, the electrical polarization increases electrostatic interactions between the charged surface of the adsorbent and adsorbates

(ions). This is important regarding that adsorption is usually inefficient at low adsorbate concentrations, for which the removal capacity of such conductive adsorbents is enhanced. On the other hand, mass transport to the electrosorption sites is also enhanced due to the contribution of migration, as the diffusion of the adsorbate tends to be limited, which could increase the removal velocity [49–51]. Then, electrosorption can increase the performance of conductive solids, such as membranes, carbon-based materials, specifically activated carbons, some clays, among other solids used in conventional water treatment processes.

Electrosorption also enables salt removal at low (sub-osmotic) pressures and room temperatures, with the primary input being a small cell voltage and an electric current whose magnitude depends on the system size. Thus, unlike reverse osmosis or distillation-based desalination systems, electrosorption does not need to be coupled to high pressure pumps or heat sources, allowing for a facile system scaling [43]. Regarding chemical and other electrochemical processes, such as (electro)coagulation and (electro)floculation, the addition of chemical species that promote the desired reactions is omitted and the energy input for electrosorption processes is usually much lower.

The most common electrode material reported for electrosorption comprise activated carbons in their different forms and presentations, from bare commercially available activated carbons [43,46,49–53] to hybrid and modified ones [54–64]. This manuscript will mainly focus on the features and characteristics of carbon-based electrodes in capacitive systems, although some other parts of the electrosorption cell will also be briefly mentioned and discussed in the next sections.

### ***1.3.1 The working electrode: activated carbon***

#### ***1.3.1.1 Physical properties***

Carbon-based materials have gained importance and attention not only due to their impressive performance for highly specialized applications, but also due to their low costs and commercial availability in several presentations. For the specific case of capacitive processes, activated carbons highlight as the most common electrode reported in the literature because of their high surface area and pore volume, but also due to their highly tunable physicochemical and electrochemical properties. Activated carbons include a wide range of amorphous carbonaceous materials that are obtained by a complete or partial combustion or thermal decomposition of a variety of carbonaceous precursors. In the words of Marsh [65]:

*“An activated carbon can be considered as molecular space (i.e., the space occupied by a molecule usually in the liquid phase), this space being contained within a three-dimensional network of carbon atoms arranged in layers composed of rings structures joined together somewhat imperfectly. This network*



*is continuous in three dimensions with some layers being stacked, roughly parallel to each other, in groups of two, or three, probably not much more.”*

Although highly simple and somewhat ambiguous, this definition implies a clear understanding of the complexity of the actual structure of activated carbons, as no definition, mathematical or physical model can really denote the highly disordered graphitic layers, the wide pore-size distribution with irregular morphologies and tortuosity and the disordered molecular arrangements, which include the presence of vacancies and structural  $sp^3$  domains.

All carbon-based materials present a degree of disorder, although there is no carbon-based material with a total or an absolute disordered arrangement. Within hexagonal graphite, the most ordered structure, the layers of hexagonal-honeycomb arrangements, described as graphene layers, do not lie immediately above and below each other but are displaced to form an ABABAB sequence. The distance between the layers is 0.335 nm and the distance between two bonded carbon atoms is 0.142 nm. Within the graphitic layers, the bonding presents trigonal  $sp^2$  with hybrid sigma-bonds with delocalized pi-bonds within the layers. As the interlayer spacing of 0.335 nm is larger than that of the C-C bond (0.124 nm), this indicates no chemical bonding between the layers and the forces of attraction are only limited to van der Waals forces. The random bonding together of these small defective polycyclic groups of carbon atoms, with linear carbon atoms, creates a space called porosity [65–69].

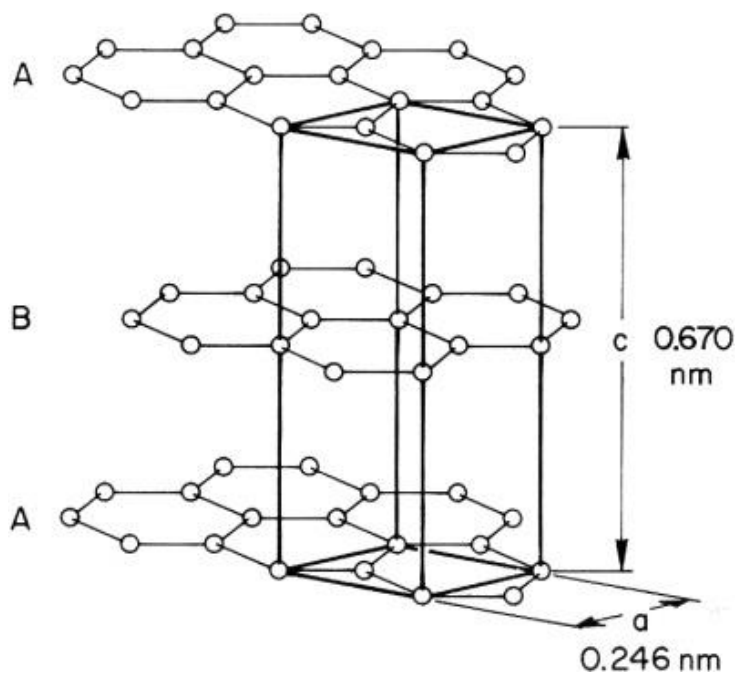


*Figure 1.2. Representation of a graphitic lattice. Each lattice comprises a graphene layer, in which a displacement of the subsequent graphene sheet can be identified [65].*

Activated carbons have high values of surface area, between 800 and 1200 m<sup>2</sup> g<sup>-1</sup>. The area of the activated carbons is given by a polydisperse capillary structure that includes pores of a wide size distribution and several shapes. The IUPAC [70] classifies the pores in macropores (> 50 nm), mesopores (2-50 nm) and micropores (< 2 nm), the latter additionally classified as supermicropores (0.7-2 nm) and ultramicropores (< 0.7 nm). The macropores and mesopores are the entrances of the adsorbate(s). In specific cases, macro and mesopores are also considered an interconnection to get to the adsorption sites, i.e., the micropores, although this only applies to hierarchical pore structures [65].

The micropores present the highest adsorption potential, which is related to the proximity of carbon atoms to each other and can retain adsorbate(s) mainly by dispersive (van der Waals) forces within the porosity. Even when any adsorbate can allocate at other preferential and closer adsorption sites (i.e., the macro or mesopores), the adsorption process is a reversible chemical reaction and that adsorbed molecules do not remain stationary at adsorption sites. This is related to thermal spikes that dislodge the adsorbed adsorbates [65]. The micropores present higher potential energy as this energy well deepens as a function of decreasing the pore size (Figure 1.3). Thus, as an adsorption process is initiated, sites of highest potential are occupied first, followed by sites of lower energy [65]. This has great coherence with the adsorption isotherm proposed by Frumkin that accounts for lateral interactions, which can be of a positive (attractive) or negative (repulsive) nature [71–73]. Then, adsorbates experience favorable positive interactions from the pore walls from several directions at the narrower pore walls.

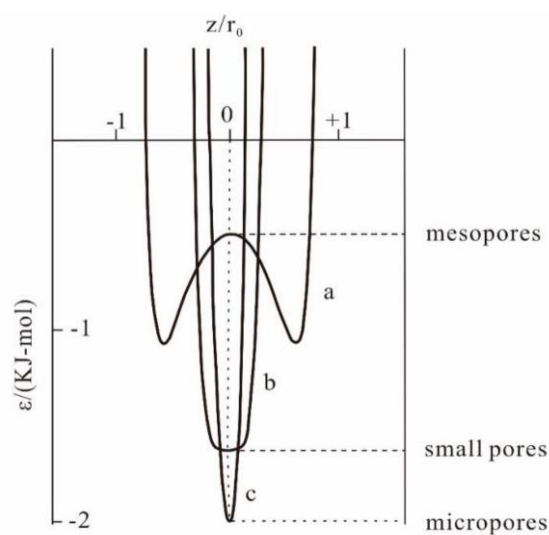


Figure 1.3. Energy peaks and distribution of the pores according to their size [65].

As can be concluded in general, the micropores are of utmost importance in activated carbons, since they represent the most energetic adsorption sites and contribute the most to the total surface area and pore volume. For the same reason, most surface chemical



properties can be associated to the surface chemistry of the micropores [68,69,74], which will be addressed upon next.

### 1.3.1.2 Chemical properties

The surface chemistry of carbon materials is a function of the presence of heteroatoms other than carbon, such as oxygen, nitrogen, hydrogen, sulfur, among others [66,67,75]. These heteroatoms are in the form of surface functional groups chemically bonded to the carbon of the structure of the graphene layer. Among the functional groups present on the carbon surface, oxygenated groups are the most common and abundant. They are represented by chemical functional groups, such as carboxyl, carbonyl, phenol, lactone, lactol, chromene, pyrone, quinone, and ether groups, distributed over the defects located on the basal plane or over the edges of the graphitic lattice [66–68,76–78]. Figure 1.4 shows the generalized structure of a graphene layer with the main oxygenated functional groups present on carbon surfaces, including the delocalized electrons from the basal planes and some  $sp^3$  domains.

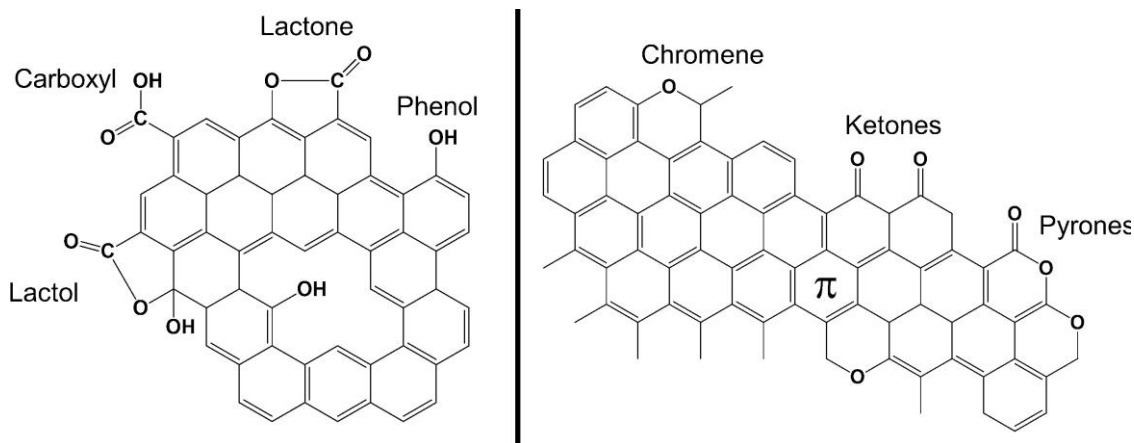
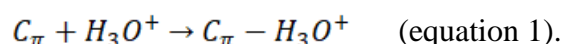


Figure 1.4. Conventional acid (left) and basic (right) groups comprising oxygen atoms on a graphene layer. The delocalized electrons of the aromatic honey-combs are also illustrated [66].

The graphitic layer and the functional groups provide specific chemical properties to all carbon-based materials. For example, a low oxygen content will decrease the polarity of the surface and thus, it will present a lower wettability or lower dispersion in aqueous solutions (the latter for the specific case of colloids). The surface chemistry also implies the development (or enhancement) of chemical reactions on its surface. For example, when immersed in an aqueous electrolyte, common reactions comprise protonation, deprotonation, coordination, ion-exchange and, of course, adsorption. Some of these reactions may promote static surface charges, which give acidic or alkaline properties to the surface, as a function of the properties of the electrolyte (e.g., the pH).

Functional groups such as carboxyl, phenol, lactol and lactone present an acid-Lewis character, which thus acidify the surface and contribute to the development of negative charges by their deprotonation at neutral and alkaline pH values [66,67,75]. Carbon basic surfaces is a subject that remains under investigation. Several authors have described that the basic character of carbon materials is associated with the presence of oxygen-containing functionalities as chromene, pyrone and quinone type [67,68,79]. However, it has been proposed that the main contribution to the basicity is by oxygen-free sites characterized by regions with  $\pi$  electron density on the carbon basal planes, which act as Lewis bases (electron donors), according to the reaction of protonation [68,69]



Therefore, the basic character of carbon has also been associated with the basal planes of the graphitic lattices with a high content of carbon atoms with  $sp^2$  hybridization, which mostly lack of oxygen-containing groups [66,67,76,79].

### ***1.3.1.3 Electrical properties***

According to the conduction band model, electrons in a carbon material occupy a continuous range of free energies. The electron that is easiest to remove is at the top of the conduction band. This energy is termed the Fermi level energy and is approximately equal (and opposite in sign) to the work function, the amount of energy required to remove an electron from the bulk material into the vacuum. The work function is strongly dependent on the surface of the carbon-based material, such as the textural properties and surface chemistry, for which the electrical conductivity vary in orders of magnitude from one carbon material to another. Carbons with only (or mostly) sigma-bonds and  $sp^3$  hybridization are generally insulators, while increasing  $\pi$ -bonds of carbon atoms with  $sp^2$  hybridization promotes the delocalization of electrons, making them available as charge carriers [66,80–83].

The oxygen content is usually associated to an increase in the resistivity of the carbon surface. For this reason, heat treatments in oxygen-free atmospheres decrease the electrical resistivity and increases the conductivity of the material. This is related to a decrease in surface  $sp^3$  domains and the subsequent increase in the domains with  $sp^2$  hybridization, which lowers the barrier for electrons [66,80–83]. Mrozowski proposed a model to interpret such changes in chars (coke): the removal of hydrogen, oxygen and low-molecular hydrocarbons (between 500 and 1200 °C) gives unpaired sigma-electrons in the peripheries of the condensed ring systems. The  $\pi$ -electrons jump from the  $\pi$ -band into the sigma state, forming a spin pair. This removes an electron from the  $\pi$ -band and creates a hole in the filled band, leading to a p-type conductivity. The large number of holes thereby created accounts for the great increase in electrical conductivity [81].

For the specific case of granular carbon-based materials, the particle size and morphology also have a profound effect in the electrical conductivity, as higher contact implies a higher conductivity between particles, which clearly lowers the global resistance value of the assembled electrode [43]. Graphite can be obtained and assembled as an electrode in a single phase of specific dimensions and geometries (e.g., prisms or cylinders made only of graphite), while granular materials must be agglomerated.

The presence of electrostatic charges on a surface in contact with a liquid promotes the formation of a complex electronic structure at such surface-electrolyte interface. Historically, this interface is known as the electrical double-layer, although most recent models consider the formation of multiple layers [LeonyLeon1993]. This is related to the fact that the implied layers promote changes in the inner potential of the electrode bulk as a function of increasing the distance from the charged surface. At this electrode-electrolyte interface, both ions and neutral species (solvent and other molecules) are distributed as a function of their thermodynamic properties and of the potential value of the surface. Although these models were first proposed to understand the interface of electrically polarized metals (electrodes) in liquid solutions, they can also describe other charged surfaces, as those of other heterogeneous systems, such as colloids and conventional surface charges that develop from chemical reactions (protonation, adsorption, etc.).

The electrode surface is the first layer at which the value of the inner potential is modified. Although it is usually schematized as a perfect pristine and planar surface, all surfaces are irregular at a nanoscopic view (Figure 1.5), which promote changes not only in the diffusion fields [84], but also in the potential (energy) distribution [85]. Changes in the potential distribution is attributed to the formation of specular dipoles at surface due to specific adsorption [86], to physical valleys and peaks [85] and even to fractal energy distributions [87]. This also implies that the planes and layers allocated at this interface will present an irregular distribution, i.e., the same ion from the same plane can be allocated at different distances from the surface [88,89].

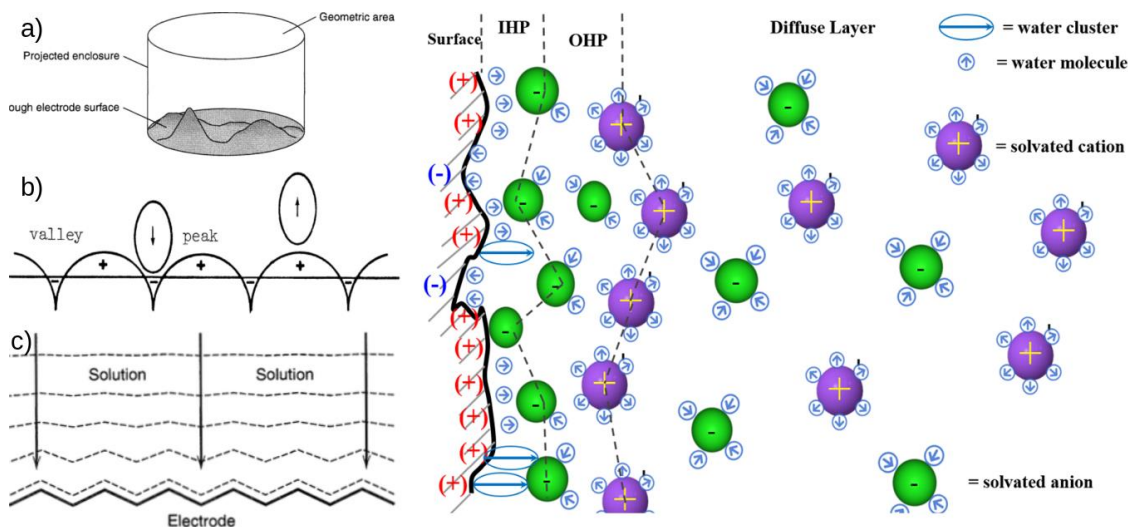


Figure 1.5. [LEFT] a) Difference between the surface area and the geometric area of an electrode [84]. b) The roughness promotes changes in the energy distribution [85,90], but also c) in the diffusion profiles to the electrode surface [84]. [RIGHT] Schematic representation of electrical layers at positively charged surfaces [84–86,88–90].

The second layer comprises a monolayer of adsorbed (fixed) water molecules [86,91], whose dipoles must not be oriented according to the charge of the surface, as this only occurs at high polarization values [92]. Some simple water dimers [86,88] are also represented. In the same layer, specifically adsorbed ions can be present, which define the inner-Helmholtz plane, whose length is half the size of the adsorbed ion. The plane of the non-specifically adsorbed ions, known as the outer Helmholtz plane, is farther away from the surface [84,86,91].

Anions are more commonly located adsorbed at positive surfaces than cations at negative surfaces [93–95]. This is due to the smaller dehydration energies of conventional inorganic anions, compared to those of inorganic cations [96–98], which promotes their partial or complete dehydration. This, in addition, promotes their approach at a distance at which van der Waals attractions overcome electrostatic repulsions [99]. These last three planes (the adsorbent solvent monolayer and the inner and outer Helmholtz planes) define the compact layer or Stern layer. The second historic layer is the diffuse layer (Figure 1.5), which extends from the outer Helmholtz plane to the bulk of the solution. The diffuse layer is composed of partially oriented but mobile water molecules and both completely solvated anions and cations; the bulk of the solution corresponds to the end of the interface and the charge of the surface does not affect the electrolyte [86].

The previous electrical layers do not present a fixed allocation and distances for all charged surfaces in all possible systems. There are certain factors that influence the development and length of these layers, such as the ionic strength of the electrolyte and the charge of the surface. The electrolyte in natural waters is highly diluted while the applied potential of the

electrode surface is limited due to the development of faradaic reactions. Both parameters increase the thickness of the formed electrical layers. In addition, the model of the electrical layers has been proposed for regular and planar surfaces, which does not account for other highly irregular and disoriented systems, as porous 3-dimensional electrodes with a wide pore-size distribution (from <1 nm to pores in the order of micrometers). Below, some models related to the formation of the electrical layers in porous structures will be reviewed.

At this point, some physical, chemical and electrochemical aspects of carbon-based materials have been briefly introduced and a first correlation between the increase in the oxygen content and the decrease of the electrical conductivity was stated above. A deeper correlation between the previous (chemical and electrical) properties consists in understanding the effect of the surface charges of these porous matrices in the electrosorption performance. Surface charges have been established as one of the most important factor to understand and even predict the performance of asymmetric electrosorption cells, which will be reviewed upon next.

### ***1.3.2 Surface charges and the electrosorption performance***

#### ***1.3.2.1 The point and potential of zero charge***

After reviewing that a charged surface promotes the formation of electrical layers at the electrode electrolyte interface, now it can be inquired how to efficiently modify such surface excess by several parameters related mostly to the electrode. The most direct approach is the value of the polarization, although it must be referred to other electrochemical parameters. As an example, there is a potential value at which the charge of the surface decreases or tends to zero [60,100,101], known as the potential of zero charge ( $E_{PZC}$ ). The  $E_{PZC}$  dictates the real polarization and charging process of the electrode surface and thus directly affects the surface excess when polarized. At more negative potentials than the  $E_{PZC}$ , the surface is negatively charged and the surface excess is mainly composed by cations; on the other hand, at more positive potentials than the  $E_{PZC}$ , the surface is positively charged and the surface excess is mainly composed by anions [84,91,102]. Electrochemical impedance spectroscopy is an adequate technique to obtain the  $E_{PZC}$  between an interval of potentials at only one frequency. Then, one must compute the capacitance from the imaginary part of the impedance spectra and graph the capacitance vs. the applied potential values. The  $E_{PZC}$  is determined as a minimum in capacitance in the obtained “V-shaped” graphs (Figure 1.6).

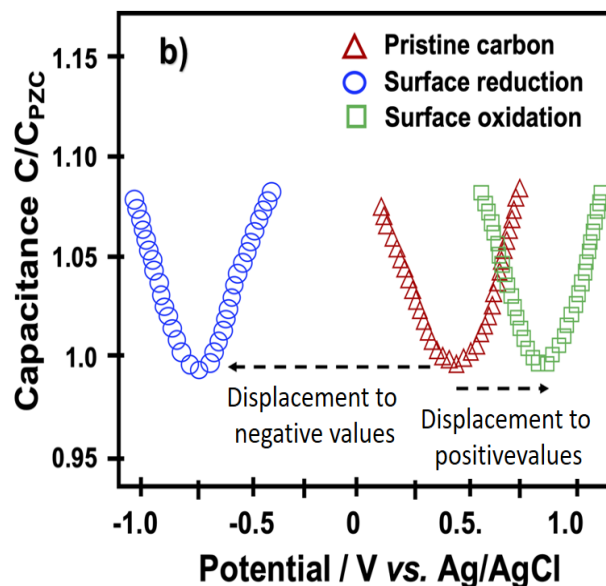


Figure 1.6. Normalized differential capacitance curves obtained from electrochemical impedance spectroscopy for two carbons with positive  $E_{PZC}$  values (red and green) and one carbon (blue) with a negative  $E_{PZC}$  [101].

The  $E_{PZC}$  is dependent on the electrical and electrochemical properties of a surface, but it is also highly dependent on the surface chemistry of the electrode, as it has been widely explored for carbon-based materials [49,50,60–62,100,103–105]. All of these reports have found that carbon-based materials with a high quantity of groups with a Brønsted-acid character increase the  $E_{PZC}$  to more positive values, while the  $E_{PZC}$  decreases to more negative values by a decrease in such functionalities and an increase of functionalities with a Brønsted-basic character.

Figure 1.6 shows such correlation, in which a pristine commercial activated carbon presented a positive  $E_{PZC}$  of  $\sim 0.45$  V (shown in red). The oxidation of the pristine carbon with nitric acid increased the content of Brønsted-acid groups and, subsequently, its  $E_{PZC}$  to a more anodic value of  $\sim 0.85$  V (shown in green), while the impregnation of the pristine carbon with amine groups decreased the  $E_{PZC}$  to the value of  $-0.75$  V (shown in blue). Usually, the farther away from the  $E_{PZC}$  implies a higher degree of electric polarization, for which there should be an agreement between the applied potential and the  $E_{PZC}$  of the electrode, i.e., the surface chemistry. This is also related to the allocation of the electrode in the electrosorption cell, as anode and cathode, which will be addressed below.

The  $E_{PZC}$  is also an indicator of the thermodynamic properties of the electrolyte, as its adsorption can change the charge distribution of the carbon surface, which affects the  $E_{PZC}$  value. Interestingly, the IUPAC [70] still defines the  $E_{PZC}$  as a parameter in the absence of specific adsorption, although Grahame [95] demonstrated the effect of electrolyte



adsorption on this parameter more than a century ago. For instance, the  $E_{PZC}$  of a mercury electrode varied as a function of the electrolyte in equimolar concentrations [95]: -0.472 V (NaF), -0.556 V (NaCl), -0.651 V (NaBr), -0.82 V (NaI) vs. the normal calomel electrode. The  $E_{PZC}$  decreased as a function of increasing the ion size of the halogen, which directly correlates with a decrease in their hydration energy. This demonstrated that bigger species with the same charge can dehydrate easier [106], promoting higher adsorption onto the electrode surface. Their adsorption increased the negative charge input at the electrode surface, promoting a more negative value of the surface potential, which was also reflected as a more negative  $E_{PZC}$ .

As hydration also depends on the electrolyte concentration, the  $E_{PZC}$  shifted to more positive potentials when decreasing the concentration (diluting) of a KI solution [95]: -0.82 V ( $10^0$  M), -0.72 V ( $10^{-1}$  M), -0.66 V ( $10^{-2}$  M), -0.59 V ( $10^{-3}$  M). Previous results indicated that the hydration energy of iodide increased with decreasing its molar concentration, thus dehydrating less and decreasing its adsorption onto the electrode surface. To summarize, the  $E_{PZC}$  is an indicator of the density and charge of species at the interface, of the energy needed to modify the surface excess, of the electrode surface chemistry, of the thermodynamic properties of the evaluated electrolyte and also to the best allocation of the electrode in the electrosorption cell.

On the other hand, activated carbons can develop charges due to several chemical reactions involving their surface functionalities without an external electrical stimulus. These reactions, as many others, are a function of the pH of an aqueous solution. One of the parameters that describe the charge distribution of a charged surface is the point of zero charge ( $pH_{PZC}$ ). The  $pH_{PZC}$  is the pH value at which the surface has no net charge and it is also indicative of the content of proton donors (Brönsted-acid character) or acceptors (Brönsted-basic character) and of their dissociation energy [80]. The surface is considered acid when the contents of proton donors is higher than that of proton acceptors; the surface is considered alkaline when the contents of proton donors is lower than that of proton acceptors. In addition, when the pH is lower than the  $pH_{PZC}$ , the surface is negatively charged; when the pH is higher than the  $pH_{PZC}$ , the surface is positively charged (Figure 1.7). In addition, a pH closer to the  $pH_{PZC}$  of a material, neutralizes and decreases its surface charges; a pH farther from the  $pH_{PZC}$  of a material, magnifies (increases) its surface charges. As the activated carbon surface contains a variety of acidic and alkaline functional groups with different  $pK_a$  values, their  $pH_{PZC}$  would correspond to an effective  $pK_a$ , representing the average surface charge of all surface functionalities [80]. The  $pH_{PZC}$  is also highly correlated with the surface chemistry of the electrode. The correct understanding of this parameter provides interfacial information and can aid in understanding and explaining such processes, such as evidencing a successful surface modification or proposing adsorption or electrosorption mechanisms, among other possible applications [36,107–109].

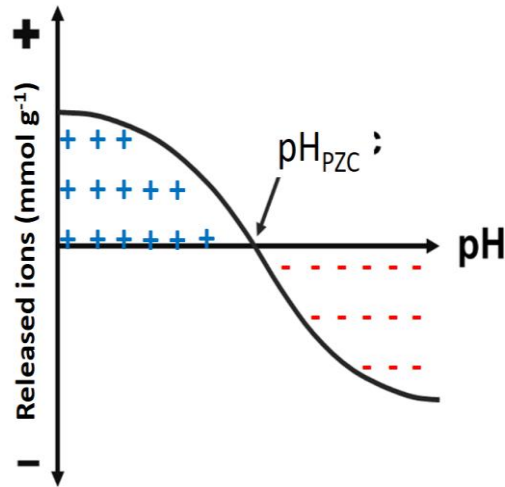


Figure 1.7. (a) Proton binding curve or released ions as a function of pH.

The  $\text{pH}_{\text{PZC}}$  and the  $E_{\text{PZC}}$  depend on the surface chemistry of the electrode, thus, there should be a correlation between them, but only few reports have evaluated such correlation. Bayram *et al.*, [110] evaluated the surface chemistry of a commercial activated carbon after its electrical polarization at different potentials. They found that the pristine carbon presented a neutral ( $\text{pH}_{\text{PZC}} = 7.4$ ) and slightly positive ( $E_{\text{PZC}} = 0.164 \text{ V vs. Ag/AgCl}$ ) surface. After the highest oxidation potential ( $5 \text{ V vs. references}$  for 90 minutes in  $\text{Na}_2\text{SO}_4$ ), the surface was acidified ( $\text{pH}_{\text{PZC}} = 3.21$ ) and became more anodic ( $E_{\text{PZC}} = 0.355 \text{ V vs. Ag/AgCl}$ ). On the other hand, the reduction potentials did not present a significant effect on the  $\text{pH}_{\text{PZC}}$  and the  $E_{\text{PZC}}$  values, and thus, on the surface chemistry of the carbon.

Another example is the one of Gao *et al.*, [111], who induced two chemical modifications on a commercial activated carbon ( $\text{pH}_{\text{PZC}} = 8.6$  and  $E_{\text{PZC}} = -0.22 \text{ V vs. SCE}$ ): i) a treatment with nitric acid and ii) an impregnation with ethylenediamine, an organic compound with a Lewis-basic character. The treatment with nitric acid promoted a decrease in the  $\text{pH}_{\text{PZC}}$  to a more acidic value (5.5) and an increase in the  $E_{\text{PZC}}$  to a more positive value (0.64 V), while the impregnation with amine-containing groups increased the  $\text{pH}_{\text{PZC}}$  to alkaline values (9.8) and decreased the  $E_{\text{PZC}}$  to a negative value (-0.38 V), compared to the values for the pristine carbon ( $\text{pH}_{\text{PZC}} = 7.4$  and  $E_{\text{PZC}} = -0.13 \text{ V}$ ).

A deeper understanding of the correlation between both parameters rely on the classification of the applied potential on the electrode-electrolyte interface. The electric potential of a charged surface can be divided in the inner potential, the surface potential and the outer potential (Figure 1.8). The inner potential is the potential difference between the bulk of two phases in contact and represents, for an electrode-electrolyte solution, the energy needed for a species to transport from the bulk of the solution to the electrode surface [84,86,91]. This movement can be divided in two steps: i) the drift from the electrolyte bulk up to the shear plane, represented by the outer potential, and ii) the drift



from the shear plane up to the electrode surface, represented by the surface potential [86,91].

Here, the outer potential is the relevant parameter in capacitive processes, as it becomes the true potential that will attract or repel certain ions located at the bulk. Then, the surface and inner potential should be in correct agreement to promote synergistic effects on the outer potential, rather than antagonistic effects. The surface potential is at the contact plane between the surface and the electrolyte, for which it is affected by the presence of static charges from functional groups, which thus affect the level of electrostatic interactions towards species at the interface, sometimes referred as the ‘surface excess.’ Then, the surface potential can be (qualitatively) inferred by measuring the  $E_{PZC}$  or indirectly by measuring the  $pH_{PZC}$ , also providing information on selecting the inner potential (the polarization of the electrode). This will be reviewed in more detail in the next section.

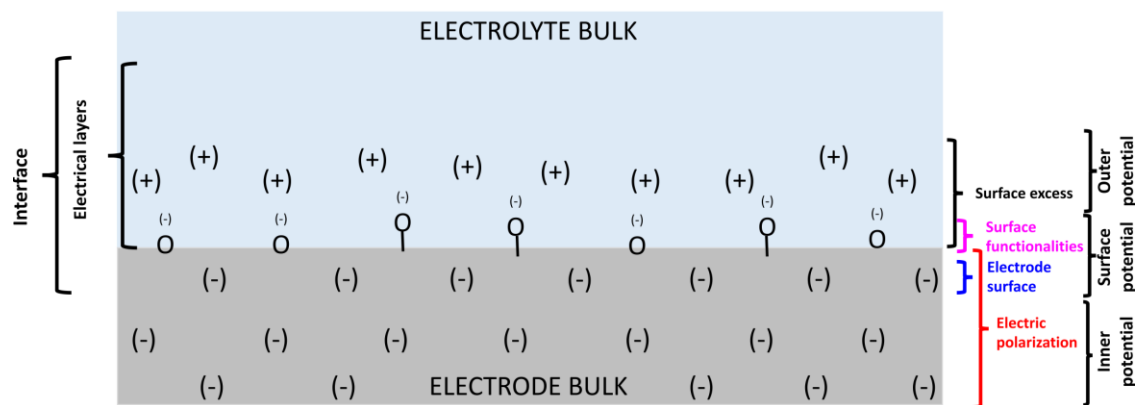


Figure 1.8. Schematic representation of a charged solid-liquid interface to highlight different electric potentials, i.e., the inner, surface and outer potentials.

### 1.3.2.2 The amphoteric Donnan model

Figure 1.8 also presents a case in which both the inner and the surface potential are negative. This represents a synergistic effect in the electrostatic interactions towards interfacial species and, as was stated above, this enhances the electrosorption removal capacity and velocity. The opposite will occur with antagonistic charges (i.e., a positive inner potential and a negative surface potential), as the inner (applied polarization) and outer (surface chemistry) potentials tend to counter, decreasing the outer potential. Opposite fixed charges to the electric polarization of the surface present an antagonist effect on electrosorption performance: they repel the adsorbate, stabilize the co-ions, and can even block the entrances of narrower pores, hindering the diffusion of the adsorbate [62,103,112]. For this, higher potentials (higher energy) are needed to counter the effect of fixed surface charges, also increasing the probability of developing redox reactions and compromising the stability of the system.

The (conventional) Donnan model considers that the electrical layers are strongly overlapped along the pore surfaces. For example, one can compute the double-layer thickness from the Gouy-Chapman equation

$$k = \left( \frac{2n^0 z^2 e^2}{\epsilon \epsilon_0 \kappa T} \right)^{1/2} \quad (\text{Equation 2})$$

where  $k$  is the double layer thickness ( $\text{cm}^{-1}$ ),  $n$  is the concentration ( $\text{mol m}^{-3}$ ),  $z$  is the charge of the symmetric electrolyte,  $e$  is the charge of an electron ( $1.60219 \times 10^{-19} \text{ C}$ ),  $\epsilon$  is the dielectric constant of the solvent (78.54 for water at 298 K),  $\epsilon_0$  is the permittivity of free space ( $8.854188 \times 10^{-12} \text{ C}^2 \text{ J}^{-1} \text{ m}^{-1}$ ),  $\kappa$  is the Boltzmann constant ( $1.38066 \times 10^{-23} \text{ J K}^{-1}$ ) and  $T$  is the temperature (K). The equation predicts a thickness of 18.67 nm (0.1 mM of a 1:1 electrolyte,  $T = 25 \text{ }^\circ\text{C}$ ,  $\epsilon_{\text{water}} = 78.54$ ), which implies that the electrical layers overlap at the micropores and, at some degree, also at the mesopores [113–116]. Then, a single electrostatic potential and concentration in each micro-region is assumed. This electrostatic potential comprises the Gouy-Chapman-Stern potential and the Donnan potential, i.e., the potential difference inside and outside the overlapped pores, which it will be different for negative and positive regions [112,117–121]. This leads to an electrical double-layer model based on the Donnan concept, in which the electrical potential makes a distinct jump from a value in the space outside the carbon particles to another value within the carbon micropores, without a further dependence of potential on the exact distance to the carbon walls [116]. For this, the Donnan approximation is the mathematical limit of the mean-field Poisson-Boltzmann theory for overlapping diffuse layers, when the Debye length greatly exceeds pore size. In this limit, the exact pore geometry is no longer of importance, and neither is the surface area. Instead, only the pore volume matters.

The amphoteric Donnan model is also a mathematical model based on the Donnan model (the Donnan potential of a porous electrode) developed to predict the salt adsorption capacity of desalination cells by porous electrodes. The feature of the amphoteric Donnan model makes it different from previous models based on the Donnan potential implying that porous electrodes (activated carbons) present both negative (acidic) and positive (alkaline) fixed chemical charges (functional groups) dispersed through their surface, which are not countered by each other. This, of course, is in excellent agreement with conventional data and knowledge of such porous matrices, previously addressed above.

The model should be physically understood by analyzing the three parameters that denote the electric charge of the system, according to the equation

$$\sigma_{\text{ionic},j} + \sigma_{\text{elect},j} + \sigma_{\text{chem},j} = 0 \quad (\text{Equation 3})$$

where  $\sigma_{\text{ionic}}$  is the charge of the ions,  $\sigma_{\text{elect}}$  is the charge of the polarization,  $\sigma_{\text{chem}}$  is the charge of the carbon surface and the subscript  $j$  denotes the positive or negative regions on

the carbon surface. Then, the mathematical model depends on experimental data rather than proposing or assuming mathematical parameters. As each micro-region is always electroneutral, the equation always equals zero, but data can be abstracted and modelled after obtaining specific information of the system. At 0  $V_{\text{cell}}$  and at the  $\text{pH}_{\text{PZC}}$ , the equation decreases to  $\sigma_{\text{ionic},j} = 0$ , i.e., the electrodes do not present any charge and thus, there is no ion removal by electrostatic interactions. At 0  $V_{\text{cell}}$  and beyond the  $\text{pH}_{\text{PZC}}$ , the equation reduces to  $\sigma_{\text{ionic},j} = -\sigma_{\text{chem},j}$ , for which ion adsorption is only dependent on the surface charges from functional groups with Brönsted character; as a contrast, at the  $\text{pH}_{\text{PZC}}$  and when electrically polarized, the equation reduces to  $\sigma_{\text{ionic},j} = -\sigma_{\text{elect},j}$ , for which ion adsorption is only dependent on the surface charge derived from the electrical stimulus.

The interesting case is the re-arranged global equation  $-\sigma_{\text{ionic},j} = \sigma_{\text{elect},j} + \sigma_{\text{chem},j}$ , at which the previously stated antagonistic or synergistic effect discussed in the previous section can be observed by a mathematical approach: when  $\sigma_{\text{elect},j}$  and  $\sigma_{\text{chem},j}$  present a different sign,  $\sigma_{\text{elect},j}$  must first neutralize the surface charges before inducing an electrostatic interaction towards the ionic species in solution; when  $\sigma_{\text{elect},j}$  and  $\sigma_{\text{chem},j}$  present the same sign, both charges are additive, thus increasing the outer potential and the removal performance of the electrode pair.

The application of the amphoteric Donnan model (Figure 1.9) implies that an electrode with a net positive charge (alkaline  $\text{pH}_{\text{PZC}}$  and/or negative  $E_{\text{PZC}}$ ) should be polarized at positive potential values and an electrode with a net negative charge should be polarized at negative potentials (acidic  $\text{pH}_{\text{PZC}}$  and/or positive  $E_{\text{PZC}}$ ). This has been mostly evaluated by measurements of the  $E_{\text{PZC}}$  on activated carbon electrodes, which can greatly influence salt removal, charge efficiency and cyclic stability in capacitive deionization cells. For example, Omosebi *et al.*, [100] studied the desalination of a pristine (Pr,  $E_{\text{PZC}} = 0.2$  V) and oxidized (Ox,  $E_{\text{PZC}} = -0.2$  V) activated carbon cloth in four cell arrangements: Ox+Pr-, Pr+Pr-, Ox+Ox-, and Pr+Ox-. The symbols represent the electrical polarization of these carbons in the desalination cell (+ is the anode and – is the cathode). When polarizing the positive carbon and the negative carbon as the positive and negative electrodes, respectively, the desalination increased 4.25 times, compared to the opposite configuration. This same tendency is observed directly or indirectly in other works [49,50,60–62,100,103–105].

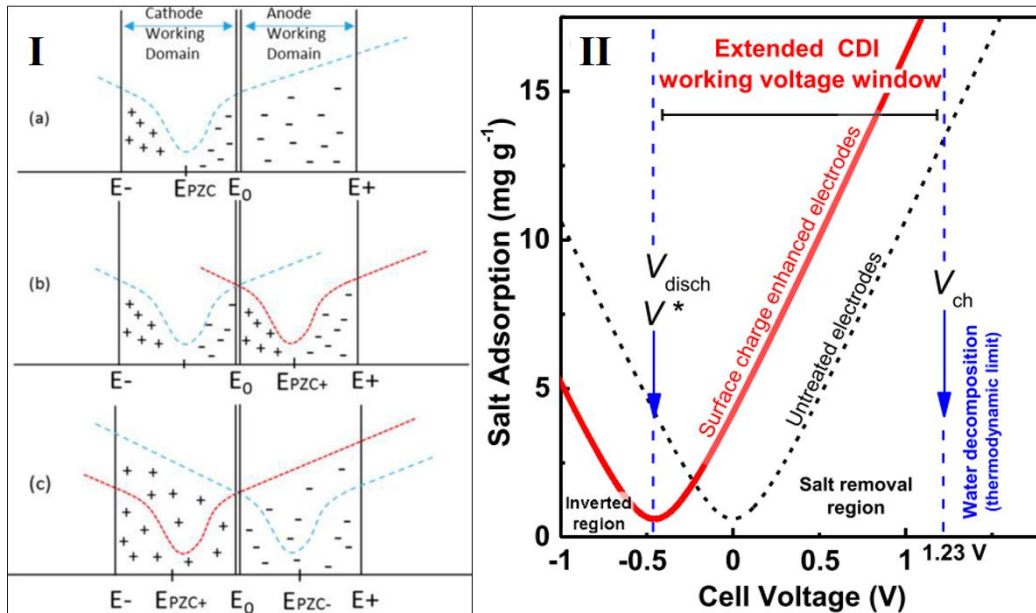


Figure 1.9. Practical application of the amphoteric Donnan model. I) The properties and allocation of the electrode influence their performance [104]. II) The correct allocation of an electrode could increase the polarization limits of the electrosorption cell by distancing the  $E_{PZC}$  from the applied potential [62].

In this section, a deep explanation of the effect of the surface charges in the electrosorption performance was established, by the understanding and correlation with the outer potential. In the next, several aspects of how to measure electrosorption performance will be revised.

### 1.3.3 Performance in electrosorption

The performance of an electrosorption cell corresponds to specific and tangible metrics, usually centered in the next aspects: costs of the process, removal capacity, removal rate, charge efficiency, selectivity, greener materials and process, stability and cyclability of the electrode, scalability, implementation of the technology, among others. Some of them will be addressed in this section, while others have been mentioned and discussed previously. It is also somewhat evident that cost could be the most important metric in water treatment processes, in general, for which most performance metrics are cost related.

#### 1.3.3.1 Charge efficiency

Charge efficiency is a parameter that correlates the removed moles of adsorbate over the measured current during the kinetics, for which it is computed as

$$\lambda = \frac{\Gamma^*F}{Q} \quad (\text{Equation 3})$$

where  $\Lambda$  is the charge efficiency (adimensional),  $\Gamma$  is the removed moles of adsorbate (moles),  $F$  is the Faraday's constant ( $C\ mol^{-1}$ ) and  $Q$  is the charge (C). As the ionic adsorbates are directly retained in the electrical double-layers formed on the porous structure, it provides information on these complex interfaces [43,116,122–124]. The charge-efficiency is also based on the Donnan concept, in which the electrical potential makes a distinct jump from a value in the space outside the carbon particles to another value within the carbon micropores, without a further dependence of potential on the exact distance to the carbon walls [116].

Theoretically, every electron provided to the carbon electrode by its electrical polarization should remove one adsorbate from solution. Nevertheless, the polarization and charging processes of the electrodes not only promote the insertion of counter-ions at the electrical layers, as co-ions also are mobilized during these processes. Then, the electrons not only attract counter-ions (i), but they also expel co-ions (ii, ion-swapping and co-ion expulsion) or can even develop faradaic reactions (iii) [43,122,123] (Figure 1.10). For this, the expected mathematical values of the charge-efficiency are between 0, in which there is no electrosorption, and 1, the ideal case in which every electron retains one ion from solution.

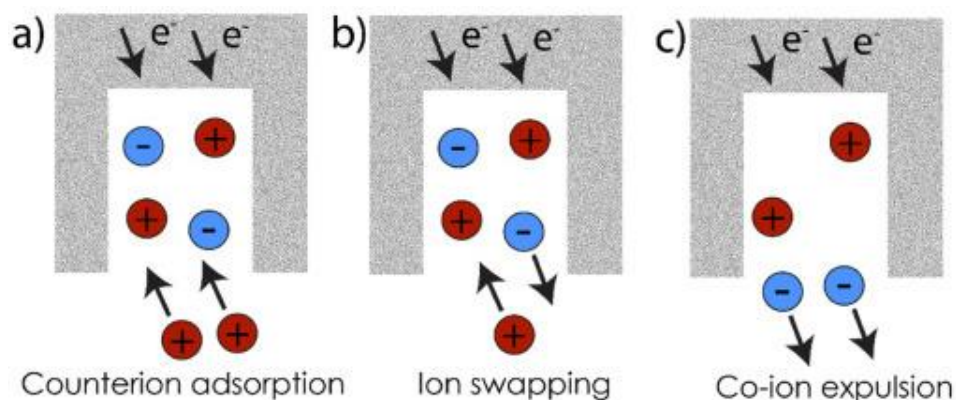


Figure 1.10. Different effects of the electrical polarization of porous adsorbents during the electrosorption process: a) counter-ion adsorption, b) ion-swapping and c) co-ion expulsion [43].

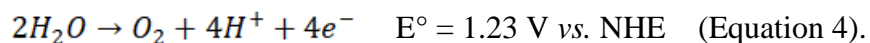
Although the charge efficiency is very useful and non-empiric parameter that provides direct data of the electrosorption performance and thus cost-related information, it does not explain several aspects of the cell. As an example, it has been extensively reported that the charge efficiency greatly increases as a function of decreasing the ionic strength of the electrolyte [43] and this has only been explained as an increase in the leakage of the co-ions through the membrane (a reduced membrane selectivity) when using membrane capacitive deionization cells. Nevertheless, this same phenomenon occurs when evaluating cells that lack a selective ion membrane, i.e., for conventional capacitive deionization cells. On the other hand, it has also been stated that charge efficiency increases by increasing the applied potential [43], although this must be specific for certain electrodes and systems. In addition,

there must be, of course, a limit in which the charge efficiency stop increasing and even decreases as a function of increasing the applied potential due to the development of parasitic faradaic reactions, which has not been established to date. Finally, there is always a lack of comparison with appropriate adsorption blanks (without polarizing), to subtract the adsorption removal to the electrosorption removal. To assume that the electrodes (or even the membrane) do not present any ion removal without the electric stimulus has biased several results, discussions and interpretations, thus obtaining overrated charge efficiencies.

### ***1.3.3.2 Faradaic reactions***

The presence of faradaic reactions decreases the electrosorption performance of electrodes, as was previously described during the charge-efficiency discussion. This basically implies that such electrons are not used to retain ions at the interface, but are instead transferred to electroactive species at the interface. Here, a deeper discussion will be settled on conventional faradaic reactions and their viability in electrosorption cells.

Regarding the applied potential and the limited polarization windows for such capacitive processes, most reports only evaluated potentials of 1.2 V<sub>cell</sub>, i.e., below the thermodynamic potential difference of water electrolysis [43,125–128]



Nevertheless, two inconveniences arise: i) such ideal and theoretical value does not consider resistances of the system (charge-transfer resistances of the electrode and the resistance of the electrolyte), which can increase the potential difference needed to the development of water electrolysis; and ii) this same potential does not give information on the kinetic limitations of the reaction over a specific electrode surface, i.e., a fast water electrolysis reaction may not be developing at the surface of activated carbon when polarized even above an overpotential, compared to certain metallic electrodes, such as platinum. Both previous reasons could imply that rapid water electrolysis could be occurring at a much higher potential difference than 1.23 V or that water electrolysis is not favorably fast at all on the studied activated carbon electrodes.

In general, a more correct and systematic understanding of parasitic reactions should imply the correlation of cell potentials with the potential of a reference electrode. For example, if the open circuit voltage of an asymmetric electrode pair presents a value of 0 V vs. the normal hydrogen electrode (NHE) in a solution with a pH value of 7, the (theoretical and ideal) potential difference for water electrolysis decreases to 0.81 V, according to its Pourbaix diagram (Figure 1.11). In addition, if the open circuit voltage is lower than -0.42 V or higher than 0.81 V vs. NHE (at pH = 7), water reduction and oxidation reactions, respectively, occur spontaneously without even polarizing the electrodes [105]. Then, water electrolysis is not only a matter of a potential difference, but also to the initial



electrochemical conditions of the system (open circuit voltage and potential of zero charges of both electrodes in the specific electrolyte).

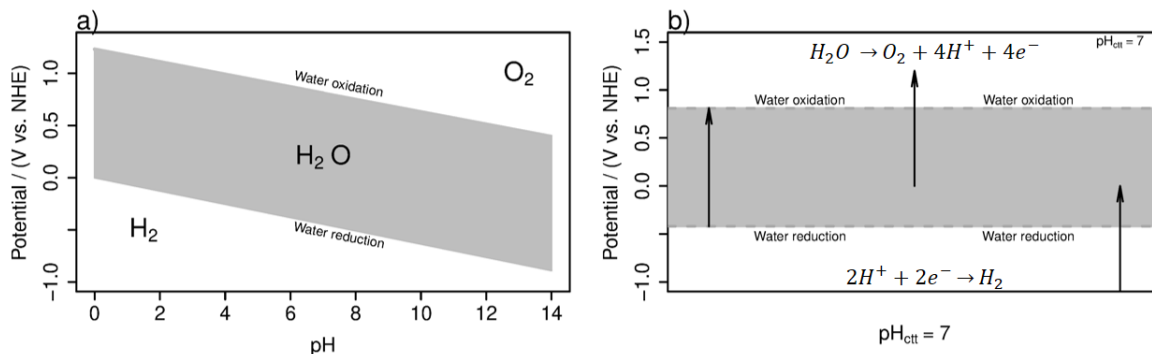
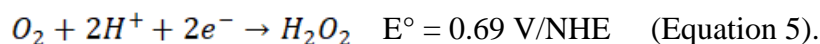


Figure 1.11 a) Pourbaix diagram of water. b) Three possible cases related to water electrolysis at pH 7 according to the open-circuit potential of the counter electrode.

Other possible and more favorable reactions comprise the oxidation of the carbon surface [49–51,104,129–133], as they can occur at much lower potential differences than 1.2 V<sub>cell</sub>. The most known and referenced electrochemical reaction is that of the quinone-type groups, although this has been mostly observed at low pH values [49,134]. Nevertheless, several functional groups on the carbon surface can be easily oxidized when electrically polarized [68,74].

It has actually been reported that activated carbons have increased its basal potential of zero charges when polarized at negative potentials [104,110], which directly relates to the oxidation of the surface and could imply that oxidation reactions are occurring immediately after immersion. In this regard, there are no standard potential values for the electrochemical reactions of the carbon functionalities [131] and clearly there is no Pourbaix Diagram for such groups on carbon-based materials. Desalination cells may induce the oxidation of chloride, for which this specific reaction must be considered in these systems, while the oxidation of fluoride is totally non-viable in aqueous solutions.

Parasitic reactions not only decrease the electrosorption performance of the electrodes, but it also presents an effect in the pH of the solution. In electrosorption cells the pH usually increases depending on the type of electrode: capacitive electrodes present lower pH increases, while pseudocapacitive electrodes present higher pH increases [114,135]. On the other hand, this increases in the pH of the solution provide a first insight of the reactions taking place at the cell. The most common and experimentally demonstrated reaction in electrosorption cells is that of oxygen reduction and peroxide formation [125,128,131,136]



The development of this reaction explains the observed increase in the pH of the solution in electrosorption cells. On the other hand, more intuitive reactions, such as the electrochemical oxidation of water and of the carbon surface, should decrease the pH of the solution. Then, there is clear evidence that such reactions take place when carbon is electrically polarized, as was stated above. Nevertheless, it seems that such oxidation parasitic reactions only occur at longer times or after several polarization cycles [100,104,133,137,138], which reiterates the importance of establishing not only the development of the reaction and its oxidation potential, but also attaining kinetic aspects of each possible reaction.

### ***1.3.3.3 Regeneration and cyclic performance***

Cyclability or the cyclic performance of electrodes used for the electrosorption process is one of the main advantages over other processes. First-of-all, the regeneration provides two marked benefits: i) the decrease of the electrostatic interactions towards the adsorbate, thus promoting its stripping and ii) the regeneration of the carbon surface from the developed electrochemical reactions (e.g., the partial electrochemical reduction of the oxidized surface after its polarization). The first point could be achieved solely by depolarizing the carbon surface, i.e., by inducing a short-circuit at the open-circuit potential or voltage. This depolarization of course is more energy-efficient than by reversing the polarization of both electrodes, although sometimes the expelling velocity of the adsorbate is much slower. The second point implies the long-term usage of the electrodes, as the oxidation reactions decrease their conductivity and thus, in their performance, which also promote marked changes in the pH of the electrolyte.

Another feature of the regeneration of electrodes is that it can be performed *in situ* and without any special procedure. In contrast, other processes must induce a certain treatment of the activated carbons or membranes. For example, the regeneration of the adsorbents with chemisorbed species requires the immersion of these materials in concentrated solutions of salts, alkalis or acids, which also increase the generation of waste products. Other regeneration processes use a thermal treatment in specific atmospheres (N<sub>2</sub>, for example), which implies increasing the temperature and using special gases or reagents, thus increasing the cost of the regeneration process. The most complicated regeneration process in electrosorption is related to fouling, in which conventional retro-washing is used.

### ***1.3.4 Fluoride removal by electrosorption processes***

As stated previously, even when electrosorption has been mainly implemented in water desalination, it has been also implemented for the selective removal of specific ions. For this, there are already reports on the electrosorption of fluoride by activated carbon electrodes and some of them will be reviewed in this section.



Dong *et al.*, [139] designed a porous biochar from waste cattail as electrodes, reaching a removal of  $1.28 \text{ mg g}^{-1}$ , although the presence of competing anions promoted a decrease in fluoride removal. Li *et al.*, [140] evaluated the electrosorption by a micropore-dominant activated carbon, decreasing by half the initial concentration ( $50 \text{ ppm F}^-$ ). Although adsorption was not evaluated, the removal at the lowest applied potential of  $0.4 \text{ V}_{\text{cell}}$  was minimal, which increased as a function of increasing the potential up to  $1.6 \text{ V}_{\text{cell}}$ . At higher potentials, water electrolysis was visually observed. They obtained a charge efficiency, of 0.98, near to the ideal theoretical value and this was attributed to the highly microporous structure which decreased the co-ion swapping and expulsion explained above.

Gaikwad *et al.*, [141] evaluated the simultaneous removal of Cr(VI) and  $\text{F}^-$  in several initial concentrations (10, 25, 50 and  $100 \text{ ppm F}^-$  and/or Cr(VI)). The (molar) removal of Cr(VI) was much higher than that of  $\text{F}^-$  and the electrosorption cell presented much higher performance (removal capacity and rate) as a function of decreasing the initial concentration of the feed. A similar report was also published by Gaikwad *et al.*, [142]. Tang *et al.*, [143] developed a mathematical model to explain the effect of salinity (0, 5 and  $20 \text{ mM NaCl}$ ) in fluoride removal by single-pass constant-voltage with high accuracy with the experimental data at different potentials ( $E_{\text{cell}} = 0.9, 1.2 \text{ and } 1.5 \text{ V}$ ) and different  $\text{F}^-$  concentrations (1, 2 and  $3 \text{ mM F}^-$ ). A similar report was also published by the works of Tang *et al.* [144,145].

Similarly, to adsorption, the State-of-the-Art in fluoride electrosorption implies the modification of activated carbon electrodes with metal phases, to promote not only higher interactions towards the adsorbent by increasing the polarity of the carbon surface, but also due to an enhancement in its electrical conductivity. Li *et al.*, [55] modified a commercial powder activated carbon with  $\text{Ti}(\text{OH})_4$  ( $V = 50 \text{ mL}$ ,  $M = 50 \text{ mg}$ ,  $C_0 = 50 \text{ ppm F}^-$ ) and increased the removal capacity in 20% ( $q = 33.6 \text{ mg g}^{-1}$ ) when polarizing at  $1.2 \text{ V}_{\text{cell}}$ . Wu *et al.*, [57] modified a commercial powder activated carbon  $\text{TiO}_2$  ( $V = 160 \text{ mL}$ ,  $M = \text{not stated}$ ,  $C_0 = 10 \text{ ppm F}^-$ ) and increased the removal capacity in 4.2 times ( $q = 1.56 \text{ mg g}^{-1}$ ) when polarizing at  $1.5 \text{ V}_{\text{cell}}$ .

The differences in the increase in removal compared to the adsorption without polarization between both modified carbons can be explained by the amphoteric Donnan model.  $\text{Ti}(\text{OH})_4$  should present a higher deprotonation and thus, a highly negative charge at the studied conditions ( $\text{pH} = 7$ ), promoting higher electrostatic repulsion towards fluoride, compared to  $\text{TiO}_2$ . Nevertheless, characterization data were not reported, as the content of the metals in the modified carbon, surface charges or any information related to these parameters. Nevertheless, the capacity of modified activated carbon with metals can be enhanced by their electrical polarization.

## 1.4 Lanthanum(III) as a modifying agent

### 1.4.1 Adsorption performance

Lanthanum is the 57th element in the periodic table and presents an atomic weight of 158 g mol<sup>-1</sup>. Lanthanum is located among the lanthanide family, which present f electrons in its electronic configuration, and its conventional oxidation state is mainly La<sup>3+</sup>, as most lanthanide and actinide elements (4f<sup>n</sup>5d<sup>0</sup>6s<sup>0</sup> or 5f<sup>n</sup>6d<sup>0</sup>7s<sup>0</sup>), although La<sup>2+</sup> is also a relevant and stable cation.

Lanthanum, due to its physical and chemical properties, classifies as a hard Lewis acid. Lewis improved the conventional theory on acids and bases by extending the definition to species that can accept or donate an electron pair, respectively, which was previously limited to accept or donate protons in aqueous solutions. Inorganic chemists have also extended the Lewis classification into hard and soft elements. Hard acids present a small ionic radii and strong solvation energy, a high charge, empty orbitals in their valence shell and high energy LUMOs, which makes them form strong and spontaneous complexes with hard bases.

Hard bases, on the other hand, present small ionic radii, are highly electronegative, are weakly polarizable, present a strong solvation and have high energy LUMOs. This classification for Lanthanum implies that it will spontaneously and strongly bond to specific functional groups with a hard Lewis character, such as the oxygenated functionalities on an activated carbon surface (carboxylic and phenolic groups); and ii) after its immobilization, it will spontaneously bond and prefer to bond to the stronger Lewis bases and fluoride is one of the strongest bases in the periodic table.

Hence, La(III) has been widely implemented for the adsorption of hard bases, such as fluoride [36,146–148]. For the scope of this manuscript, only data from the adsorption kinetics will be described. As an example, Rao *et al.*, [149] removed more than 90% of fluoride by lanthanum oxide after one hour of contact in two different mass:volume ratios (V = 50 mL, C<sub>0</sub> = 4 ppm). Sahu *et al.*, [150] obtained approximately the same performance by modifying poly-o-toluidine with lanthanum phosphate by sol-gel polymerization (M = 20-250 mg, V = 100 mL, C<sub>0</sub> = 5, 10 and 20 ppm). Yu *et al.*, [151] produced a carbon material from *Sargassum*, which was mixed with silica gel impregnated with La(III) and reached a capacity of 50 mg g<sup>-1</sup> (M:V = 0.4 g L<sup>-1</sup>, C<sub>0</sub> = 20 ppm, pH<sub>0</sub> = 7).

Then, La(III) presents not only high affinity and thus high adsorption capacities and velocities towards this anion, but it also performs efficiently at neutral pH values, with a high selectivity and with lower costs of implementation, compared to other rare earths, such as Sc(III), Ho(III), Sm(III), Ce(IV), Nd(III), Y(III) Pr(III,IV), among others [64,152–156]. In addition, La(III) presents low toxicity and bio accumulation [157,158], which depends

on the dose, the uptake forms (free cation or ion pair, cluster or crystal size, etc.) and its physicochemical properties [159–161].

Lanthanum has been previously immobilized on a commercial activated carbon for fluoride adsorption. This work, by Vences-Alvarez *et al.*, [36] used the bituminous activated carbon F-400 and the impregnation process was experimentally optimized by evaluating several La(III) concentrations and contact times. The experimental optimization was based upon the fluoride removal by adsorption points, in which the optimum materials were impregnated in a 0.05 M La(III) solution for 2 days, in which the best modified adsorbent was impregnated with a 2.1% of La(III) (w/w).

The materials with higher La(III) content decreased the textural properties of the activated carbon by blocking most of the micropores, for which their adsorption increased no further, which was also corroborated by SEM-EDS micrographs and mappings. The presence of the crystalline forms of La(OH)<sub>3</sub> and La<sub>2</sub>O<sub>3</sub> were confirmed by XRD analysis (M = 0.1 g, V = 30 mL, pH<sub>0</sub> = 7, C<sub>0</sub> = 20 ppm). These forms favored a mechanism in which the fluoride was chemisorbed to the modified surface via a ligand-exchange with the exposed hydroxyls from the formed La(III) clusters, for which the pH increased substantially during adsorption. Finally, an analysis of the kinetics showed that the modified activated carbon removed 8 times more fluoride than the pristine carbon and the effect of co-existing anions only presented an effect when their initial concentrations were of 50 ppm, i.e., 2.5 times the initial concentration of fluoride.

The development of the ligand-exchange mechanism was corroborated by analyzing the pK<sub>a</sub> distribution of conventional functional groups of carbon-based materials before and after fluoride chemisorption. The modified carbon presented an intense peak at the interval of pK<sub>a</sub>s between 7 and 9, associated to hydroxyls groups [68], which was almost absent when performing the same analysis after fluoride adsorption. On the other hand, the capacity of the same modified carbon decreased when evaluated in real tap water samples, although its performance was still much higher than that of the adsorption blank, i.e., the pristine carbon in deionized water.

#### ***1.4.2 Capacitive performance***

Considering that the graphitic structure of the modified carbon remains unaffected by the impregnation process, the modified activated carbon discussed previously could still present good electrical properties (conductivity) and could be electrically polarized to further increase its fluoride removal. Nevertheless, as the micropores represent the most conductive zones of the activated carbon, a lower range of La(III) contents should be studied. As stated above, the micropore volume decreased after the impregnation due to the formation of La(III) clusters.

On the other hand, the addition of La(III) to the activated carbon seems viable considering the capacitive properties and cyclability performance of several lanthanum compounds [162–170]. From the literature, lanthanum oxide has been reported the most, although there are other capacitive compounds. As an example, Yadav *et al.*, [165] synthesized thin films of La<sub>2</sub>O<sub>3</sub> with a microrod structure, which were grown over stainless-steel surface by hydrothermal method. Their electrode presented a specific capacitance of 250 F at a scan rate of 5 mV s<sup>-1</sup>. This material showed a stable cyclic performance during 1000 cycles, in which its capacitance was reduced by 19%.

The work of Rajagopal *et al.*, [168] on doped nanosheets of reduced graphene oxide with lanthanum oxide/hydroxide nanoparticles evaluated three different ratios of the reagents substrates. The material with a lanthanum - graphene ratio of 1:2 presented the highest capacitance of 889.29 F cm<sup>2</sup> compared to the other higher ratios and the pristine materials (lanthanum nanoparticles and reduce graphene oxide), which was only reduced by 16% after 1000 cycles. Zhang *et al.*, [163] synthesized LaN via the calcination of La<sub>2</sub>O<sub>3</sub> in NH<sub>3</sub> atmosphere, reaching a volumetric capacitance of 951.3 F cm<sup>-3</sup> with 1 A g<sup>-1</sup> of current density. The volumetric capacitance decreases in less than 1% after 1000 cycles at three different current densities. Then, the electrochemical properties of several lanthanum phases is worth to highlight.

For all previous reasons, the incorporation of La(III) to an activated carbon and its subsequent polarization at positive potentials could provide beneficial capacitive properties to this matrix, similar to those observed in a double-layer capacitor reported above, thus increasing both the adsorption capacity (without polarizing) of the modified lanthanum - activated carbon matrix by chemisorption interactions with the La(III) clusters and the electrosorption capacity of the pristine activated carbon by its electric polarization.

## Motivation of this research

High fluoride concentrations in arid and semi-arid zones due to groundwater overexploitation promotes its consumption above the recommended national and international standards, negatively affecting human health. As most water treatment plants present an adsorption step with activated carbon and considering its electrical properties, activated carbons can be electrically polarized to enhance electrostatic interactions towards this highly polar anion, possibly increasing its removal capacity and even its removal velocity. Furthermore, due to their versatility, most carbon-based materials can be chemically modified by their impregnation with diverse compounds, in which the modification with specific metal phases could not only enhance the polarity of the surface and present a much higher chemical affinity towards fluoride, but also enhance the electrical properties of the whole matrix (metal - activated carbon hybrid). Regarding this, lanthanum highlights as both an excellent fluoride sorbent and a capacitive material in several of its forms, for which a hybrid La(III)-activated carbon can be expected to increase the removal capacity and velocity of fluoride when polarized, compared to conventional adsorption.

## **Hypothesis**

The electrical polarization of a commercial activated carbon impregnated with La(III) will increase the removal capacity and velocity towards fluoride, due to higher electrostatic interactions and migration effects. The performance of the modified electrodes will be better (higher and faster fluoride removal) than that of the pristine unmodified carbon and than the performance obtained by conventional adsorption. In addition, water electrolysis will not be thermodynamically nor kinetically favored in the studied system.

## **General objective**

The purpose of this work is to evaluate different lanthanum impregnation contents, polarization values and polarization profiles to identify the best conditions of fluoride removal capacity and velocity by the studied electrodes. Furthermore, evaluate the selectivity towards fluoride by electrosorption against other anions of environmental relevance.

## **Specific objectives**

- \* To identify the effect of the pore-size distribution on fluoride electrosorption by two commercial activated carbons with standardized surface area, surface chemistry and polarization and charging processes.
- \* To describe the effect of the applied potential in fluoride removal by the previous commercial carbons to corroborate that water electrolysis is not an impeding reaction on the electrosorption performance in the studied conditions.
- \* To identify the effect of the La(III) loading, of the polarization value and of the polarization profile (polarizing from the beginning and after the adsorption equilibrium) of the modified carbons by batch experiments to provide the best conditions for fluoride electrosorption removal (capacity, velocity, cyclability and stability).
- \* To establish the effect of competing anions of environmental relevance in equimolar initial concentrations in the electrosorption performance of fluoride.

## Chapter two: Exploring the polarization window during fluoride electrosorption in activated carbons with differences in their pore-size distribution

Adapted from the following published work:

**D.R. Martinez-Vargas**, L.F. Chazaro-Ruiz, J.R. Rangel-Mendez, Exploring the polarization window during fluoride electrosorption in two activated carbons with significant differences in their pore-size distribution, *Sep. Purif. Technol.* 295 (2022) 121360. <https://doi.org/10.1016/j.seppur.2022.121360>.

### 2.1. Introduction

Fluorine is an essential element at concentrations below 1.5 ppm in water for human consumption [30,31]. Nevertheless, its overexposure and chronic consumption above such limit promotes dental and skeletal fluorosis, an undesired condition spread worldwide [30,31]. Electrosorption is a treatment option for either organic or inorganic ions present in different water reservoirs at low concentrations [43]. The applied electric field not only increases the electrostatic interactions towards the adsorbate(s), but it also enhances the mass-transport to the electrode surface due to migration effects [49–51], thus, increasing the removal capacity and rate compared to a conventional adsorption process.

Electrodes for electrosorption usually comprise porous adsorbents with good electrical conductivity and carbon-based materials have become one of the most common electrodes [43,46]. The electrosorption performance depends on several factors, as there should be a correct agreement between the properties of the adsorbate (charge, hydrated energy and hydrated size, etc.) and of the electrosorption cell (physicochemical and electrochemical properties of the electrode pair, polarization potential, cell configuration and architecture, flow rate, etc.) [43,46,123,171].

Most reports have mainly focused in increasing the electrical conductivity of the electrode pair and the available surface for the adsorbate(s), for which the effect of textural properties (surface area, pore volume and pore-size distribution) has been widely addressed for capacitive processes, in general [113,114,129,172–175]. On the other hand, our research group has identified that activated carbon electrodes can perform significantly different as a function of their surface chemistry without significantly altering their textural properties [49,50], i.e., alkaline surfaces with a net positive surface charge are better for the electrosorption of anions, such as arsenate [49] and fluoride [50]. Then, the surface chemistry should be ideally standardized between electrodes with marked differences in



their textural properties to better isolate and understand the effect of the latter on the electrosorption performance. Fluoride electrosorption has been widely addressed by several carbon-based electrodes [50,55,57,139–141,176–178], although there are no reports on the effect of the textural properties nor the surface chemistry nor the combination of both factors.

Another situation comprises that most reports on capacitive processes have fixed the polarization potential below 1.23 V, the potential difference associated with water electrolysis and the most conventional Faradaic parasitic reaction assumed in electrosorption cells [43,125,128]. Nevertheless, water electrolysis and other faradaic reactions are probably occurring at higher potential differences due to conventional cell resistances in these diluted media, such as charge-transfer resistances and the resistance of the electrolyte, for which 1.23 V could not be the upper limit of an electrode pair in aqueous solutions. Furthermore, even when water electrolysis could thermodynamically occur at 1.23 V, the reaction could be kinetically limited on the surface of activated carbon electrodes. In this regard, some studies have reported an enhancement in the performance of their studied electrodes when polarizing beyond this potential limit of 1.23 V [50,57,125,140,144,174,177]. For this, we propose that the polarization potential is a parameter that should be experimentally evaluated and even optimized in every electrosorption cell and not just adjusted to the theoretical and ideal thermodynamic value of water electrolysis.

This work centers in tackling both previous hypothesis in one experimental design. First, to evaluate the electrosorption of fluoride by two commercial activated carbons with significant differences in their pore-size distributions, but with alike surface chemistry, which should isolate the effect of the pore-size distribution and promote a better understanding of this parameter. The second aspect is to evaluate the effect of the applied potential on the electrode performance by selecting potentials beyond 1.2 V<sub>cell</sub>, the most conventional polarization limit due to water electrolysis, which will be explored up to a potential at which the electrosorption performance increases no further.

## ***2.2. Materials and methods***

### ***2.2.1 Material standardization and characterization***

Two granular activated carbons from different precursors were selected: a bituminous carbon (F-400, Calgon) and a coconut-shell carbon. Both carbons were ground and sieved to obtain particle sizes between 250 and 500 µm. Fine material was removed by rinsing with deionized water (18.2 MΩ) and the carbons were then dried overnight at 85 °C.

The textural properties were determined by N<sub>2</sub> physisorption analysis at 77 K in a Micrometrics Accelerated Surface Area and Porosimetry Analyzer 2020. The point of zero charge was determined by potentiometric titrations: 0.1 g of the carbons were immersed overnight in 50 mL of a 0.1 M NaCl solution (Sigma Aldrich), previously adjusting the pH to 3 with 0.1 M HCl (J.T. Baker). Then, the solution was titrated with 0.1 M NaOH (J.T. Baker) by an automatic titrator (Mettler-Toledo T70) under inert N<sub>2</sub> atmosphere. The released ions was then computed by the formula

$$released\ ions = \frac{(C_{HCl} * V_{HCl}) + (C_{NaOH} * V_{NaOH}) - (V_{sol} + V_{HCl} + V_{NaOH}) * (10^{-pH} - 10^{-pOH})}{a/M}$$

(Equation 6),

where C<sub>HCl</sub> and V<sub>HCl</sub> are the concentration and the volume of the titrant (0.1 M HCl), C<sub>NaOH</sub> and V<sub>NaOH</sub> are the concentration and the volume of the added base (0.1 M NaOH), V<sub>sol</sub> is the initial volume of the solution (50 mL), a is the activity of the species in the working solution (0.1 M), M is the mass of carbon (0.1 g) and the released ions are given in (mmol g<sup>-1</sup>). Finally, the released ion was graphed vs. the measured pH of the solution. The pK<sub>a</sub> distribution was obtained with the software SAIEUS-pk-Dist © (1994).

For the electrochemical characterization, the carbons were packed in sacks made of stainless-steel mesh (#304), which served as the working electrode (1.32 cm<sup>2</sup>). The counter electrode consisted of a stainless-steel mesh (SSM) without carbon (1.32 cm<sup>2</sup>) and the reference electrode was Ag/AgCl/3M NaCl (ALS Co., Ltd). For further comparison, the potential difference of this electrode *versus* the normal hydrogen electrode is of 209 mV at 25 °C. Both the working electrode and the counter electrode were assembled by placing a Teflon membrane between them to minimize their separation and avoid short-circuit. The electrode design is presented in Figure 2.1. The electrodes were then placed in boiling water to degas the pores. All three electrodes were then immersed in specific aqueous solutions and connected to a Potentiostat/Galvanostat (Bio-Logic VMP multichannel, controlled by the EC Lab software) for their characterization.

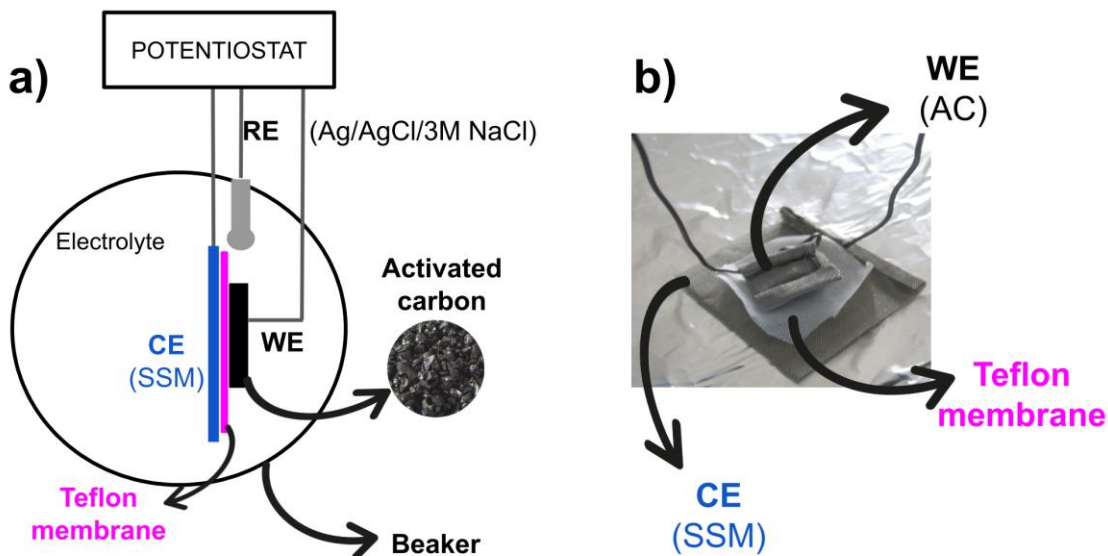


Figure 2.1. a) Schematic representation of the electrosorption cell. b) Photo of the assembled electrode pair (working electrode (WE) and counter electrode (CE) separated by a Teflon membrane).

Afterwards, all three electrodes were immersed in specific aqueous solutions and connected to a Potentiostat/Galvanostat (Bio-Logic VMP multichannel, controlled by the EC Lab software) for their characterization. Cyclic voltammetry was carried out in 0.1 M  $K_2SO_4$ , scanning at different sweep rates between -0.25 and 0.25 V vs. Ag/AgCl/3M NaCl. The gravimetric capacitance was computed using the formula

$$C = \frac{q}{\Delta V \cdot M} \quad (\text{Equation 7}),$$

where  $C$  is the gravimetric capacitance ( $F\ g^{-1}$ ),  $Q$  is the charge (C),  $\Delta E$  is the potential window (V) and  $M$  is the mass of carbon (g). Linear sweep voltammetry was performed in a 5 ppm F solution with constant stirring at  $0.1\ mV\ s^{-1}$ , from  $-0.1\ V_{cell}$  to  $2.5\ V_{cell}$ . For this experimental setup, two channels of the Galvanostat/Potentiostat were coupled to simultaneously measure the half-cell potentials of the working and counter electrode with different channels. By this, we could directly relate the potentials of the reference electrode (Ag/AgCl/3M NaCl) to cell potential values ( $E_{cell}$ ), such as those selected during the electrosorption kinetics. The mass:volume ratio for all the characterization was fixed to 2:1.

### 2.2.2 Kinetics

Kinetics were performed using sacrifice electrosorption cells ( $C_0 = 5\ ppm\ F^-$ ,  $M = 50\ mg$ ,  $V = 25\ mL$ ,  $pH_0 = 7$ ,  $T = 25\ ^\circ C$ ) by polarizing at  $E_{cell} = 0, 1.2, 1.6, 2$  and  $2.4\ V$  immediately after their immersion and with a constant stirring of 120-130 rpm. The initial concentration ( $C_0 = 5\ ppm\ F^-$ ) was selected to obtain an overlapping of the developed electrical double-

layers for most of the micro and mesopores computed from the Gouy-Chapman equation (Equation 2). In addition, this concentration is similar to those found in real waters in the city of San Luis Potosí [179]. Finally, it is worth to highlight that fluoride oxidation is non-viable even at such higher potentials, for which fluoride is also an adequate model pollutant for capacitive processes [125].

Each of the sacrifice cells were depolarized and disconnected at different time intervals, collecting the solution in 50 mL Falcon tubes to measure the fluoride concentration with the fluoride selective electrode (9409BN, Thermo Scientific) and the pH (ORION 8156BNUWP ROSS), both connected to a potentiometer (Orion VeraStar Pro, Thermo Scientific). Fluoride removal capacity was determined by the equation

$$q = \frac{(C_0 - C_i) * V}{M} \quad (\text{Equation 8}),$$

where  $q$  is the fluoride removal capacity ( $\text{mg g}^{-1}$ ),  $[F]_0$  is the initial fluoride concentration (ppm),  $[F]_i$  is the measured concentration of fluoride at different time intervals during the kinetics (ppm),  $V$  is the volume of the solution (L) and  $M$  is the mass of the carbons (g). The charge efficiency was computed using Equation 3.

The evaluation of the cyclic performance was carried out inducing continuous electrosorption-desorption cycles in both carbons in the same previous conditions ( $C_0 = 5$  ppm  $F^-$ ,  $M = 50$  mg,  $V = 25$  mL,  $\text{pH}_0 = 7$ ,  $T = 25$  °C). A cycle consisted in the electric polarization of the electrodes at  $2 V_{\text{cell}}$  for 1 hour; afterwards, the polarization of the electrodes were reversed to  $-2 V_{\text{cell}}$ . This procedure was repeated 4 more times to attain a total of 5 consecutive electrosorption cycles.

## 2.3. Results and discussion

### 2.3.1 Characterization

Figure 2.1a and 2.1b show the textural analysis for both carbons from  $N_2$  adsorption-desorption isotherms at 77 K and the cumulative pore volume, respectively, which is summarized in Table 2.1. The data indicates that both the bituminous and the coconut-shell carbon have a similar value of surface area ( $S_{\text{BET-Bituminous}} = 905 \text{ m}^2 \text{ g}^{-1}$  and  $S_{\text{BET-Coconut}} = 820 \text{ m}^2 \text{ g}^{-1}$ ). The  $N_2$  isotherms (Figure 1a) particularly display a highly microporous structure at the first shoulder at low relative pressures [65,180], for which both carbons presented a very similar contribution of the micropores to their total surface area of ~80% (680 and 730  $\text{m}^2 \text{ g}^{-1}$  for the coconut-shell and bituminous carbon, respectively).

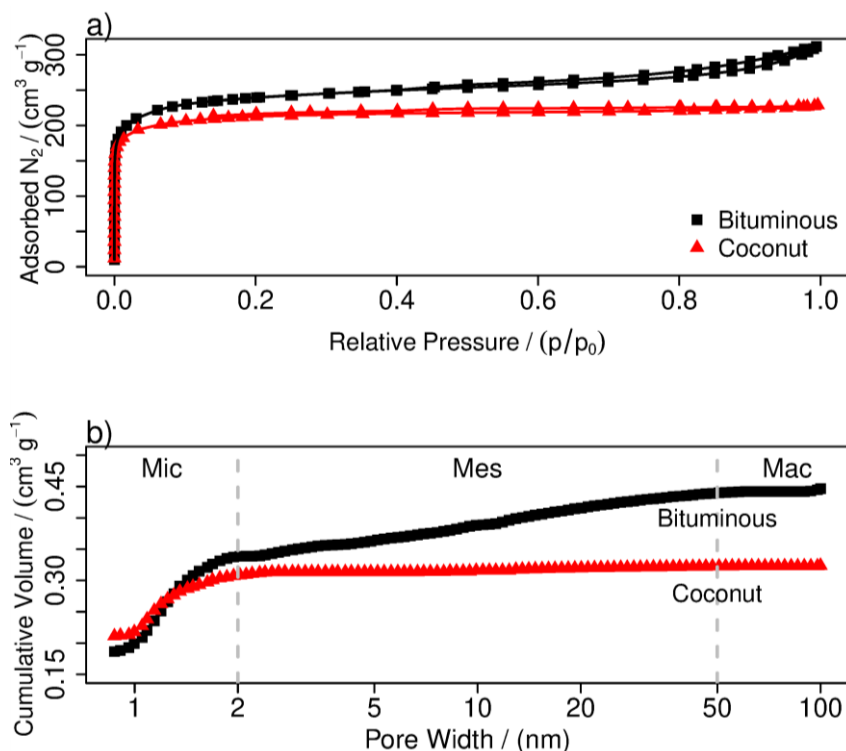


Figure 2.2. a) Adsorption-desorption isotherms of  $N_2$  at 77 K. b) Cumulative pore volume obtained by non-linear density functional theory (Mic = micropores, Mes = mesopores, Mac = macropores, “X” axis in logarithmic scale).

Table 2.1. Textural properties.

Adsorbent	$S_{BET}$ ( $m^2 g^{-1}$ )	$V_{TOTAL}$ ( $cm^3 g^{-1}$ )	$V_{MIC}$ ( $cm^3 g^{-1}$ )	$V_{MES}$ ( $cm^3 g^{-1}$ )	AVP (nm)
Bituminous	905	0.447	0.338 (75.8%)	0.101 (22.7%)	2.1
Coconut-shell	820	0.324	0.308 (95.2%)	0.014 (4.4%)	1.74

After this shoulder in Figure 1a, the bituminous carbon further increased its  $N_2$  adsorption, which is associated with the completion of the adsorption monolayer and the beginning of micropore and mesopore filling (capillary condensation) [65]. This increase implies that the bituminous carbon also presented a percentage of mesopores, while the coconut-shell carbon practically lacks mesoporosity. This is in excellent agreement with the minimal increase in the cumulative pore volume (Figure 2.2b) at pore widths higher than 2 nm (i.e., the mesopore range). Then, the coconut-shell carbon is mainly microporous, as they represent 95% ( $0.308 cm^3 g^{-1}$ ) of the total pore volume, while the bituminous carbon presents both micro (75%,  $0.338 cm^3 g^{-1}$ ) and mesoporosity (25%,  $0.101 cm^3 g^{-1}$ ), as

reported in Table 1. For this same reason, the average pore diameter is larger for the bituminous carbon, 2.1 nm, compared to that of the coconut-shell carbon, 1.71 nm.

Surface chemistry was studied by obtaining the points of zero charge ( $\text{pH}_{\text{PZC}}$ ) and the  $\text{pK}_a$  distribution of both carbons by potentiometric titrations [80]. Both  $\text{pH}_{\text{PZC}}$  values were very similar:  $\text{pH}_{\text{PZC-coconut}} = 8.3$  and  $\text{pH}_{\text{PZC-bituminous}} = 8.8$  (Figure 2.3a). The alkaline  $\text{pH}_{\text{PZC}}$  values of both carbons imply a higher content of functional groups with Lewis-basic character, for which both carbons will present a net positive surface charge in neutral and acid solutions and thus, favorable electrostatic interactions towards fluoride.

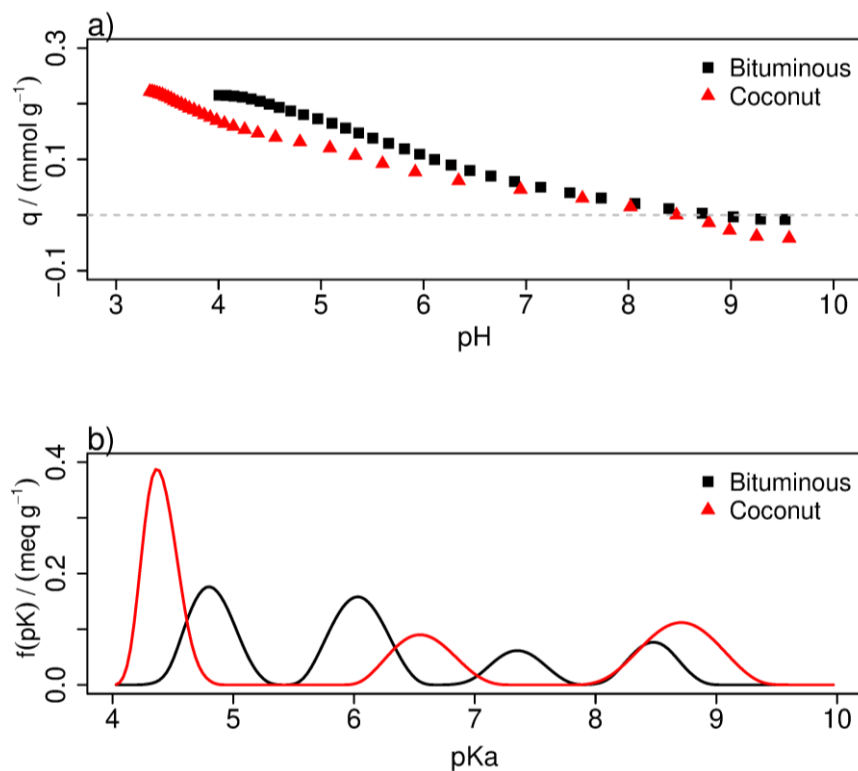


Figure 2.3. a) Surface charge distribution and b)  $\text{pK}_a$  distribution (in 0.1 M NaCl,  $M = 100$  mg,  $V = 50$  mL,  $T = 25$  °C, deaerated with  $\text{N}_2$ ).

The  $\text{pK}_a$  distribution (Figure 2.3b) showed a first insight of the slight difference in their  $\text{pH}_{\text{PZC}}$  values. This analysis relies on the understanding that the surfaces of real solids are inherently complex and possess a continuous distribution of adsorption energies, rather than discrete adsorption energy values [181,182]. This promotes that the exact same functional group develops a sequential dissociation along a specific pH interval, for which the  $\text{pK}_a$  distribution provides a semi-quantitative analysis of their concentration [80]. As can be observed (Figure 2.3b), both carbons present well-defined peaks of subset of functional groups with a similar dissociation energy, being the most energetic those at lower  $\text{pK}_a$  values, i.e., the carboxylic groups ( $4 \leq \text{pK}_a \leq 6$  [80]). For this, the more acidic  $\text{pH}_{\text{PZC}}$  for the coconut-shell carbon can be attributed to a higher content of carboxylic groups, as the

concentration of lactonic ( $7 \leq \text{p}K_a \leq 9$ ) [80]) and phenolic ( $8 \leq \text{p}K_a \leq 11$  [80]) groups are not appreciably different.

Cyclic voltammetry was performed to study the capacitive response of the carbons by their potentiodynamic polarization at different sweep rates. The voltammetric response at  $1 \text{ mV}^{-1}$  resemble a double-layer capacitor (Figure 2.4a), being the capacitance of the bituminous carbon higher than that of the coconut-shell carbon. This is related to a higher and more accessible pore volume of the bituminous carbon in the evaluated electrolyte due to the presence of mesopores. The marked differences at the positive potentials were attributed to the significant differences in the hydrated radii ( $\text{K}^+ = 0.331 \text{ nm}$  and  $\text{SO}_4^{2-} = 0.379 \text{ nm}$  [96]) and the hydrated energy ( $\text{K}^+ = -322 \text{ kJ mol}^{-1}$  and  $\text{SO}_4^{2-} = -1059 \text{ kJ mol}^{-1}$  [183]) in this asymmetric electrolyte. For the bituminous carbon, the presence of mesopores helped to allocate the bulkier anion, for which the capacitance remained symmetric during the studied potential window; for the coconut-shell carbon, its asymmetric response is in excellent agreement with other voltammetric responses of highly microporous carbons in asymmetric electrolytes [184,185].

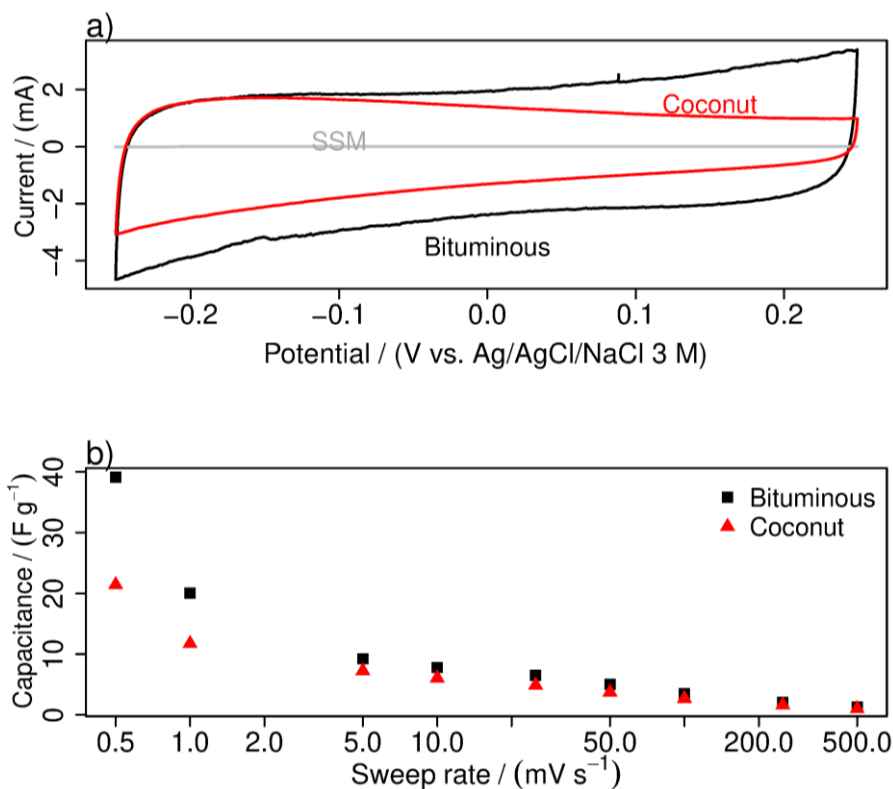


Figure 2.4. a) Cyclic voltammetry at  $1 \text{ mV s}^{-1}$  in the anodic direction and b) gravimetric capacitances at different sweep rates ('x' axis in log-scale). The reported voltammograms and the computed capacitances correspond to the 3rd cycle (in  $0.1 \text{ M K}_2\text{SO}_4$ ,  $M = 50 \text{ mg}$ ,  $V = 25 \text{ mL}$ ,  $T = 25 \text{ }^\circ\text{C}$ ,  $\text{Ag/AgCl/3M NaCl}$  as the reference electrode and SSM as the counter electrode, undeaerated solution).

The gravimetric capacitance of both carbons decreased as a function of increasing the sweep rate (Figure 2.4b), which implies less ion accumulation in the narrower pores at higher sweep rates. At higher sweep rates, similar values for both carbons were observed, probably associated with the capacitance of the most exposed surface. The decrease in the gravimetric capacitance for the coconut-shell carbon was lower at higher sweep rates, reiterating that a percentage of its polarizable area was inaccessible to the electrolyte.

### ***2.3.2 Kinetics and the overlapping of the electrical layers***

Figure 2.5 shows the results from the adsorption and electrosorption kinetics by both carbons in 5 ppm  $F^-$  solutions. Both carbons barely adsorbed fluoride, although their electrical polarization did increase the removal of the anion at different degrees. The low adsorption capacity of carbon-based materials towards fluoride has been widely reported, even at much higher initial concentrations of the anion, which can be related to the high polarity of fluoride and the slightly polar surface of the studied carbons. The  $F^-$  adsorption capacity of the bituminous carbon was only of  $0.0735 \text{ mg g}^{-1}$  ( $C_0 = 5 \text{ ppm } F^-$ ,  $\text{pH}_0 = 7$ ), which increased to 0.147, 0.235, 0.431 and  $0.445 \text{ mg g}^{-1}$  when polarized at 1.2, 1.6, 2 and  $2.4 \text{ V}_{\text{cell}}$ , respectively (Figure 2.5a). For the coconut-shell carbon (Figure 2.5b), its adsorption capacity was even lower than for the bituminous carbon,  $0.047 \text{ mg g}^{-1}$ , which increased to 0.065, 0.098, 0.256 and  $0.227 \text{ mg g}^{-1}$  by its polarization at the same potentials, respectively. As can be observed, the more significant increases occurred at  $2 \text{ V}_{\text{cell}}$ , which were of a similar magnitude,  $\sim 6$  and 5.4 times the capacity of conventional adsorption (at  $0 \text{ V}_{\text{cell}}$ ) for the bituminous and coconut-shell carbons, respectively. The comparison of the capacities is summarized in Figure 2.5c, in which it can be observed that the bituminous carbon achieved higher fluoride removal capacities.



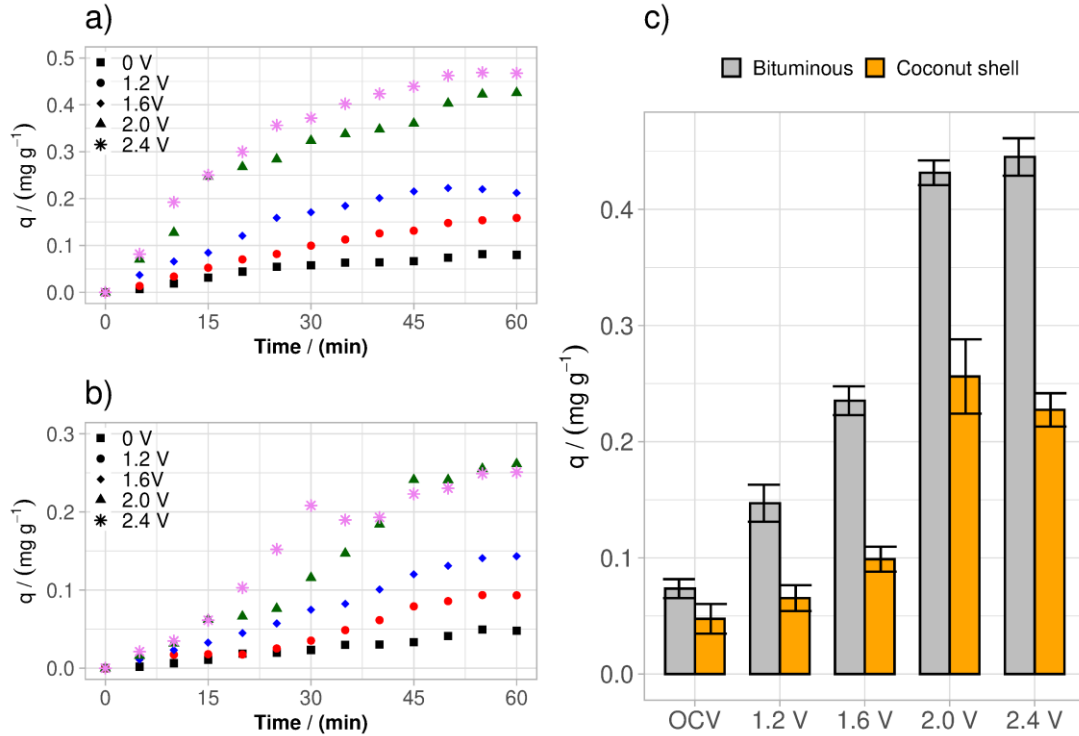


Figure 2.5. Adsorption and electrosorption kinetics of fluoride for a) bituminous and b) coconut-shell carbon at different potentials (y-axis in different scale). c) Comparison of the capacities between both carbons at each of the applied potentials for the bituminous (gray) and coconut-shell (orange) carbon ( $C_0 = 5 \text{ ppm F}$ ,  $M = 50 \text{ mg}$ ,  $V = 25 \text{ mL}$ ,  $\text{pH}_0 = 7$ ,  $T = 25 \text{ }^\circ\text{C}$  and 120-130 rpm, SSM as counter electrode).

The electrical polarization had a more profound effect in the fluoride removal velocities. First, the bituminous carbon presented a more positive slope as a function of increasing the applied potential, compared to those of the coconut-shell carbon. This can be visually observed by comparing Figure 2.5a and 2.5b, and Table 2.2 comprises the results of the slopes computed at  $t = 25 \text{ min}$ . To corroborate this, the ratio of the obtained capacities

$$\frac{q_{\text{bituminous}}}{q_{\text{coconut}}} \quad (\text{Equation 8})$$

during the kinetics at each applied potential was computed and graphed (Figure 2.6). In general, the ratio is higher than 1, which reiterates that the capacity of bituminous carbon was higher than that of the coconut-shell carbon. In addition, the ratio from Equation 8 presents its highest values at short times ( $\sim 4$  times) than at times near the equilibrium ( $> 30 \text{ min}$ ). This corroborates that the removal rate of the bituminous carbon was faster, i.e., this carbon removed more fluoride at lower times due to an enhanced mass-transport promoted by the mesopores.

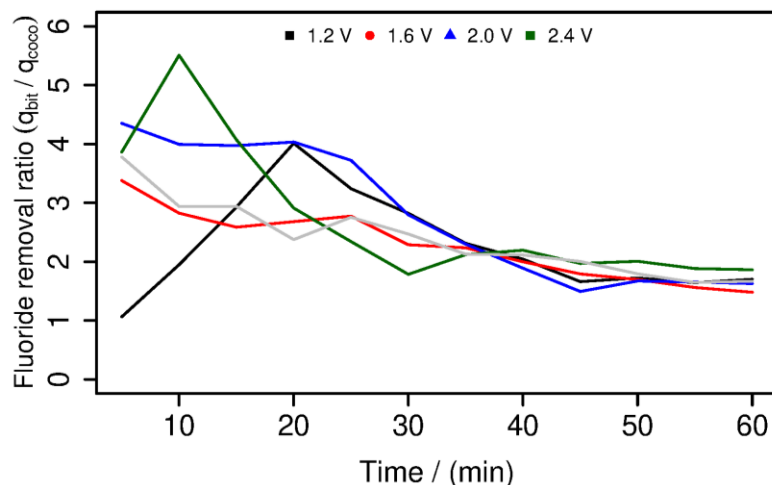


Figure 2.6. Fluoride removal ratio ( $q_{bit} / q_{coconut}$ ) during fluoride kinetics ( $C_0 = 5 \text{ ppm } F^{-1}$ ,  $M = 50 \text{ g}$ ,  $V = 25 \text{ mL}$ ,  $T = 25 \text{ }^\circ\text{C}$ , 120-130 rpm, SSM as the counter electrode).

Table 2.2. Removal velocities by adsorption and electrosorption in  $\text{mg g}^{-1} \text{ hr}^{-1}$  (obtained at  $t = 25 \text{ min}$ ,  $M = 50 \text{ mg}$ ,  $V = 25 \text{ mL}$ ,  $C_0 = 5 \text{ ppm } F^{-}$ ,  $\text{pH}_0 = 7$ , rpm = 120-130,  $T = 25 \text{ }^\circ\text{C}$ ).

Carbon	OCV	1.2 $V_{\text{cell}}$	1.6 $V_{\text{cell}}$	2 $V_{\text{cell}}$	2.4 $V_{\text{cell}}$
Bituminous	0.1325	0.2106	0.3619	0.8021	0.8996
Coconut-shell	0.0558	0.0525	0.135	0.1988	0.309

As can be observed from Figure 2.5, the coconut-shell carbon increased to a lesser degree its fluoride removal when polarized at 1.2 and 1.6  $V_{\text{cell}}$  and presented a more limited mass-transport, compared to the bituminous carbon at these same potentials. On the other hand, both carbons presented a marked increase at 2  $V_{\text{cell}}$ , while there were insignificant increases in removal between 2 and 2.4  $V_{\text{cell}}$ . These results could be related to differences in the polarization processes of the carbons. Nevertheless, the current and charge profiles of both carbons (Figure 2.7a and 2.7b, respectively) presented similar values and a stable behavior during the whole polarization time, for most potentials. This is sufficient to establish that both carbons presented not only similar values of surface area ( $S_{\text{BET}}$ ) and surface chemistry ( $\text{pH}_{\text{PZC}}$ ), but also similar charging processes, which was also reflected in the similar increases in capacity during the kinetics. In addition, this suggests that the results from the kinetics could be solely attributed to differences in the pore-size distributions of the studied carbons, which will be addressed below. Finally, the current profiles (Figure 2.7a) showed a marked increase in the recorded current at short times when polarized at 2.4  $V_{\text{cell}}$ , probably attributed to the development of fast faradaic reactions, which could explain the insignificant differences in the performance at 2 and 2.4  $V_{\text{cell}}$ . Then, 2  $V_{\text{cell}}$  was experimentally established as the polarization limit in the studied conditions.

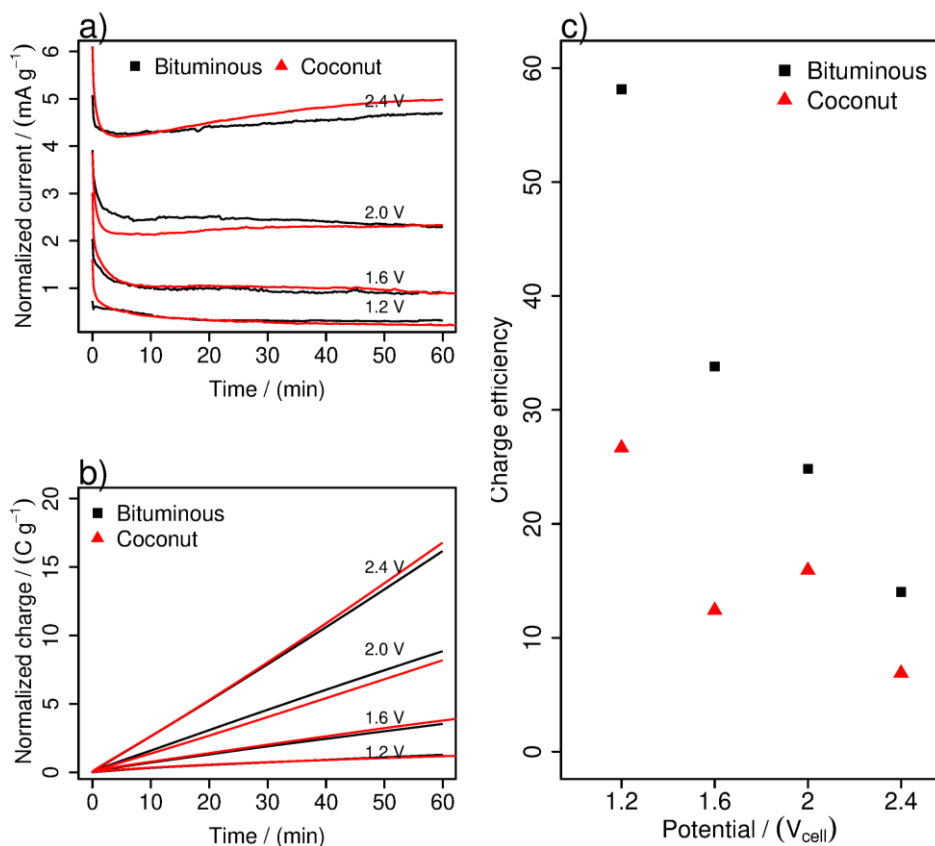


Figure 2.7. Recorded a) current and b) charge, both normalized per carbon mass during the electrosorption kinetics. c) Charge efficiency ( $M = 50$  mg,  $V = 25$  mL,  $C_0 = 5$  ppm  $F^-$ ,  $pH_0 = 7$ ,  $rpm = 120-130$ ,  $T = 25$  °C).

Figure 2.7c shows the charge efficiency computed for both electrodes at the evaluated potentials. As can be observed, the highest charge efficiency is obtained when polarizing at 1.2 V<sub>cell</sub> and decreased as a function of increasing the applied potential. As ion-swapping and co-ion expulsion usually occur at lower potentials [43], the decrease in the charge efficiency must be related to the presence of parasitic faradaic reactions. This was corroborated by performing linear sweep voltammetry (Figure 2.8) in the same conditions than the electrosorption kinetics (5 ppm  $F^-$  solution and with constant stirring), in which significant increases in current were observed at  $\sim 0.5$  V<sub>cell</sub>. Even when there are no punctual studies that correlate the current increases observed in linear sweep voltammetry (or other potentiodynamic technique) and unstable current profiles in amperometry (a potentiostatic technique), there are reports that have addressed some correlations. For example, it is well-known that unstable current profiles are related to the development of faradaic parasitic reactions on the electrode surface, mainly, the oxidation of the carbon surface, which are observed after several electrosorption cycles [50,104,129].

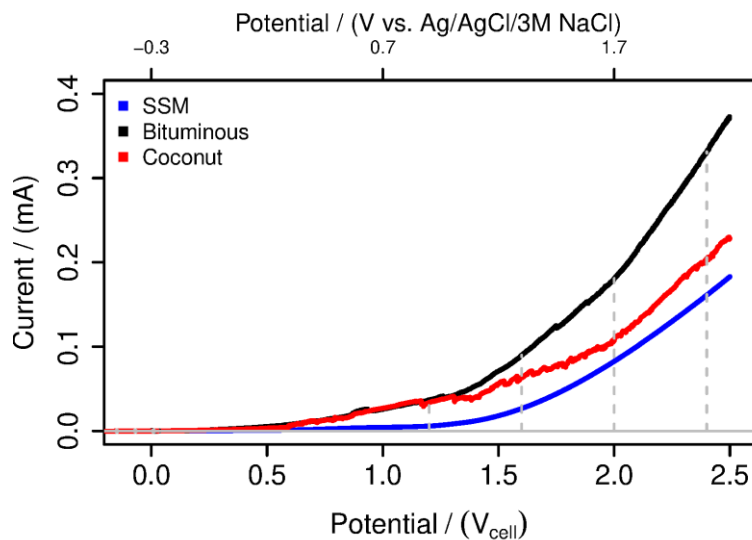


Figure 2.8. Linear sweep voltammetry for the studied electrodes in 5 ppm  $F^{-1}$  with constant agitation ( $v = 0.1 \text{ mV s}^{-1}$ ,  $M = 50 \text{ g}$ ,  $V = 25 \text{ mL}$ ,  $T = 25 \text{ }^{\circ}\text{C}$ , 120-130 rpm, SSM as the counter electrode).

The presence of micropores has been widely associated with better performances in capacitive process for water treatment [120], as they account not only for most of the surface area and pore volume in porous materials [80], but also because of their higher electrical conductivity [186]. Nevertheless, the micropores need to be reached by the hydrated adsorbates in solution. For this reason, the textural properties of the electrode should be in excellent agreement with the properties of the adsorbate (hydration energy and hydrated size, charge, etc.). On the other hand, several works have reported that the presence of mesoporosity enhances both the removal capacity and the mass-transport of adsorbates [129,172–175], mostly due to a better allocation of the electrical double-layers (EDLs) and the subsequent decrease in their overlapping at the micropores, which will be addressed upon next.

An approximation using the Gouy-Chapman equation (Equation 2) computes a double-layer thickness of 18.67 nm in the studied conditions (0.263 mM for a 1:1 electrolyte,  $T = 25 \text{ }^{\circ}\text{C}$ ,  $\epsilon_{\text{water}} = 78.54$ ), for which the EDLs are clearly overlapped at the micropores and most of the mesopores. On the other hand, recent models on the formation of the EDLs in nanometric spaces based on field-dependent permittivity propose that the EDL thickness is much narrower, compared to that computed from the Gouy-Chapman approximation [187], which is in excellent agreement with experimental and theoretical reports on the contribution of the micropores to the formation of the EDL [113,188]. Nevertheless, all models consider that the EDLs indeed overlap at the micropores and, even at some degree, at the mesopores [113,114], which decreases the available surface area and pore volume for the electrosorption of ionic species (Figure 2.9a). Then, if the evaluated carbons are

behaving as double-layer capacitors, it is reasonable to consider that the microporous coconut-shell carbon presented higher EDL overlapping, which can be translated as less available surface for fluoride removal. This can be observed from the minimal increases in fluoride removal at 1.2 and 1.6  $V_{\text{cell}}$  for this carbon. For the bituminous carbon, the presence of mesopores aided in allocating the formed EDLs, for which its fluoride removal did significantly increase when polarized at these same potentials.

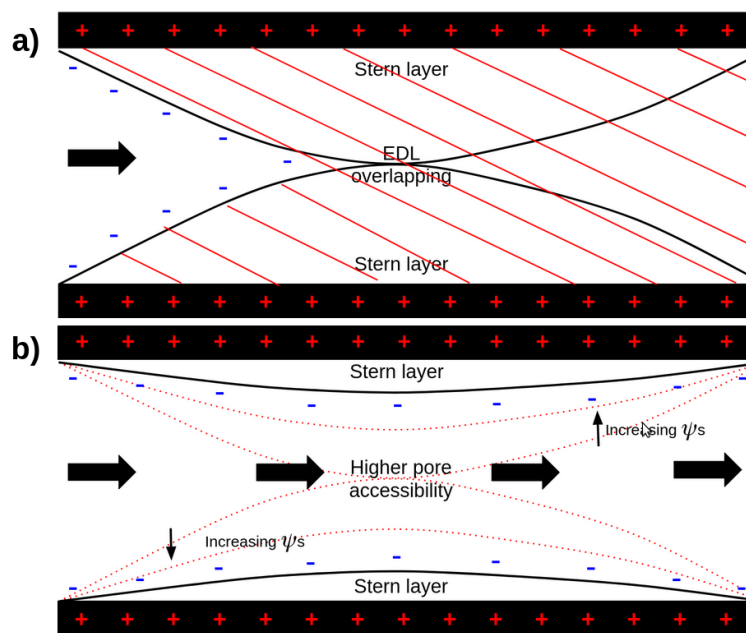


Figure 2.9. a) EDL overlapping in a slit-shaped pore ( $\Psi_s =$  surface potential). b) Decrease of the EDL overlapping as a function of increasing the potential ( $\Psi_s$ ). c) Allocation of the fluoride anions at the Stern layer in a microporous carbon.

It is well-known that the EDL thickness decreases as a function of increasing the charge of the particle or of the electrolyte, the ionic strength of the electrolyte and the applied potential of the electrode (Figure 2.9b) [84,86,91,102,189,190]. Then, at the highest applied potentials of 2 and 2.4  $V_{\text{cell}}$ , the EDLs became narrower, which may suggest that their overlapping also decreased, thus unblocking a portion of the pore volume (Figure 2.9c). This could explain or reflect the marked increases in fluoride removal for both carbons at these potentials and would be in excellent agreement with other works that have addressed this phenomenon [189–192].

A first quantitative approximation of the decrease of the overlapping was obtained by computing the projected area of the removed fluoride moles at the equilibrium (Figure 2.5c), which were then contrasted to the available surface area above the theoretical EDL thickness of 18.67 nm. First, the surface area above a pore width of 18.67 nm was subtracted from the total surface area of the carbons ( $S_{\text{BET}}$  in Table 2.1), as this value of EDL thickness should have blocked all the area provided from the carbon pores until this

width (i.e., the micropores and most mesopores). This corresponds to an available surface area of only  $6.54 \text{ m}^2 \text{ g}^{-1}$  and  $0.79 \text{ m}^2 \text{ g}^{-1}$  for the bituminous and coconut-shell carbon, respectively, according to the NLDFT analysis. At  $2 V_{\text{cell}}$ , the projected area of the removed fluoride moles were 4 times higher than the available surface area for the coconut-shell carbon, while it was only of 83% of the total available surface for the bituminous carbon, which must be an indicator of the decrease in the EDL thickness. The surface area excess was added to the previous available surface area computed by the overlapping ( $0.79 \text{ m}^2 \text{ g}^{-1}$ ), which corresponded to a surface area provided by a pore width of  $\sim 9.5 \text{ nm}$ . By this, it is viable to propose that the overlapping decreased  $\sim 50\%$  for this carbon, from an initial overlapping at  $18.67 \text{ nm}$  and down to  $9.5 \text{ nm}$ . Probably, the same was occurring for the bituminous carbon, although it was not appreciable due to its higher available surface.

Even when the removal of fluoride by the formation of multilayers seems also a feasible explanation of this phenomenon, the surface potential practically fades at short distances ( $\sim 1 \text{ nm}$ ) from the surface, for which most fluoride interactions must have been at very short distances. It is also worth to highlight that the projected surface area of the removed fluoride ions should be higher than that computed above, due to negative lateral interactions that forbids the allocation of the counter-ions at the electrical layers directly in contact and next to each other without any separation among them. That slight separation must also be considered and added to the projected area and the calculations performed above. In addition and as was stated above, the Gouy-Chapman approximation provides a more thicker EDLs than those observed by more recent molecular dynamics, for which probably fluoride anions reached even smaller pore widths. For these reasons, the approach here used must be solely suggestive in a quantitative form and it is reiterated that it was only used to demonstrate that the EDL thickness decreased as a function of increasing the applied potential, which unblocked the nanometric pores in the activated carbon electrode.

Continuing with the previous idea, the EDL overlapping could also explain part of the restrictive mass-transport observed for the coconut-shell carbon. The formation of the EDL is considered an instantaneous process for planar surfaces, while, in porous electrodes, it depends on the transport and allocation of the counter-ions inside the pore. Then, the EDL formation in such narrower spaces is a function of the thermodynamic properties of the adsorbate, its transport, the length of the pore and the presence of convection [193]. Kwak et al. [194] demonstrated that the equilibrium of electrically polarized nanopores with significant EDL overlapping effects is established quite slowly, due to slow axial transport through the pore. Then, mass-transport limitations for the coconut-shell carbon, especially at short times, could be due to the slow allocation of fluorides while penetrating its highly microporous structure.

### 2.3.3 Polarization limits and parasitic reactions

As stated above, the objective of evaluating several polarization potentials was to identify the polarization limit in the studied system, i.e., the potential at which the electrosorption performance increased no further. Most reports only evaluated potentials of 1.2 V<sub>cell</sub>, below the thermodynamic potential difference of water electrolysis (Equation 3). Nevertheless, two inconveniences arise: i) such ideal and theoretical value does not consider the conventional resistances of the system (charge-transfer resistances of the electrode and the resistance of the electrolyte), which can increase the potential difference needed to the development of water electrolysis; and ii) this same potential does not give information on the kinetic limitations of the reaction over a specific electrode surface, i.e., a fast water electrolysis reaction may not be developing at the surface of activated carbon when polarized even above an overpotential, compared to certain metallic electrodes. Both previous reasons could imply that rapid water electrolysis could be occurring at a much higher potential difference than 1.23 V or that water electrolysis is not favorably fast at all on the studied activated carbon electrodes.

Parasitic reactions not only decrease the electrosorption performance of the electrodes, as was observed in the charge efficiency of the carbons (Figure 2.7c), but they also present an effect on the pH of the solution. Nevertheless, in our studied system, pH fluctuations were minimal ( $\Delta\text{pH}_{\text{max}} = +0.4$  at  $E_{\text{cell}} = 2.4$  V), which are typical increases of solely capacitive systems. The increase in the pH is a conventional phenomenon of the anode compartment [135] or of asymmetric cells in which the activated carbon is only present in the anode [114], although this is also dependent on the surface chemistry of the studied carbon-based materials. In addition to the previous discussion, the minimal fluctuations of the pH can also be attributed to the low mass:volume ratio used, to the  $\text{pH}_{\text{PZC}}$  values close to neutrality and that fluoride electrosorption does not present a pH-dependent mechanism at the evaluated electrodes. On the other hand, this increases in the pH of the solution provide a first insight of the reactions taking place at the cell, addressed upon next.

As was observed in Figure 2.8, current increases detected by linear sweep voltammetry occurred at a potential of  $\sim 0.5$  V<sub>cell</sub>, i.e., a potential difference much lower than 1.23 V. Nevertheless, as activated carbons and the current collector (stainless-steel mesh) are not ideal electrodes for water electrolysis, the increases in current should be associated to other faradaic reactions. The most common and experimentally demonstrated reaction in electrosorption cells is that of oxygen reduction and peroxide formation [125,128] (Equation 5), which occurs at 0.69 V vs. NHE (or  $\sim 0.49$  V vs. Ag/AgCl/3M NaCl) and explains the increase in the pH of the solution.

The main conclusion of this section seems to be that the polarization potential should not be fixed to a constant value below the theoretical potential of water electrolysis, but it must be evaluated and even optimized, according to the needs of every system (water quality,

energy efficiency, removal capacity and rate, etc.). The commercial activated carbon electrodes here evaluated can be polarized beyond  $1.2 V_{\text{cell}}$ , increasing their fluoride removal capacity and rate. This is in good agreement with other reports in which the electrosorption performance was enhanced by polarizing beyond  $1.2 V_{\text{cell}}$  [50,57,125,140,144,174,177]. On the other hand, there are also reports in which no significant enhancement beyond  $1.2 V_{\text{cell}}$  was observed [49,51] which reiterates that there are still aspects to truly understand why and in which system water electrolysis will be promoted. In addition, water electrolysis is just one specific reaction that can occur in aqueous solutions, while there are other more viable reactions, such as oxygen reduction and the oxidation of the carbon surface, which are practically never taken into account when establishing polarization limits.

#### ***2.3.4 Cyclic performance***

Figure 2.10 shows the cyclic performance of both carbons for 5 consecutive cycles. The first graphs (Figure 2.10a and 2.10b) comprise the removal capacities when polarized at  $2 V_{\text{cell}}$  and includes the subsequent regeneration of the carbon surface after fluoride desorption process by polarizing at  $-2 V_{\text{cell}}$ . As it is well-known, the system is considered stable if the removal capacity is relatively constant, which was the case for both the bituminous and coconut-shell carbon during the 5 cycles. Even when faradaic reactions were induced during this high polarization value, fluoride was efficiently expelled when polarizing at  $-2 V_{\text{cell}}$  (>90% regeneration for both carbons).



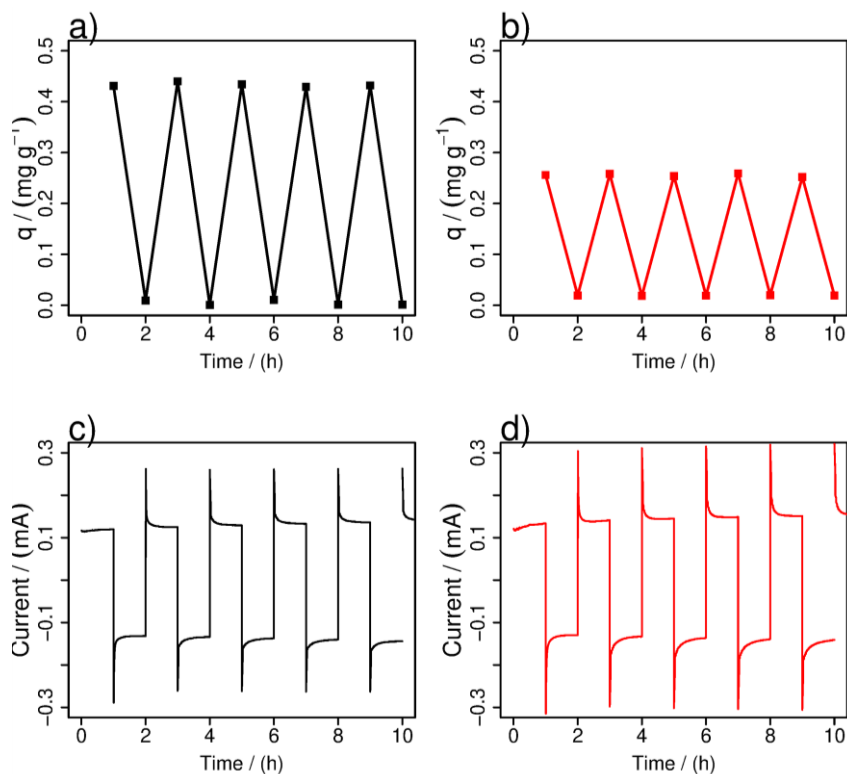


Figure 2.10. Electro sorption and desorption (a) and (b) and current profiles (c) and (d) during five electro sorption cycles for the bituminous and the coconut-shell carbon, respectively ( $C_0 = 5 \text{ ppm F}$ ,  $M = 50 \text{ mg}$ ,  $V = 25 \text{ mL}$ ,  $\text{pH}_0 = 7$ ,  $T = 25 \text{ }^\circ\text{C}$  and 120-130 rpm, SSM as counter electrode).

Figure 2.10c and 2.10d display the recorded current during the electro sorption cycles for both carbons to reiterate that the surface was correctly regenerated. Several works have already reported and discussed that stable and symmetric current profiles during electro sorption cycles are associated to a correct regeneration of the surface [100,104,129]. This is due to the oxidation of the carbon surface has implications in decreasing the electrical conductivity of the material. In a previous publication [50], the same bituminous activated carbon was depolarized, i.e., without reversing the polarization at negative potential and decreased its capacitive behavior at each cycle. Then, the most marked effect of the oxidation reactions taking place during the polarization were those related to the charge efficiency of the electrodes (Figure 2.7c) and not in the removal capacities.

## 2.4. Conclusions

The two commercial activated carbons selected for this study present a similar surface area ( $S_{\text{BET}}$ ), surface chemistry ( $\text{pH}_{\text{PZC}}$ ), and even similar current and charge profiles during their polarization. Nevertheless, the bituminous carbon presented five times more mesopore

percentage (25%), compared to the coconut-shell carbon (5%). During the kinetics, the bituminous carbon performed better as an electrode, as it presented a higher removal, although higher increases were observed in the removal velocity, being ~4 times higher at short times.

The poor performance of the coconut-shell carbon at 1.2 and 1.6  $V_{\text{cell}}$  was attributed to the overlapping of the EDLs in its highly microporous structure. This was not observed for the bituminous carbon, in which its higher mesopore content helped to allocate the EDLs. At 2  $V_{\text{cell}}$ , both carbons increased more their removal performance, which was explained by a ~50% decrease in the EDL thickness, from ~18.67 nm to ~9.5 nm, which reduced their overlapping and increased the available pore space. Parasitic faradic reactions were developed at all applied potentials, although their effect was more significantly observed at 2.4  $V_{\text{cell}}$ .

The applied potential in capacitive processes is a factor to evaluate and optimize. As has been here demonstrated and has been observed in other works, it is feasible to polarize beyond 1.2  $V_{\text{cell}}$  and significantly increase the performance of some electrosorption cells. Nevertheless, this had a pronounced effect in one charge efficiency of the electrode. Finally, although water electrolysis is thermodynamically viable in these systems, it could not be developing due to kinetic limitations.

## Chapter three: Fluoride Electrosorption by Hybrid Lanthanum-Carbon Electrodes

Adapted from the following published works:

**D.R. Martinez-Vargas**, E.R. Larios-Durán, L.F. Cházaro-Ruiz, J.R. Rangel-Méndez, Correlation between physicochemical and electrochemical properties of an activated carbon doped with lanthanum for fluoride electrosorption, *Sep.Purif. Technol.* 268 (2021). <https://doi.org/10.1016/j.seppur.2021.118702>.

**D.R. Martinez-Vargas**, J.R. Rangel-Méndez, L.F. Cházaro-Ruiz, Fluoride electrosorption by hybrid La(III)-activated carbon electrodes under the influence of the La(III) content and the polarization profile, *J. Environ. Chem. Eng.* 10 (2022) 106926. <https://doi.org/10.1016/j.jece.2021.106926>.

### 3.1 Introduction

Fluorine is an essential element for human health at low doses, but its excessive and chronic consumption promotes undesired health conditions, such as dental weakness and skeletal deformations [195,196]. For this, the World Health Organization established a maximum concentration limit of 1.5 ppm in waters for human consumption [195–197]. Electrosorption is an emerging treatment process for waters containing either organic or inorganic ions, even at low concentrations [52]. This process, also known as desalination or capacitive deionization, consists in polarizing adsorbents with high surface area and good electrical conductivity, promoting the migration of species to the electrode surface with opposite electric charge. The electrosorption performance depends on several parameters, mainly on the physicochemical and electrochemical properties of the electrodes and of the adsorbate, the electrode configuration, the cell architecture, the applied voltage, the flow rate, among other parameters [43,46,53,123,131,171,198–201]. Nevertheless, the electrode design and their configuration in the cell have received higher attention, as observed in a higher number of reports solely on these topics.

Carbon-based materials are commonly selected as electrodes for the electrosorption and desalination processes because of their high surface area, good electrical conductivity, and tunable physicochemical and electrochemical properties [43,46,52,53]. In addition, several reports have focused on the surface modification of commercial activated carbons to develop hybrid materials with higher capacity and rate removal towards different adsorbates. Some of the modifications comprise the addition of specific functional groups, as specific metal phases [54–59,202], but also, of larger chemical entities, as surfactants, polymers and ion-exchangers [60–64,103,203]. Regarding metals, certain metal

phases present a higher electrical conductivity than carbon-based electrodes and their addition may also promote the removal of the desired species by conventional adsorption. For this, there are several reports on the modification of different carbon-based electrodes with several metal phases for water desalination [54,56,58,59,202], while on fluoride electrosorption there are only reports with Ti(IV) [55,57] and La(III) [50].

All reports on capacitive processes consider two polarization profiles: polarizing the adsorbents from the beginning and polarizing the adsorbents after conventional adsorption. Conventionally and to this day, insignificant differences have been observed in capacity by both profiles, while the removal rate does increase by polarizing the electrodes from the beginning [50,54,56], making this profile the most reported one. Nevertheless, polarizing after the adsorption equilibrium could be viable for electrodes in which significant interfacial changes occur after the adsorption process. In general and for carbon-based materials, several studies have already reported changes in the surface charge after the adsorption of different adsorbates [36,107–109] and, furthermore, surface charges have been established as a key parameter to increase the electrode performance in capacitive processes [61,62,103,104,112]. Then, a new electrode interface with more favorable properties for electrosorption could be developed after conventional adsorption, which could promote a better performance of the electrode.

For the previous reasons, the objective of this research is to study fluoride removal on activated carbon electrodes impregnated with different La(III) percentages by both polarization profiles. Besides studying the effect on fluoride removal capacity and rate by the electrical stimulus of these modified matrices, the authors expect differences between both profiles for the electrodes of this study, as these electrodes undergo interfacial changes related to their net surface charge during the adsorption process. Such differences will be evaluated by several *in situ* characterization techniques before and after the adsorption of fluoride, as these techniques could also provide information on the processes and mechanisms taking place at the interface, according to the previously proposed mechanism [36]. Further analysis of the surface charge distribution and the interfacial changes that took place at such matrices include the recordings of the open circuit potentials and their correlation to the charging and polarization process.

## ***3.2 Materials and methods***

### ***3.2.1 Material standardization and physicochemical characterization***

Granular activated carbon (F-400, Calgon) was ground and particles between 250 and 500  $\mu\text{m}$  were collected and rinsed with deionized water (18.2 M $\Omega$ ) until fine material was removed. Then, the activated carbon was dried overnight at 85 °C. For the impregnation with lanthanum below 1% (w/w), 0.6 g of activated carbon was immersed in 100 mL of

0.15 M  $\text{La}(\text{NO}_3)_3$  (Aldrich) solution for 2 days, at 25 °C and constant stirring (120-130 rpm). For higher La percentages, 0.1 g of AC were immersed in 10 mL of either 0.3 or 0.5 M  $\text{La}(\text{NO}_3)_3$  solutions at the same conditions stated previously. The adsorbents were centrifuged, decanted, washed three times with deionized water and dried overnight at 85 °C. All samples were stored in  $\text{N}_2$  atmosphere until their use.

The surface area, pore volume and pore-size distribution were determined by  $\text{N}_2$  adsorption-desorption isotherms at 77 K in a Micrometrics Accelerated Surface Area and Porosimetry Analyzer 2020. The content of La(III) was quantified by digesting 20 mg of the carbons with 20 mL of  $\text{HCl-H}_2\text{SO}_4$  molar ratio of 1:5 (Fermont) in a Microwave Advanced Digestion System (Milestone), from 25 to 150 °C in 10 minutes and maintaining that temperature during 35 minutes. The final solution was diluted to 50 mL with deionized water and La(III) was determined using inductively coupled plasma-optical emission spectrophotometer (Varian 730-ES) at 379.47 nm. Scanning electron microscopy and energy-dispersive-ray spectroscopy (Quanta 200) were performed to obtain the La(III) mapping of the carbons. X-Ray Diffraction (XDR SmartLab Rigaku) was implemented to obtain the crystallographic patterns and phases with a  $\text{Cu K}_\alpha$  radiation  $\lambda = 1.546 \text{ \AA}$ , with a step time of 10 s and  $2\theta$  of  $0.02^\circ$ . The carbons were crushed before obtaining both the micrographs and diffractograms.

The point of zero charge was determined by placing 0.1 mg of the adsorbents in 50 mL of 0.1 M NaCl or in 0.1 M NaF (Sigma Aldrich) and stirring for 14 hours. The pH was adjusted to 11 with a solution of 0.1 M NaOH (J.T. Baker); then, the samples were titrated with 0.1 M HCl (J.T. Baker) by an automatic titrator (Mettler-Toledo T70) under  $\text{N}_2$  atmosphere. Afterwards, the released ions and the  $\text{pK}_a$  distribution were obtained as was stated in Section 2.2.1.

### ***3.2.2 Cell arrangement and electrochemical characterization***

For the electrochemical characterization, the carbons were again packed in sacks made of stainless-steel mesh (#304), which served as the working electrode. The counter electrode consisted of a stainless-steel mesh (SSM) without carbon and the reference electrode was Ag/AgCl/3M NaCl (ALS Co., Ltd). The working electrode was deaerated in boiling water and a Teflon membrane was placed between the working and the counter electrode to avoid short-circuit. All electrodes were then immersed in specific aqueous solutions and connected to a Potentiostat/Galvanostat (Bio-Logic VMP multichannel, controlled by EC Lab software).

Cyclic voltammetry was carried out in 0.1 M NaF, scanning between -0.5 and 0.5 V vs. Ag/AgCl/3M NaCl at different sweep rates. The gravimetric capacitance was computed using the Equa 7. The potential of zero charge was determined in a 20 ppm F solution, polarizing the carbons from -0.2 to 0.6 V (vs. Ag/AgCl/3M NaCl) in 0.05 V increments,

with a potential amplitude of 10 mV, using a frequency range from 100 kHz to 100 mHz and 10 points per decade. The capacitance was computed with the formula

$$C = \frac{1}{2\pi f \cdot \text{Im}} \quad (\text{Equation 9}),$$

where C is the capacitance (F), f is the lowest value of frequency (Hz) and -Im is the imaginary component ( $\Omega$ ) and the potential of zero charge was identified as the lowest value of capacitance among the applied potentials. Two sets of measurements were performed with freshly prepared electrodes: i) immediately after immersion and ii) after reaching the adsorption equilibrium. All values of capacitance were then graphed versus the polarization potential and the capacitance minimum was selected as the potential of zero charge. Linear sweep voltammetry was performed in a 20 ppm F<sup>-</sup> solution, i.e., the working solution, sweeping at 0.2 mV s<sup>-1</sup> from -0.2 V to 1.2 V (vs. Ag/AgCl/3M NaCl).

### 3.2.3 Kinetics

For this specific chapter, the initial concentration was increased to 20 ppm F<sup>-</sup> mainly, due to the weight of the working electrode, which limited the amount of mass of carbon and thus, the thickness of the electrode and the dimensions of the projected area.

For fluoride electrosorption, the cell (V = 0.5 L, pH<sub>0</sub> = 7, C<sub>0</sub> = 20 ppm F, 120-130 rpm) consisted of 0.25 g of activated carbon packed in a SSM (working electrode, 6.25 cm<sup>2</sup> of projected area), a SSM without activated carbon (counter electrode, 25 cm<sup>2</sup> of projected area) and Ag/AgCl/3 M NaCl as the reference electrode. The working electrode was deaerated in boiling water before its immersion in the electrolyte. Kinetics were first performed by polarizing only at 0.8 V (vs. Ag/AgCl/3M NaCl) in two polarization profiles: i) polarizing from the beginning and ii) polarizing after the adsorption equilibrium at the same potential value. This potential corresponds to ~1.1 V<sub>cell</sub> and was selected according to the results of the potential of zero charge and due to the results of previous reports [49,50]. During the kinetics, the concentration of fluoride was measured with the fluoride selective electrode (Thermo Scientific) and the pH of the solution was measured with a potentiometer (Thermo Scientific Potentiometer) at different time intervals. Fluoride removal capacity (mg g<sup>-1</sup>) was calculated by Equation 8. The release of Lanthanum from the modified electrodes was determined by ICP-OES (Varian 730-ES) at 379.47 nm at the adsorption and electrosorption equilibria.

Another set of electrosorption kinetics were performed by polarizing at 0.4, 0.8 and 1.2 V (vs. Ag/AgCl/3M NaCl) and both previous polarization profiles: stepped-potential increases (including the open circuit potential (OCP)) and polarizing at a single value from the beginning. Desorption was evaluated by depolarizing the electrodes (at the OCP) and by reversing the polarization at -0.5 V and -1.0 V (vs. Ag/AgCl/3M NaCl). Electrochemical impedance spectroscopy was performed during the desorption experiments at the OCP to

track interfacial changes on the carbon surface. The technique was performed at the OCP using a perturbation of 10 mV of amplitude, in a frequency range from 100 kHz to 10 mHz, with 10 points per decade. The system was allowed to stabilize until attaining a  $\Delta E_{\text{OCP}} = 1 \text{ mV h}^{-1}$ .

### ***3.3 Results and discussion***

#### ***3.3.1 Characterization***

##### ***3.3.1.1 Textural properties***

Table 3.1 shows the La(III) content in the carbon matrices, obtained from acid digestion, which confirms a successful impregnation of La(III) with significant differences in their w/w percentages. The labels of the carbons in this study were according to their lanthanum content: GAC, for the pristine carbon, and La-0.5%, La-1.5% and La-2.0% for the modified carbons. The textural analysis of the carbons (Table 3.1 and Figure 3.2a) shows a marked decrease in the surface area and pore volume as a function of increasing the La(III) content in the carbons. Lanthanum, as other metals, can anchor and agglomerate onto the carbon surface mainly due to their coordination with phenolic and carboxylic surface groups [204,205]. The decrease in the textural properties of the modified carbons can be attributed to the formed clusters that blocked some of the pores, especially the narrower ones [36]. Both the pristine carbon ( $905 \text{ m}^2 \text{ g}^{-1}$  and  $0.447 \text{ cm}^3 \text{ g}^{-1}$ ) and La-0.5% ( $895 \text{ m}^2 \text{ g}^{-1}$  and  $0.438 \text{ cm}^3 \text{ g}^{-1}$ ) presented a similar surface area and pore volume, which is in good agreement with the low impregnation percentage of this modified carbon. On the other hand, the surface area and pore volume did significantly decrease for La-1.5% ( $802 \text{ m}^2 \text{ g}^{-1}$  and  $0.396 \text{ cm}^3 \text{ g}^{-1}$ ) and La-2.0% ( $752 \text{ m}^2 \text{ g}^{-1}$  and  $0.375 \text{ cm}^3 \text{ g}^{-1}$ ). These losses can be associated specifically to micropores ( $< 2 \text{ nm}$ ), as they decreased more than other pore sections (Table 3.1 and Figure 3.1a).

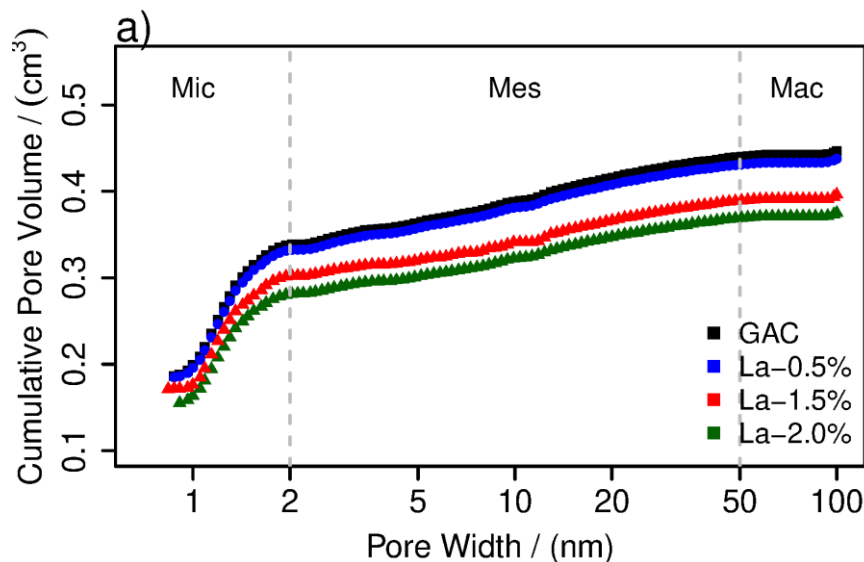


Figure 3.1. Cumulative pore volume by  $N_2$  adsorption-desorption isotherms at 77 K, obtained by non-linear density functional theory (x-axis in logarithmic scale, Mic = micropores, Mes = mesopores and Mac =, macropores).

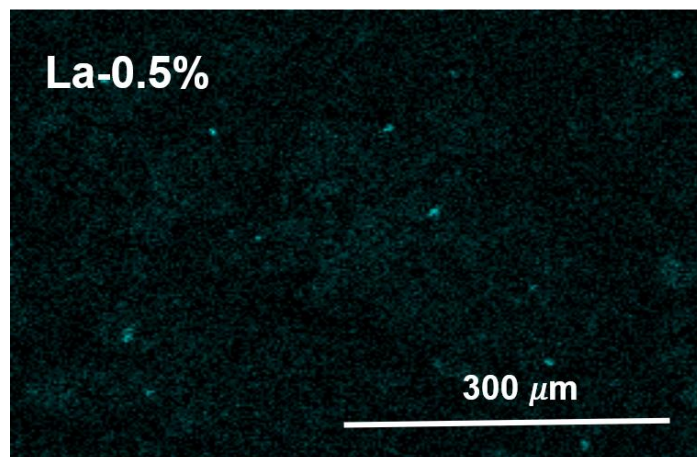
Table 3.1. Textural, physicochemical and electrochemical properties of the studied carbons.

Adsorbent	%La (w/w)	$S_{BET}$ ( $m^2 g^{-1}$ )	$V_{mic}$ ( $cm^3 g^{-1}$ )	$V_{mes}$ ( $cm^3 g^{-1}$ )	$V_{tot}$ ( $cm^3 g^{-1}$ )	pH <sub>PZC</sub>	$E_{PZC}$ (V vs. ref)
GAC	ND	905	0.338	0.101	0.447	8.5	0.0
La-0.5%	0.52	895	0.331	0.099	0.438	4.91	0.1
La-1.5%	1.58	802	0.302	0.087	0.396	4.68	0.45
La-2.0%	1.96	752	0.281	0.088	0.375	4.43	0.55

Scanning electron microscopy coupled to energy dispersive X-ray spectroscopy was performed to corroborate the formation of La(III) clusters and to evaluate their dispersion on the carbon surface by elemental mappings of the micrographs in sample La-0.5%. As can be observed, lanthanum particles, represented in blue color (Figure 3.2a), indeed formed several clusters. The clusters are well-dispersed, but greatly differ in size, ranging from ~200 nm and up to ~3  $\mu m$ . Nevertheless, the smaller clusters are more abundant in this sample. This difference in the clusters size was expected, since the activated carbon used in this study has a highly disordered and irregular pore structure [205,206]. Finally, due to the low content of lanthanum, no diffraction peaks were observed by X-ray diffraction (Figure 3.2.b), although,  $La_2O_3$  and  $La(OH)_3$  phases were identified in [36].



a)



b)

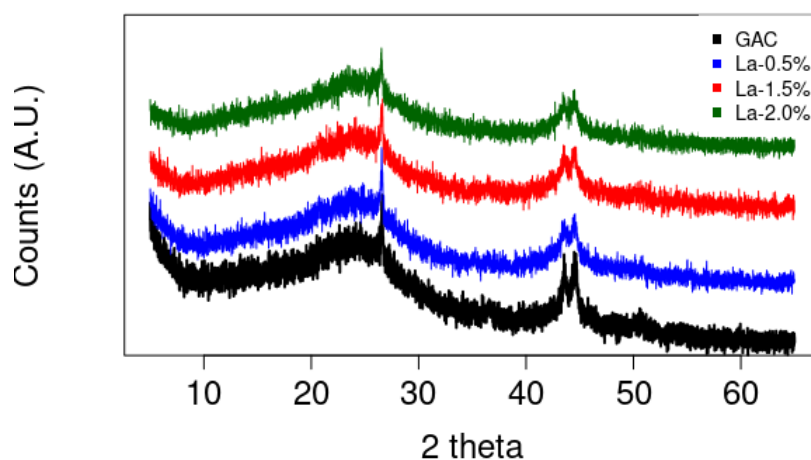


Figure 3.2. a) SEM-EDS mapping of Lanthanum (in blue color) for the modified carbon La-0.5% at 250x. b) Diffractograms of the adsorbents (Cu K $\alpha$  radiation  $\lambda = 1.546 \text{ \AA}$ , step time =  $0.02^\circ$  every 10 s).

### 3.3.1.2 Surface chemistry and surface charges

The anchoring of lanthanum also promoted significant changes in the surface chemistry of the carbon. La(III) clusters provided a higher polarity to the surface because of the exposed hydroxyl terminations. These hydroxyl functionalities also changed the net charge of the surface, as they can deprotonate as a function of the solution pH, which was evaluated by the determination of the point of zero charge ( $\text{pH}_{\text{PZC}}$ ). For the pristine carbon, the  $\text{pH}_{\text{PZC}}$

was 8.5 (Table 3.1), implying a positive charge at neutral solutions. On the other hand, the  $pH_{PZC}$  of the modified carbons decreased to acidic pH values as function of increasing the La(III) content (4.9, 4.68 and 4.43 for La-0.5%, La-1.5% and La-2.0%, respectively), for which their surface will present a negative charge at neutral solutions. Even when fluoride can present electrostatic repulsion towards the negative charges from the deprotonation of these surface hydroxyls, the presence of these groups promotes fluoride chemisorption by a ligand-exchange mechanism [36], which will be further addressed below.

In addition, the direct effect of surface charges on an electrode for capacitive processes can be evaluated by the potential of zero charge ( $E_{PZC}$ ). The  $E_{PZC}$  is the potential value with a minimum capacitance value and reflects the composition of ions at the interface, also termed as the surface excess: when  $E > E_{PZC}$ , the interface will be composed mainly by anions; when  $E < E_{PZC}$ , the interface will be composed mainly by cations. The pristine carbon presented the lowest  $E_{PZC}$ , 0.0 V (vs. Ag/AgCl/3M NaCl), while the  $E_{PZC}$  of the modified carbons increased to more positive values as a function of increasing the La(III) content (0.1, 0.45 and 0.55 V for La-0.5%, La-1.5% and La-2.0%, respectively). The increase in the  $E_{PZC}$  for the modified carbons implies that they will require higher polarization values to change their surface excess and remove fluoride. Due to this result, 0.8 V (vs. Ag/AgCl/3M NaCl or  $\sim 1.1 V_{cell}$ ) was selected as the polarization potential for the electrosorption experiments, i.e., above the highest  $E_{PZC}$ , but not high enough to promote the expulsion of lanthanum.

### 3.3.1.3 Cyclic voltammetry

One common approach for electrosorption is to study the capacitive properties of adsorbents. When polarized, capacitive electrodes accumulate charge as ions at the interphase. In addition, the decrease in surface area due to the occlusion of pores could also imply changes in the polarizable area of the modified carbons, as micropores provide higher area and can present higher electrical conductivity than other pore sections [207–209]. For this, cyclic voltammetry was carried out to evaluate changes in the response by the potentiodynamic polarization of the carbons. All voltammetric responses (1 mV s<sup>-1</sup>, Figure 3.3) resemble a double-layer capacitor with a marked variation on the capacitance of the electrodes (the width of the response) between carbons. Again, insignificant differences were observed between La-0.5% and the pristine carbon, while the modified carbons with more La(III) decreased their capacitance as a function of increasing the La(III) content. Then, more occluded pores decreased the polarizable surface of the carbons, which decreased their ability to retain ions at the interface. This corroborates that lanthanum clusters blocked a significant part of the polarizable area of the modified carbons and that the polarizable area was located mainly at micropores.

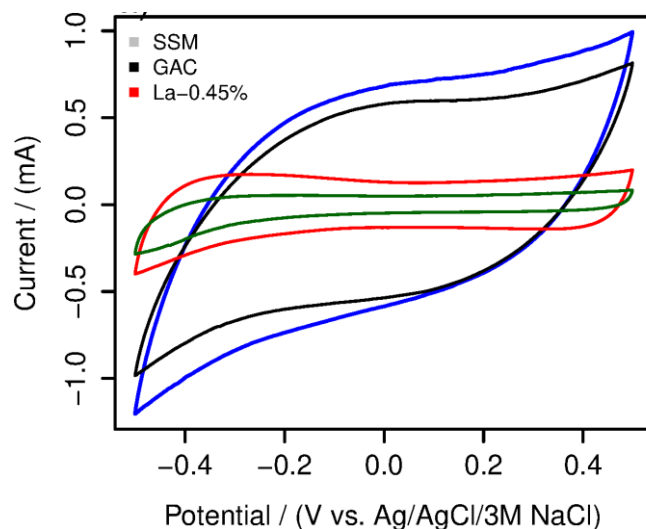


Figure 3.3. Cyclic voltammetry in 0.1 M NaF, from -0.5 to 0.5 V a) at  $1 \text{ mV s}^{-1}$  for all the carbons ( $M = 0.025 \text{ g}$ ,  $V = 0.050 \text{ L}$ ,  $\text{rpm} = 120\text{-}130$ ,  $T = 25 \text{ }^\circ\text{C}$ ). The measurements correspond to the 3rd cycle.

Figure 3.4 shows the voltammetric response of the modified carbon La-0.5% as a function of different sweep rates. As can be observed, the voltammetric response deformed at higher sweep rates, which also decreased the gravimetric capacitance of this electrode. This is related to insufficient time for the ions to enter into the narrower pores at faster sweep rates, which decreased the quantity of ions accumulated at the interphase, thus decreasing the capacitance. This same tendency, the deformation of the characteristic response of a double-layer capacitor and the marked decrease in the gravimetric capacitance by increasing the sweep rate, was similar for the other carbons, including the pristine carbon.

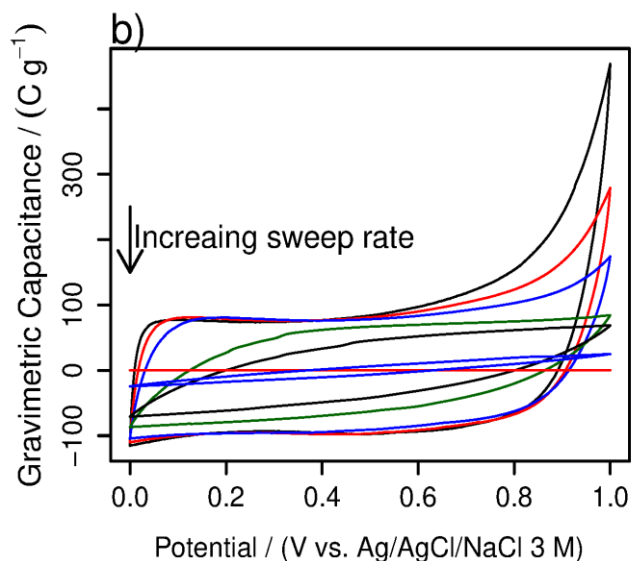


Figure 3.4. Gravimetric capacitances obtained from cyclic voltammetry in 0.1 M NaF, from -0.5 to 0.5 V at several sweep rates for La-0.5% ( $M = 0.025$  g,  $V = 0.050$  L, rpm = 120-130,  $T = 25$  °C). The measurements correspond to the 3rd cycle.

### 3.3.2 Kinetics

#### 3.3.2.1 Conventional adsorption vs electrosorption

Figure 3.4 shows the kinetics from conventional adsorption at the open circuit potential (OCP, i.e., without polarizing the carbons, Figure 3.4a), the electrosorption kinetics (Figure 3.4b) and the comparison of the obtained capacities between both processes for all the electrodes (Figure 3.4c). Conventional adsorption kinetics at the OCP (Figure 3.4a) showed an increase in the adsorption capacity and velocity as a function of increasing the La(III) content. The pristine carbon presented the lowest capacity ( $0.77$  mg g<sup>-1</sup>), while the modified carbons increased their adsorption capacity to  $1.95$  mg g<sup>-1</sup>,  $6.13$  mg g<sup>-1</sup>, and  $7.86$  mg g<sup>-1</sup> for La-0.5%, La-1.5% and La-2.0%, respectively. When polarized from the beginning at 0.8 V (vs. Ag/AgCl/3M NaCl, Figure 3.4b), the pristine carbon increased its capacity to  $1.23$  mg g<sup>-1</sup>, while the modified carbons presented a capacity of  $3.13$  mg g<sup>-1</sup>,  $6.21$  mg g<sup>-1</sup> and  $6.56$  mg g<sup>-1</sup> for La-0.5%, La-1.5% and La-2.0%, respectively. When comparing both processes (Figure 3.4c), it can be observed that the electrical polarization only benefited the pristine carbon and La-0.5%, compared to the removal at the OCP. On the other hand, the electrosorption capacity of La-1.5% presented no significant difference while the electrosorption of La-2.0% decreased, compared to their capacity at the OCP. Other differences were observed in the removal rates of both adsorption and electrosorption kinetics (Table 3.2). Finally, La(III) concentration was determined by ICP-OES at the equilibrium, but was only detected for samples from the electrode La-2.0%. This explains the decrease in the electrosorption capacity compared to conventional adsorption, as the

La(III) content decreased due to the electrical polarization, which also implies that this electrode is not suitable to be polarized, as even this minimal polarization from its  $E_{PZC}$  (0.55 V) expelled La(III).

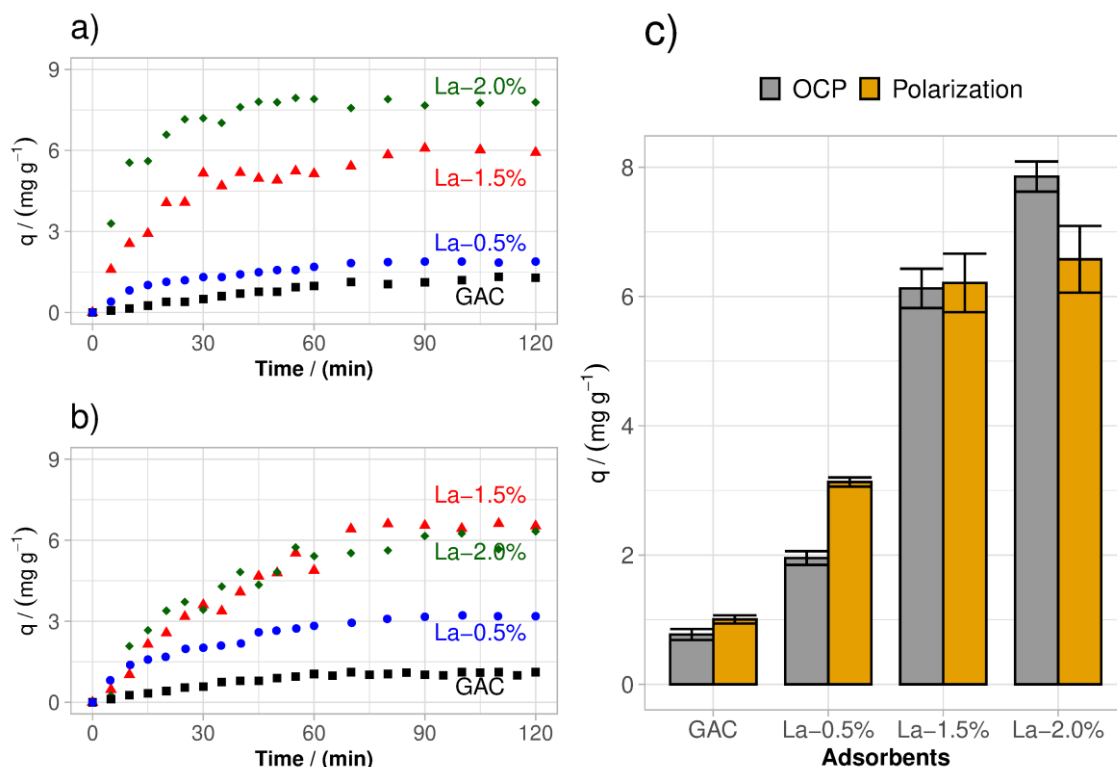


Figure 3.5. Adsorption kinetics for the adsorbents a) without polarization and b) polarizing at 0.8 V. c) Comparison of the obtained capacities by both adsorption and electrosorption kinetics ( $M = 0.25$  g,  $V = 0.5$  L,  $C_0 = 20$  ppm F,  $pH_0 = 7$ ,  $rpm = 120-130$ ,  $T = 25$  °C).

Table 3.2. Removal velocities by adsorption and electrosorption in  $mg\ g^{-1}\ h^{-1}$  ( $M = 0.25$  g,  $V = 0.5$  L,  $C_0 = 20$  ppm F<sup>-1</sup>,  $pH_0 = 7$ ,  $rpm = 120-130$ ,  $T = 25$  °C).

Electrode	Conventional adsorption (at the open-circuit potential)	Electrosorption (0.8 V vs. Ag/AgCl/3M NaCl)
GAC	0.615	1.32
La-0.5%	2.863	4.714
La-1.5%	9.785	7.61
La-2.0%	17.169	8.928

Previous analysis helped to discern the real effect of the electrical polarization on these modified carbon matrices. The removal of fluoride at the OCP increased as a function of increasing the La(III) content, as the anchoring of La(III) increased the number of adsorption sites for fluoride on the modified carbons, i.e., the exposed hydroxyls from La(III) clusters [36]. On the other hand, the deprotonation of some of these oxygenated functionalities provided a net negative charge on the surface at our working system ( $C_0 = 20$  ppm F,  $pH_0 = 7$ ), corroborated by a decrease in the  $pH_{PZC}$  and an increase in the  $E_{PZC}$ . These negative charges competed with the positive polarization of the carbon when polarized from the beginning. Opposite charges to the polarization of the electrode present an antagonistic effect by repelling the adsorbate (fluoride) and stabilizing cations such as sodium.

As explained above, an electrode with a higher  $E_{PZC}$  will need higher potentials (higher energy) to counter the exposed antagonistic charges and start electrosorbing fluoride. On the other hand, if the surface charges are of the same sign as the electrical polarization of the electrode, there is a synergy and the electrosorption capacity and rate is enhanced, as has been studied by the amphoteric-Donnan model [62,112,210,211]. For this reason, the carbons with the lowest  $E_{PZC}$  increased more its removal capacity when polarized at the selected potential. Even due to all previous factors and discussion related to the correlation between the surface chemistry, the surface charges and the electrosorption performance, the performance of the modified carbons was significantly better compared to the performance of the pristine carbon, which reiterates the importance of the surface modification with metal phases in fluoride removal.

### ***3.3.2.2 The polarization profile and interfacial changes after adsorption***

Figure 3.5a shows the electrosorption results of the modified carbons La-0.5% and La-1.5% when polarized at 0.8 V vs. Ag/AgCl/3M NaCl after the adsorption equilibrium (filled figures). Previous electrosorption results (polarizing from the beginning, unfilled figures) were added to the graph to compare both processes. As can be observed for La-0.5%, there are no significant differences in the removal capacity as a function of the polarization profile, but the adsorption velocity did increase when polarizing from the beginning. On the other hand, the stepped polarization promoted a removal of  $8.92 \text{ mg g}^{-1}$  for La-1.5%, increasing the fluoride removal in 50%, compared to the adsorption and the electrosorption processes individually ( $\sim 6 \text{ mg g}^{-1}$ ). Before explaining the processes taking place at the stepped kinetics (polarizing after the adsorption equilibrium), the adsorption mechanism of fluoride into these matrices will be further detailed and experimentally verified upon next.

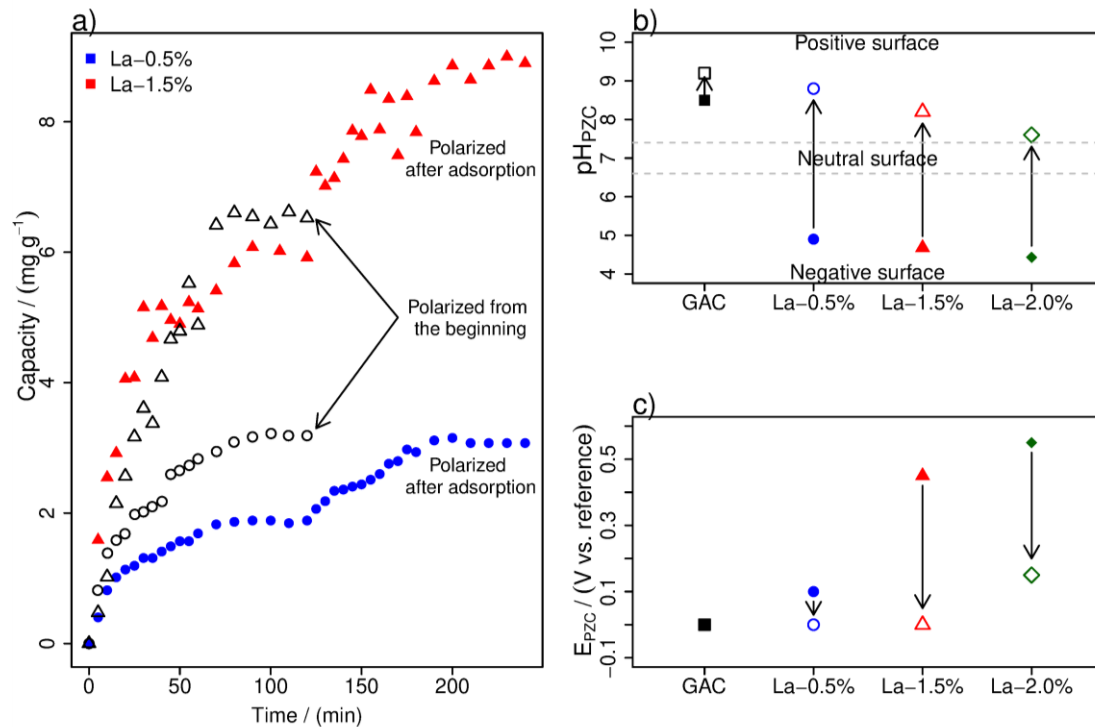


Figure 3.6. a) Comparison of conventional adsorption kinetics and stepped electrosorption kinetics for La-0.5% and La-1.5% ( $E_{pol} = 0.8$  V,  $M = 0.25$  g,  $V = 0.5$  L,  $C_0 = 20$  ppm F,  $pH_0 = 7$ ,  $rpm = 120-130$ ,  $T = 25$  °C). Shift in the b)  $pH_{PZC}$  and c)  $E_{PZC}$  due to fluoride adsorption. The filled figures correspond to the initial determination, before fluoride adsorption; the unfilled figures to the determination after fluoride adsorption ( $M = 0.025$  g,  $V = 0.05$  L,  $pH_0 = 7$ ,  $rpm = 120-130$ ,  $T = 25$  °C,  $E_{amp} = 10$  mV).

Fluoride chemisorbs onto the modified carbons by a ligand-exchange mechanism, in which the exposed hydroxyls of La(III) are involved [36]. This was observed by increases in the measured pH of the solution, FT-IR signals, analysis of the pKa distribution [36] and due to the absence of fluoride liberation when depolarizing the electrode [50]. Because some of these hydroxyls are exchanged by fluorides in solution, the input of negative charges on the carbon surface should decrease after the adsorption equilibrium. This was tracked and corroborated by measuring both the  $pH_{PZC}$  and the  $E_{PZC}$  after fluoride adsorption. The  $pH_{PZC}$  (Figure 3.6b) of all carbons increased to more alkaline values (unfilled figures), even for the pristine carbon ( $pH_{PZC} = 8.7, 8.2, 7.6$ , for La-0.5%, La-1.5% and La-2.0%, respectively), which is indicative of the change in the surface charge from negative to positive at our working conditions. The same tendency is observed in the  $E_{PZC}$  (Figure 3.5c), as the obtained values became less positive, compared to the values before fluoride adsorption (unfilled symbols), except for the pristine carbon. Then, the ligand-exchange mechanism was taking place and it promoted significant interfacial changes related to the surface charges after fluoride adsorption.



These changes in the net surface charge (from negative to positive values) could explain the better performance for La-1.5% when polarized after the adsorption equilibrium. According to the amphoteric Donnan model, a positive surface is better suited for anion electrosorption, due to a decrease in the energy needed to modify the surface excess (less co-ion expulsion) and higher electrode charging (higher potential difference from the  $E_{PZC}$ ), which translates as higher attraction of adsorbates towards the surface [62,118]. Previous statement should be understood as a synergy between the inner potential (the applied potential, 0.8 V vs. Ag/AgCl/3M NaCl) and the surface potential (associated to the surface chemistry of the electrode), i.e., the global attraction towards fluoride increases when both potentials are positive, as occurred when polarizing after the adsorption equilibrium.

#### ***3.3.2.2.1 The electrical pore blockage of the micropores***

Independently from previous discussion, there is still a gap in understanding the differences between the two polarization profiles related to the available surface before and after fluoride adsorption. Formally, no differences in removal should be attained by both polarization profiles if the available surface and pore volume that interacts with fluoride remains the same. All the accessible functionalities and polarizable surface inside the narrower pores should have contributed to fluoride removal independently of the profile, although this was probably not the case. Then, it seems feasible to propose that there were not only changes in the net surface charges, but also in the available polarizable surface after fluoride adsorption. A fraction of the polarizable surface was unreachable at the beginning of the kinetics. The previous statement must be referred specifically to the micropores, as they present higher deployment of functionalities and are responsible for the alkaline or acidic surface characteristics of these materials, present higher conductivity and, of course, are more prone to be obstructed or unavailable to solvated species [36,74,80,209,212]. Then, as it has been widely reported, there is an unavailable micropore space in aqueous solution [213,113,114,214], compared to the reported values obtained by physisorption analysis.

Due to this, it is here proposed that the narrower pores were not only obstructed physically, due to the presence and growth of La(III) clusters, but also electrically, due to the exposed antagonistic charges from deprotonated hydroxyl groups at their entrances (Figure 3.7), similar to a conventional electron-shielding effect in atoms. Then, the exchange of the hydroxyl groups decreased the concentration of negative surface charges, the micropores unblocked and the available micropore space increased, thus increasing the interaction towards fluoride and promoting higher fluoride removal for the modified carbon La-1.5%.



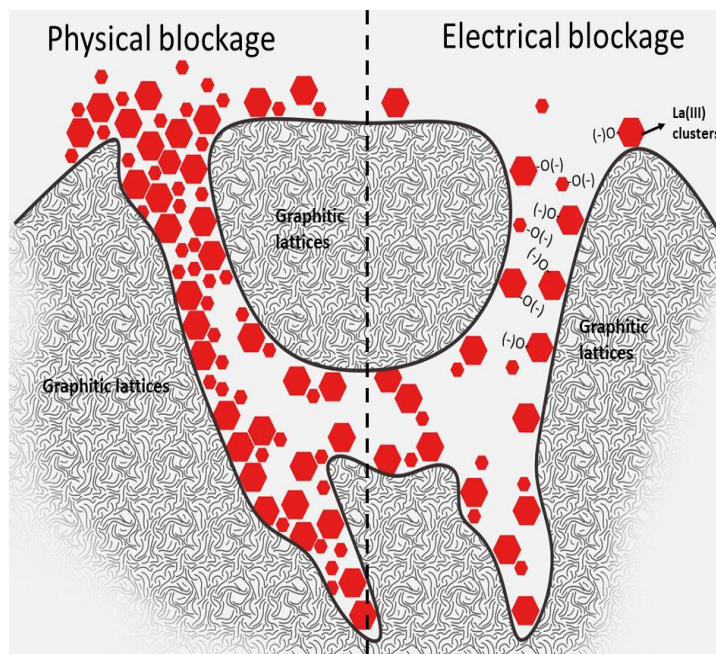


Figure 3.7. Schematic differentiation between a physical (left) and electrical (right) pore blockage.

On the other hand, La-0.5% did not present significant differences between the two polarization profiles as its pores were less blocked, both physically and electrically. This can also be analyzed from its lower  $E_{PZC}$  value (0.1 V), for which it was easier to counter the negative charges of the deprotonated hydroxyls when polarized at 0.8 V. All these results imply that marked improvements could be observed by selecting a stepped polarization profile (polarizing after the adsorption equilibrium) for electrodes that present significant interfacial changes related to their net surface charges after the adsorption process, as occurred for La-1.5%. Another approach consists in determining the  $E_{PZC}$  and applying sufficient energy (polarization value) far from this value to overcome antagonistic surface charges, as occurred for La-0.5%. Even when both previous approaches should promote better performances, in the former, the removal capacities could be different according to the polarization profile; in the latter, the removal capacities for both processes should be similar. Nevertheless, the electrosorption potential presents energetic and efficiency limits, while the polarization profile is not limited by such aspects, although may be indeed limited by a slow or inefficient adsorption step.

### 3.3.2.2.2 Polarization and charging processes

If the observed differences in fluoride removal for La-1.5% are indeed attributed to changes in the available polarizable surface after the adsorption step, then the current and charge profiles should also present differences as a function of the polarization profile for this same electrode. First of all, the current profiles of porous conductive matrices present a high initial stimulus of current, which decreases as a function of time. Electrodes with

higher surface area and pore volume (or higher electrical conductivity) require higher current to be electrically polarized. Figures 3.8a and 3.8b show the measured current (polarization profile) and charge (charging process), respectively, of the studied electrodes La-0.5% and La-1.5% during the electrosorption kinetics by both profiles. As can be observed, La-0.5% presented insignificant differences in the measured current and charge, which can be correlated to a similar polarization process independently of the polarization profile, as was stated in the previous section. On the other hand, La-1.5% shows a marked increase in the measured current and charge when polarized after the adsorption equilibrium, compared to its polarization from the beginning and can be attributed to a more efficient polarization and charging processes. This could also be associated to the fact that the available polarizable surface for La-1.5% was different depending on the polarization profile, i.e., polarizing after the adsorption equilibrium there was a higher polarizable surface than at the beginning of the kinetics.

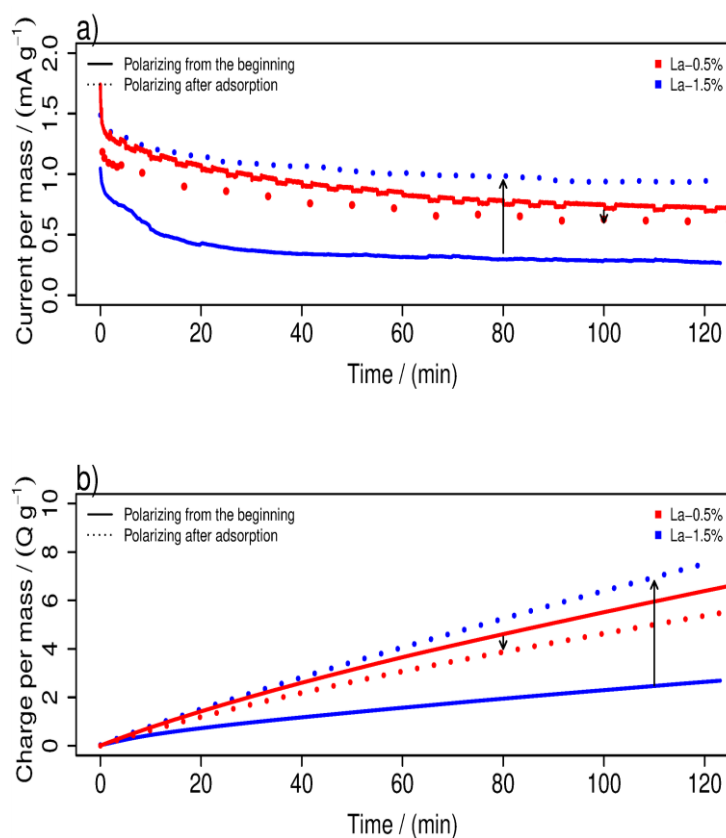


Figure 3.8. a) Current and b) charge profiles for La-0.5% and La-1.5% during the electrosorption kinetics. The arrows indicate the difference between both polarization profiles by the same electrode.

An additional analysis relies on the correlation between the  $E_{PZC}$  and the open-circuit potentials (OCPs). Figure 3.9 shows the OCPs before agitating the solution, i.e., before adsorbing fluoride (OCP recordings) and during fluoride adsorption (without polarizing the

carbons). First of all, the OCP is another reported method to obtain the  $E_{PZC}$  of porous electrodes [215]. The OCP of the pristine carbon was the lowest value, while the modified carbons increased their OCP as a function of increasing their La(III) content in a similar tendency as for the reported  $E_{PZC}$  by electrochemical impedance spectroscopy in Table 3.1. The recordings before adsorbing fluoride indeed show a stable behavior, as practically no fluoride is being adsorbed at this stage. After starting to agitate the solution, the OCPs of the modified carbons increased to more positive values and reached a new steady state at ~25 minutes. On the other hand, the pristine carbon increased its OCP at a much slower rate than the modified carbons, probably due to its less polar surface that promoted a slower and less spontaneous wetting process of this electrode.

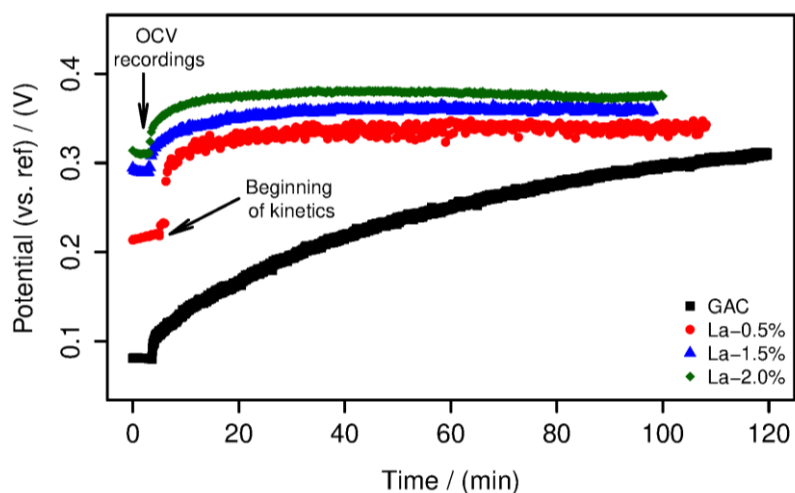


Figure 3.9. Recording of the open-circuit potential (OCP) values for the electrodes during a kinetics.

Figure 3.10 represents a schematic illustration of the useful and non-useful polarization for the modified carbon La-1.5%, as a function of specific electrochemical values: the potential of zero charge,  $E_{PZC}$ , the open circuit potential, OCP, and the polarization potential,  $E_{POL}$ . The  $E_{PZC}$ , as discussed above, represents the value at which the electrode is uncharged and polarizing beyond this value promotes a specific charge (positive or negative) on the electrode surface. The OCP represents an electrodynamic equilibrium value of the electrochemical system and its importance is related to the difference between this value and  $E^{POL}$  (0.8 V vs. Ag/AgCl/3M NaCl). As can be observed, when La-1.5% is electrically polarized from the beginning, there is a potential difference of 0.5 V between the OCP (0.3 V) and  $E_{POL}$  (0.8 V). Nevertheless, this electrode presents a positive charge at the  $E_{PZC}$  (0.45 V), for which the real potential difference was only of 0.35 V. This implies that there is a non-useful polarization of ~0.15 V, probably related to the energy wasted in expelling the co-ions and in counter the deprotonated surface functionalities. On the other hand, when this electrode is polarized after the adsorption equilibrium, the OCP increased to ~0.35 V, but the  $E_{PZC}$  decreased down to 0.0 V, for which there is a potential difference of 0.45 V

between the OCP and  $E_{POL}$ . The absence of non-useful polarization by this profile and a higher potential difference between the  $E_{PZC}$  and  $E_{POL}$  also explains the higher performance by this electrode and by polarizing after the adsorption equilibrium, even when the potential difference between both profiles is rather small. This also correlates adequately with the better polarization and charging processes observed for this modified carbon (Figure 3.8). This same schematization of the electrochemical parameters for La-0.5% (before adsorption:  $E_{PZC} = 0.1$  V, OCP = 0.21 V; after adsorption:  $E_{PZC} = 0.0$  V, OCP = 0.33 V;  $E_{POL} = 0.8$  V) would not show a significant difference by the obtained  $E_{PZC}$  values, and thus, in its polarization and charging process.

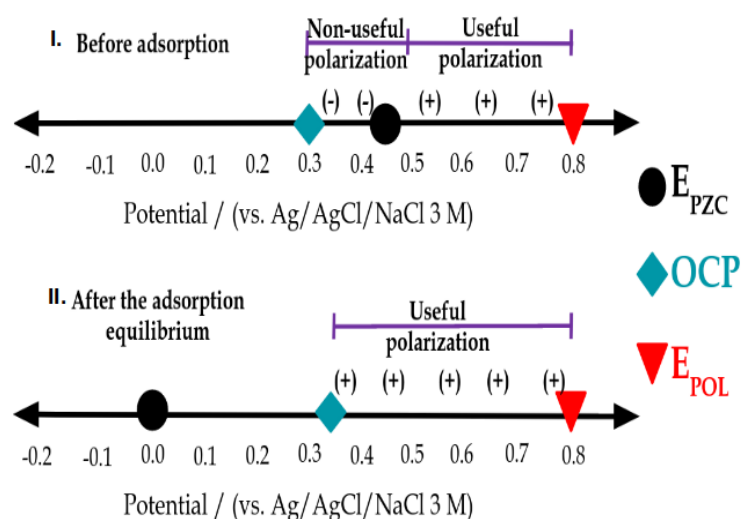


Figure 3.10. Schematic representation of useful and non-useful polarization using the values of the electrode La-1.5% I) before and II) after reaching the adsorption equilibrium, based on the electrochemical values of the potential of zero charge ( $E_{PZC}$ ), the open-circuit potentials (OCP) and the polarization potential ( $E_{POL}$ ).

### 3.3.2.2.3 Comparison to other works

Even when there are a few reports on fluoride electrosorption by activated carbon electrodes modified with metals [50,55,57], only one polarized their electrodes after the adsorption equilibrium. For this reason and to observe the effect of the polarization profile, the performances of other activated carbon electrodes modified with metals applied to water desalination were analyzed and were added to the discussion. The reported capacities were obtained from the kinetics experiments, once at the equilibrium. As an example, Chang *et al.*, [54], modified an activated carbon with  $TiO_2$  and increased its desalination ~15 times by polarizing the electrode after the adsorption equilibrium, compared to its adsorption capacity ( $C_0 = 500$  ppm NaCl, 1.2  $V_{cell}$ ). Ryoo and Seo [56] modified an activated carbon with Si(IV), Al(III), Zr(IV) and Ti(IV), polarizing their adsorbents again only after the adsorption equilibrium. The lowest increase in desalination was of 2.78 times higher than the adsorption capacity (without polarizing the electrode), but the carbon

modified with Ti(IV) increased its removal ~15 times ( $C_0 = 3.54$  ppm NaCl,  $1.0 V_{\text{cell}}$ ). These two previous examples evidence the importance of the polarization profile on these hybrid matrices, although the other polarization profile, polarizing the electrodes from the beginning, was not evaluated. On the other hand, when polarized from the beginning, most carbon electrodes modified with metals only increased their removal less than ~2 times [54,58,59,202]. The exceptional case was observed in the work of Yasin *et al.*, [58], in which an activated carbon electrode modified with  $\text{TiO}_2$  and  $\text{ZrO}_2$  increased its desalination 2.11 times and its subsequent doping with nitrogen achieved an increase in 2.84 times the desalination capacity of the unmodified electrode ( $C_0 = 50$  ppm NaCl,  $1.0 V_{\text{cell}}$ ). It is also worth to highlight that those last reports on modified electrodes did increase their removal velocity by polarizing from the beginning.

From previous reports, it can be observed that polarizing from the beginning is the most evaluated profile, but the few reports that evaluated the stepped polarization (polarizing after the adsorption equilibrium) showed better improvements in removal. Compared to our work, even when only an increase of 50% in removal was observed due to the polarization profile, our global removal is much higher than others reported for fluoride electrosorption. In addition, better results could also be obtained by controlling the La(III) cluster size, or by considering activated carbon-based electrodes with higher surface area, higher conductivity or a less heterogeneous surface. Again, this tendency is of special interest for porous electrodes modified with metals in which substantial interfacial changes related to surface charges occur after the adsorption process. In addition, this is not particular of fluoride and La(III), as the ligand-exchange mechanism has been observed between other anions and metals [153,216–219].

### **3.3.3 Electrosorption at other polarization potentials**

Another set of electrosorption kinetics by several stepped-potential increases (Figure 3.11a) were performed in order to evaluate the effect of the applied potential on fluoride removal, but only for the pristine carbon and La-0.5%. In addition, the potential value was extended to a higher value of 1.2 V (*vs.* Ag/AgCl/3M NaCl). All potential increases were standardized to the slowest equilibrium time observed for these set of kinetics, i.e., 3 hours. Results show that both carbons increased their removal capacities at each of the applied potentials. The adsorption capacity of the pristine carbon increased 3.9 times (from 1.12 to 4.26 mg g<sup>-1</sup>) at the last polarization step of 1.2 V (*vs.* Ag/AgCl/3M NaCl), while La-0.5% increased its adsorption capacity 2.55 times (from 2.33 to 5.93 mg g<sup>-1</sup>). The graph bars at Figure 3.11b showed a clear effect of the addition of La(III) to the carbon surface, when compared between samples, but also the effect of the polarization on their removal capacities, obtaining a marked and significant increase in fluoride removal.

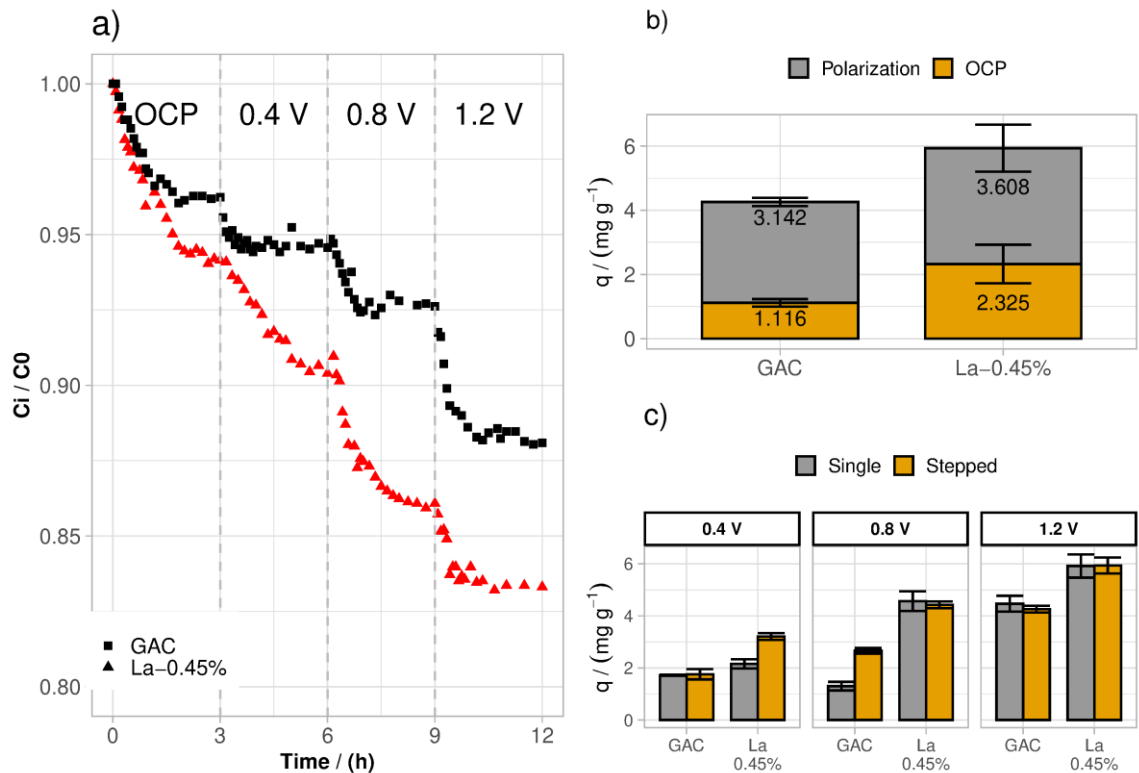


Figure 3.11. a) Stepped-potential kinetics for fluoride; b) capacities from OCP adsorption (gray) and electrosorption (orange) for the stepped-potential sequence; c) comparison of the capacities between both sequences for each of the applied potentials: stepped-potential (gray) and single-potential (orange) ( $C_0 = 20 \text{ ppm F}$ ,  $M = 0.3 \text{ g}$ ,  $V = 0.5 \text{ L}$ ,  $\text{pH}_0 = 7$ ,  $T = 25 \text{ }^\circ\text{C}$  and 120-130 rpm).

Now, the electrosorption kinetics by polarizing from the beginning at these same potentials (0.4, 0.8 and 1.2 V) will be discussed. When polarizing at 0.4 V (vs. Ag/AgCl/3M NaCl), the capacity of La-0.5% decreased, compared to the capacity from the stepped-potential profile, while the capacity of the pristine carbon was similar for both kinetics at this potential (Figure 3.11c). The first adsorption step (without polarization) in the stepped-potential profile contributed to neutralize some of the deprotonated lanthanum hydroxyls due to the ligand-exchange mechanism [36]. This charge neutralization made possible a further increase in fluoride removal when polarizing at 0.4 V afterwards. When polarizing at 0.4 V from the beginning, the positive polarization of the surface competed with the deprotonated hydroxyls. These adsorption sites were not previously neutralized as in the stepped-increase kinetics. At this polarization potential, not enough energy was applied to repel the sodium cations adsorbed at the interface, thus diminishing the removal of fluoride. A larger potential value was needed to overcome this charge effect, as was observed at higher polarization values, explained upon next and as was explained above in section 3.3.2.2.2.



When polarizing at 0.8 V (vs. Ag/AgCl/3M NaCl), the adsorption capacity of La-0.45% was the same for both single and stepped profiles, while for the pristine carbon was lower than for the stepped-potential profile and even lower than the capacity at 0.4 V. On the other hand, at 1.2 V, the adsorption capacities were similar to those obtained from the stepped-potential profile. The inconsistent adsorption capacity at 0.8 V for the pristine carbon could be due to competing faradaic reactions, observed in the linear sweep voltammetry (Figure 3.12a) and corroborated below (section 3.5.1). Probably, some of these faradaic reactions took place faster at 1.2 V, explaining why no significant differences in capacities were observed between different potential sequences at 1.2 V. Nevertheless, the current profiles (Figure 3.12b and 3.12c) obtained from these potentiostatic stimuli showed constant and stable measurements  $< 2.7 \text{ mA g}^{-1}$  at all polarization potentials. Finally, the stainless-steel mesh, presented no visual oxidation when polarized at this potentiostatic regime.

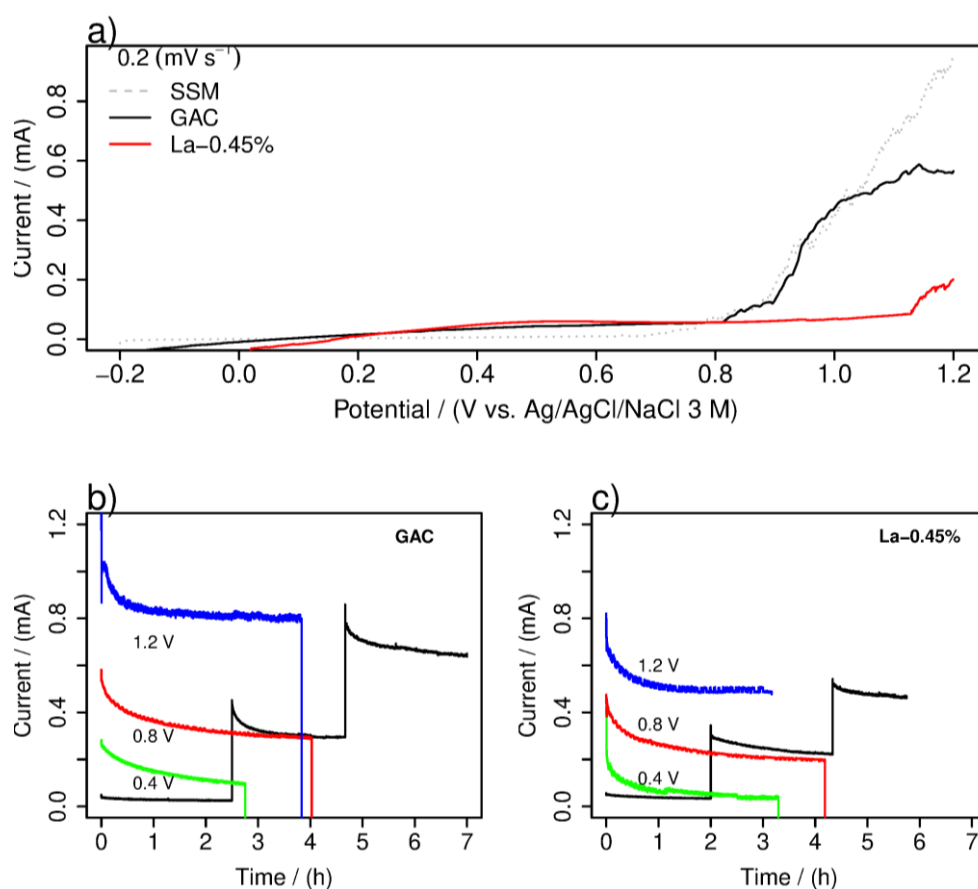


Figure 3.12. a) Linear sweep voltammetry at  $\nu = 0.2 \text{ mV s}^{-1}$ . b) Current profiles from stepped-potential and single potential kinetics for the b) pristine carbon and c) La-0.5%. The black lines represent the current measured during the kinetics by stepped-potential increases. ( $C_0 = 20 \text{ ppm F}$ ,  $M = 0.3 \text{ g}$ ,  $V = 0.5 \text{ L}$ ,  $\text{pH}_0 = 7$ ,  $T = 25 \text{ }^\circ\text{C}$  and 120-130 rpm, SSM as the counter electrode.)

Due to previous results, the polarization window can be extended to 1.2 V (vs. Ag/AgCl/3M NaCl), for which this potential will be used for further characterization of the electrosorption cell in the next sections.

### ***3.3.4 Electrosorption cycles by depolarization***

#### ***3.3.4.1 Depolarization at the OCP***

A whole cycle of electrosorption ( $C_0 = 20$  ppm F,  $\text{pH}_0 = 7$ ) consisted in polarizing at 1.2 V for 3 hours, the time needed to reach the electrosorption equilibrium, and then depolarizing the carbon at the open circuit potential with constant agitation until reaching a constant fluoride concentration. This process was then repeated 5 more times. The modified carbon did not desorb fluoride when depolarized (Figure 3.13a), although desorption was feasible by reversing the polarization of the electrode, as will be discussed in section 3.3.4.2. After the 2nd cycle and further, the adsorption capacity increased ~23% for La-0.5% ( $q_{\sim 1\text{st cycle}} = 5.53$  mg g<sup>-1</sup> vs.  $q_{\sim 2\text{nd-6th cycles}} = 6.82$  mg g<sup>-1</sup>). The lack of desorption at the open circuit potentials corroborated that fluoride was retained by a chemisorption process, even when polarized. The chemisorption process is attained by a ligand-exchange mechanism, in which fluoride is exchanged by the hydroxyl from the La(III) clusters [36].



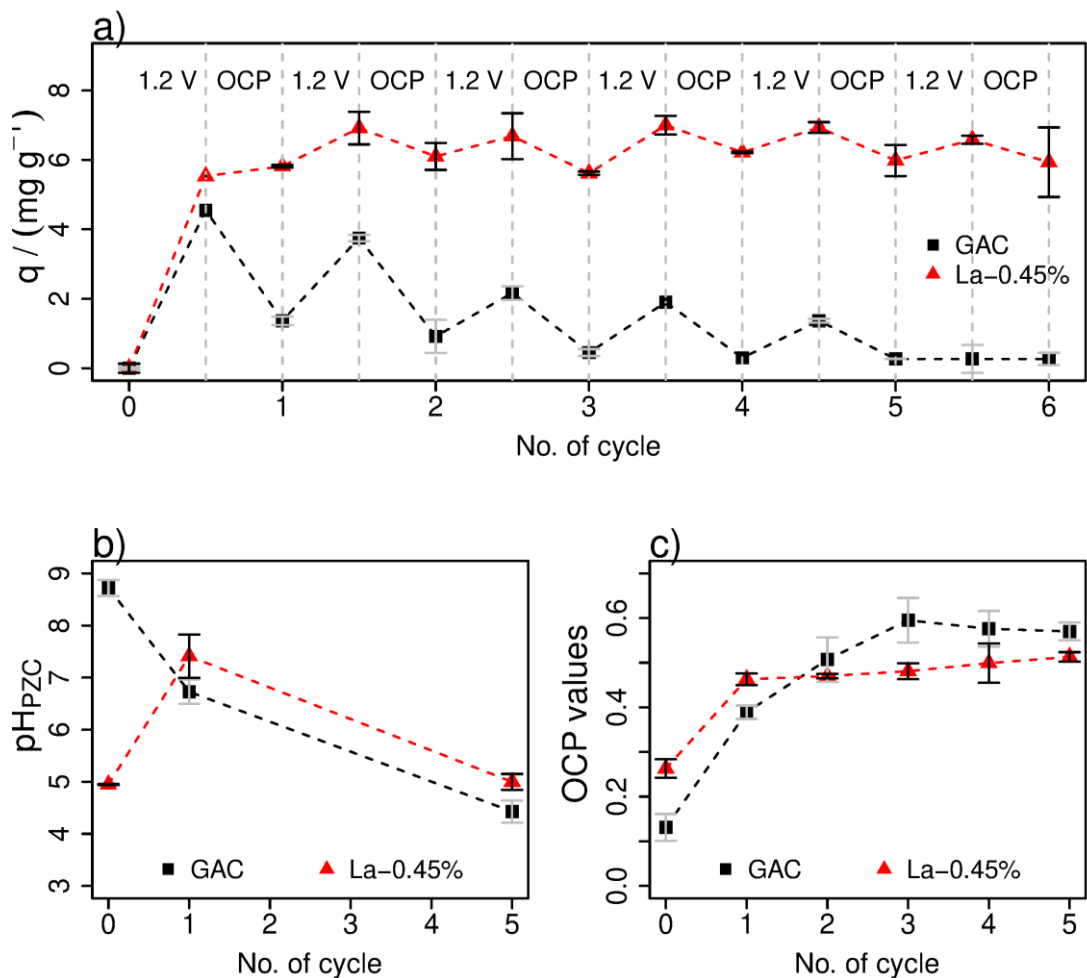


Figure 3.13. a) Electrosorption-desorption cycles ( $C_0 = 20$  ppm fluoride,  $M = 0.3$  g,  $V = 0.5$  L,  $\text{pH}_0 = 7$ ,  $T = 298$  K and 120-130 rpm, Ag/AgCl/3M NaCl as reference electrode, SSM as counter electrode, POL = polarization, OCP = open circuit potential). b) Point of zero charge values determined before polarizing or basal determination, after the 1st polarization and after the 6th polarization. c) Open circuit potential recorded before each polarization step.

Probably, the increase in fluoride concentration at the electrode surface promoted further chemisorption to take place, as a conventional Le-Chatelier principle. The increases in capacity for the consecutive cycles could be associated to a purely capacitive retention inside the carbon pores, as fluoride continues to migrate when the carbons are polarized. On the other hand, the capacity of the pristine carbon decreased in each cycle, reaching a 60% decrease at the 5th cycle ( $0.27 \text{ mg g}^{-1}$ ) and practically no electrosorption capacity at the 6th cycle. Then, the pristine carbon can only be polarized twice before losing most of its capacity.

During the polarization, interfacial changes were taking place for both carbons that can explain their difference in their performance, mainly, the oxidation of the surface and La(III) expulsion, the latter only for the modified carbon. Activated carbons oxidize when polarized [49,104,133], which can be confirmed by techniques that provide information on oxygen content or surface charges, as the  $pH_{PZC}$  and the  $E_{PZC}$ , among others. The  $pH_{PZC}$  for the pristine carbon decreased from 8.9 to 7.1 after the 1st cycle, and to 4.1 after the 6th cycle (Figure 3.13b), which clearly demonstrates the oxidation of the carbon surface due to its polarization. The oxidation of the surface increased the density of oxygenated functionalities with an acid-Lewis character and, subsequently, the density of negative charges and the electrostatic repulsion after each cycle. Also, the oxidation of the surface implies a decrease in its graphitization and thus, in its conductivity. Both previous factors explain the decrease in the electrosorption capacity after each subsequent polarization. In addition to the oxidation of its surface, La-0.5% expelled lanthanum.

For La-0.5%, its  $pH_{PZC}$  increased from 4.9 to 7.4 while its La(III) content decreased to 0.39% w/w after the 1st cycle. This is related to a decrease in the negative surface charges due to the expulsion of La(III) clusters. At the end of the 6th cycle, the  $pH_{PZC}$  decreased to 5.2, which is associated to the surface oxidation, while the La(III) content decreased to 0.32%. Nevertheless, the fact that the  $pH_{PZC}$  decreased after the 6th cycle to a lesser degree than for the pristine carbon implies that the presence of La(III) stabilized the oxidation of the modified carbon. This correlates adequately with the discussion of linear sweep voltammetry results (Figure 3.10), in which current increases were observed at higher potential values for the modified carbon. More detailed studies should take place to evaluate if lanthanum expulsion was due to the polarization potential, to consider lower potential value, or due to the polarization time.

The open circuit potential (OCP), also reported as the immersion potential [215], can be used to obtain information about the surface chemistry of carbon electrodes. The OCP values of both carbons increased as a function of increasing the number of electrosorption cycles (Figure 3.13c). Globally, the pristine carbon increased more its OCP values, from 0.13 V before the 1st polarization, to 0.57 V, after the 6th polarization; while the modified carbon increased from 0.26 to 0.51 V for these same polarizations. These increases in the OCP could be related to changes in the electrolyte composition, as the electrical polarization promoted the expulsion of adsorbed protons and of lanthanum. In addition, the surface oxidation increased the number of oxygenated functionalities that deprotonated at the working electrolyte, also changing the electrolyte composition at some degree. Nevertheless, these changes were minimal compared to the concentration of the working electrolyte ( $C_0 = 20 \text{ ppm F} \approx 10^{-3} \text{ M F}$ ).

On the other hand, the oxidation of the carbon surface decreased the number of functional groups that can oxidize, also decreasing the ratio of species that can be oxidized vs. the species that can be reduced. This ratio is directly related to the OCP values, according to

the Nernst equation. As can be observed, the pristine carbon increased had the highest increase in its OCP (0.57 V), compared to the modified carbon (0.51 V), which is equivalent to a higher oxidation of its surface. Then, this again corroborates that the presence of La(III) stabilized the oxidation of the modified carbon. It was observed that the electric polarization of the carbon surface promoted interfacial changes of the pristine electrode in contrast with the modified carbon. The pristine carbon decreased its electrical conductivity after the polarization by decreasing its graphitization while the presence of La(III) aided in stabilizing the surface chemistry, since it protects the surface from the oxidation process.

### 3.3.4.2 By reversing the polarization at negative potentials

Both carbons were polarized at negative potential values to study the desorption of fluoride. Figure 3.14 shows that desorption was achieved in only 1 hour when polarizing at -0.5 V. After reversing the polarization, 93.7% and 51.1% fluoride desorption was reached for the pristine carbon and La-0.5%, respectively. Nevertheless, the mesh oxidized at the second desorption cycle using this negative potential. At -1.0 V, the desorption rate was slightly faster, but this potential also increased the oxidation of the counter-electrode (SSM). Further experiments on desorption with a different counter electrode and in different electrolyte media should be considered for future desorption performance.

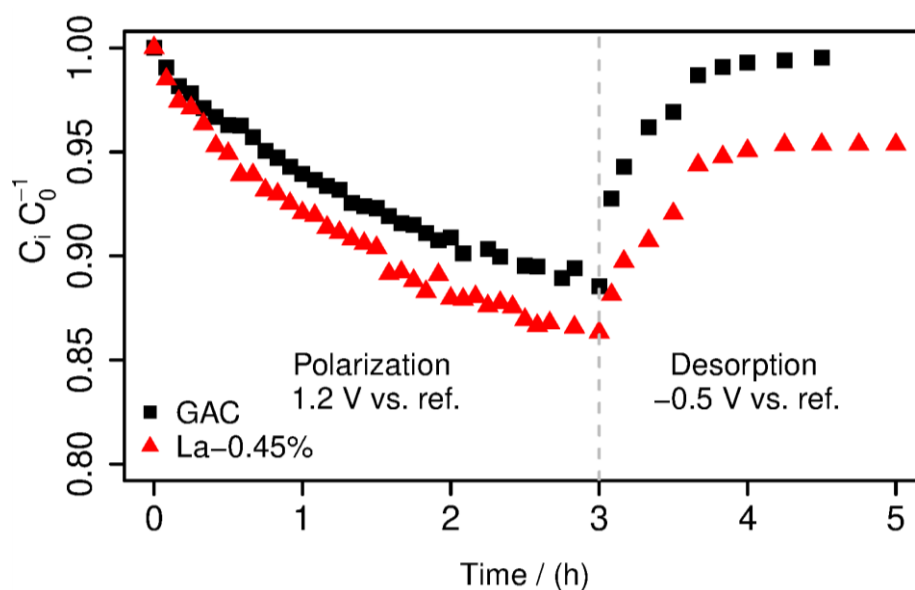


Figure 3.14. Electrosorption-desorption cycle of fluoride by reversing the polarization of the working electrode ( $M = 0.3$  g,  $C_0 = 20$  ppm F,  $V = 0.5$  L,  $pH_0 = 7$ ,  $T = 298$  K and 120-130 rpm, Ag/AgCl/3M NaCl as reference electrode, SSM as counter electrode).

### 3.4 Conclusions

The modification of a commercial activated carbon with different percentages of La(III) was achieved. The formed La(III) clusters partially blocked the entrances to narrower pores, promoting significant changes in their textural and capacitive properties, which correlated directly with their La(III) content. The addition of La(III) increased the number of sorption sites, increasing their adsorption capacity. Nevertheless, the electrical polarization of the modified electrodes promoted contrasting results. The electrical polarization of the modified activated carbons only benefited the carbon with the lowest La(III) content, increasing its removal capacity and kinetics, independently of the polarization profile. On the other hand, the other two carbons with higher La(III) content presented a similar or lower removal than that obtained by conventional adsorption (without polarizing the electrode). Even when La-1.5% presented a similar removal by conventional adsorption and electrosorption (polarized from the beginning), its polarization after the adsorption equilibrium promoted higher removal than by both processes individually. Due to these results, the polarization profile should be considered as a parameter to improve the electrosorption process in which the net surface charges of the electrodes change during the adsorption step, as in certain activated carbon electrodes modified with metals.

The two fundamental determinations to understand the charge distribution at these interfaces are the point and the potential of zero charge. These two parameters demonstrated that fluoride was chemisorbed by a ligand-exchange mechanism and that the hybrid carbons presented changes in their surface charge distribution after fluoride adsorption. The determination of both parameters before and after adsorption provided sufficient evidence to deduce that La(III) clusters partially blocked the entrances to the narrower pores both physically and electrically (due to the presence of antagonist charges).

The subsequent set of kinetics evaluated at other potential values showed that both the pristine carbon and La-0.5% could also be polarized at potentials beyond 1.2 V<sub>cell</sub> (0.8 V vs. Ag/AgCl/3M NaCl), increasing their removal rate and capacity. The same capacity was obtained independently of the polarization profile used, although polarizing from the beginning increased the removal velocity for both carbons. The modified carbon chemisorbed fluoride by a ligand-exchange mechanism, even during its electrical polarization. Because of this chemisorption process, fluoride did not desorb after the depolarization of the electrode. On the other hand, the pristine carbon did release fluoride when depolarized and its adsorption capacity decreased down to less than 10% of the initial capacity after the 6th cycle. When reversing the polarization of the electrodes at -0.5 V, fluoride desorption was attained for the modified carbon and at a much faster rate. Nevertheless, the stainless steel mesh (the counter electrode) oxidized when polarized at such negative potentials, for which it is not suitable as a counter electrode material for the evaluating the cyclic performance of the carbons.

The polarization process promoted the oxidation of the surface of both carbons, which was observed by a marked increase in the point and potential of zero charge after each subsequent cycle. However, the presence of lanthanum stabilized the oxidation process at some degree. On the other hand, a certain percentage of this metal was released during the polarization process. Finally, electrochemical impedance spectroscopy provided was a useful indicator to track interfacial changes and processes occurring during the electrosorption cycles.

## Chapter four: Fluoride electrosorption in the presence of competing anions of environmental relevance

Under review in *Electrochimica Acta*.

### 4.1 Introduction

Excessive and chronic fluoride consumption is associated to severe health implications, such as dental weakness and skeletal deformations [30,31]. For this, international standards have established a limit of 1.5 ppm in drinking waters for human consumption [30,31]. Electrosorption is an option for waters containing either organic or inorganic ions [52], as the electrical stimulus enhances electrostatic interactions towards ions. Carbon-based materials are excellent electrodes for the electrosorption process due to their high surface area and pore volume [52]. In addition, carbon-based materials can be modified with different chemical entities to develop hybrid electrodes with a better chemical and electrical properties to increase the electrosorption performance [50,54–57,178]. For the specific case of fluoride, only Ti(IV) [55,57] and La(III) [50,178] have been used as a modifying agent for activated carbons.

To date, there are some reports that have evaluated fluoride selectivity from different matrices against anions by capacitive processes [47,55,139,176,220,221]. In this regard, some works have fixed the concentration of the competing anions to resemble those of environmental conditions. Nevertheless, the concentration of species in natural environments can significantly vary in even small temporal and spatial lapses, for which such performance will be a function of the season, the temperature and any specific event that can promote concentration variations. Another approach consists in evaluating equimolar initial concentrations of the competing adsorbates to provide a first screening of the selectivity of a particular process or its conditions [47,55,176].

To best of our knowledge, there is only one report on fluoride electrosorption by a modified activated carbon with the metallic compound  $\text{Ti}(\text{OH})_4$ , which presented a remarkable selectivity in the presence of other anions in equimolar initial concentrations [55]. On the other hand, our research group has previously reported the impregnation of a commercial bituminous activated carbon with La(III), which mainly agglomerated at the carbon surface in the form of  $\text{La}(\text{OH})_3$ . The modified matrices have significantly outperformed the performance of the pristine unmodified carbon in both adsorption [36] and electrosorption [50,178]. The hybrid matrices were completely characterized and their electrosorption performances were extensively evaluated under different conditions. From there, the next

and last step comprises to evaluate the selectivity of these electrodes towards fluoride in the presence of anions of environmental relevance. Some of their properties will be mentioned below during the discussion and experimentally corroborated by electrochemical impedance spectroscopy.

## ***4.2 Materials and methods***

### ***4.2.1 Material standardization and modification***

Granular activated carbon (F-400, Calgon) with particle sizes between 250 and 500  $\mu\text{m}$  were selected for the impregnation step. For the synthesis of La-0.5%, 6 g of activated carbon were immersed in 100 mL of  $\text{La}(\text{NO}_3)_3$  0.15 M (Aldrich) solution for 2 days, at 25  $^\circ\text{C}$  under constant stirring (120-130 rpm). For La-1.5%, activated carbon was immersed in 0.3 M  $\text{La}(\text{NO}_3)_3$  solution in the mass:volume ratio of 0.1g:10 mL at the same conditions stated previously. The adsorbents were centrifuged, decanted, washed with deionized water and dried overnight at 85  $^\circ\text{C}$ .

### ***4.2.2 Cell configuration and electrochemical characterization***

The cell configuration consisted of 50 mg of activated carbon packed in a stainless steel mesh (working electrode, 2.6  $\text{cm}^2$  of projected area), a stainless steel mesh without activated carbon (counter electrode, 25  $\text{cm}^2$  of projected area) and a Teflon membrane between the electrodes. The electrodes were placed in boiling water for 5 minutes before its immersion in the cell to release accumulated air in their pores and to increase its wettability. Then, the electrodes were immersed in the electrosorption cell and were connected to a Potentiostat/Galvanostat (Bio-Logic VMP multichannel, controlled by EC Lab software).

Electrochemical impedance spectroscopy was carried out in two experimental sets. The first set was performed in 0.1 M NaF and 5 ppm  $\text{F}^-$  (0.263 mM, the working solution) at the open circuit potential (*vs.* Ag/AgCl/3M NaCl), with a potential amplitude of 10 mV, using a frequency range from 100 kHz to 10 mHz and 10 points per decade. The diluted system is of interest as it is the working solution and could provide different and better information of the electrical processes when decreasing the ionic strength of the system. The results were analyzed by an equivalent circuit approach to characterize the resistivity and capacitive nature of the working electrode, using the Levenberg-Marquardt algorithm (Chi-squared of  $10^{-3}$ ). The second set was performed to obtain the potential of zero charge in the working electrolyte (5 ppm  $\text{F}^-$  solution) by polarizing from -0.2 to 0.8 V (*vs.* Ag/AgCl/3M NaCl) in 0.05 V increments, with a potential amplitude of 10 mV and a frequency of 100 mHz. The capacitance was computed with Equation 9.

The electrosorption kinetics were performed using sacrifice cells ( $M = 50 \text{ mg}$ ,  $V = 50 \text{ mL}$ ,  $\text{pH}_0 = 7$ ). The cells were depolarized at different time intervals and the solution was then collected in Falcon tubes ( $50 \text{ mL}$ ) for the determination of the anions. The solutions were binary mixtures ( $\text{F}^-$  vs. anion) in equimolar initial concentrations ( $0.263 \text{ mM}$ ) of each anion (Sigma Aldrich): fluoride (from  $\text{NaF}$ ), chloride (from  $\text{NaCl}$ ), nitrate (from  $\text{NaNO}_3$ ), sulfate (from  $\text{Na}_2\text{SO}_4$ ), phosphate (from  $\text{Na}_2\text{HPO}_4$ ) and arsenate (from  $\text{Na}_2\text{HAsO}_4 \cdot 7 \text{ H}_2\text{O}$ ). Fluoride electrosorption was also evaluated in a complex mixture comprising all anions simultaneously in equimolar initial concentrations ( $0.263 \text{ mM}$  of each anion). Considering the speciation, two different species of phosphate ( $\text{HPO}_4^{2-}$  and  $\text{H}_2\text{PO}_4^{-1}$ ) and of arsenate ( $\text{HAsO}_4^{2-}$  and  $\text{H}_2\text{AsO}_4^{-1}$ ) were present in the studied conditions (Figure 4.1) in a very similar proportion.

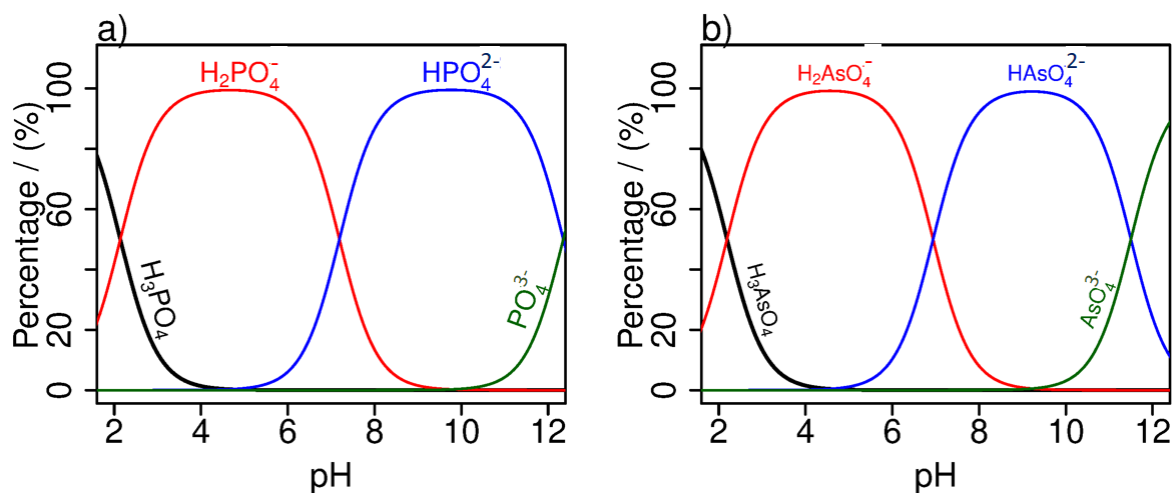


Figure 4.1. Speciation diagrams of a) phosphate and b) arsenate.

#### 4.2.3 Analytical determinations

Fluoride concentration was measured with a fluoride selective electrode (Thermo Scientific); nitrate concentration, by UV-VIS spectrophotometry (Aquamate Thermospectronic); chloride concentration, by means of a chloride selective electrode (ORION 9417BN); and As, P, S, Fe and La were determined by ICP-OES (Varian 730-ES). The analytical determination of iron and lanthanum concentrations in water were included to evaluate the stability of the electrochemical system, i.e., the oxidation of the stainless-steel mesh (Fe) and the expulsion of the anchored La to the solution. The pH (ORION 8156BNUWP ROSS) and the conductivity (cell ORION 013005MD) were measured with the potentiometer Orion VeraStar Pro (Thermo Scientific).



## 4.3 Results and discussion

### 4.3.1 Characterization

Both modified carbons were fully characterized in the previous chapter and were labelled as a function of their La(III) content in w/w%: GAC for the pristine carbon without lanthanum, La-0.5% contains a 0.5 w/w% of Lanthanum and La-1.5% contains a 1.5 w/w%. Due to its lower La(III) content, La-0.5% developed smaller and well-dispersed clusters, which affected lesser its surface area ( $S_{\text{BET}} = 895 \text{ m}^2 \text{ g}^{-1}$ ) and pore volume ( $V_{\text{TOT}} = 0.438 \text{ cm}^3 \text{ g}^{-1}$ ) compared to those of the pristine carbon ( $S_{\text{BET}} = 905 \text{ m}^2 \text{ g}^{-1}$  and  $V_{\text{TOT}} = 0.447 \text{ cm}^3 \text{ g}^{-1}$ ). On the other hand, La-1.5% developed bigger clusters, which decreased these same parameters more significantly ( $S_{\text{BET}} = 802 \text{ m}^2 \text{ g}^{-1}$  and  $V_{\text{TOT}} = 0.396 \text{ cm}^3 \text{ g}^{-1}$ ). The formation of La(III) clusters provided terminal hydroxyls to the activated carbon surface, which not only increased in number as a function of increasing the La(III) content in the impregnation solution, but also increased the oxidation degree of the surface. These terminal hydroxyls presented a Lewis-acid character, i.e., they can deprotonate at neutral and alkaline pH solutions, for which they changed the net surface charge to negative values. This was directly observed in the acidification of the points of zero charge and the increase of the potentials of zero charge to more positive values.

It was also previously observed that the interaction towards fluoride during both adsorption and electrosorption experiments was favored by the presence of Lanthanum hydroxyls, and for this reason La-0.5% increased more its fluoride removal due to a synergistic effect of chemisorption (by the presence of La(III) clusters) and of electrostatic interactions (by the polarization). This was attributed to its low potential of zero charge ( $E_{\text{PZC}}$ ) of only 0.1 V above that of the pristine carbon, while La-1.5% was 0.45 V above the  $E_{\text{PZC}}$  of the latter. For this, La-0.5% needed lower energy to change its surface excess and start electrosorbing anions, which is in excellent agreement with the amphoteric Donnan model [62,178]. In contrast, La-1.5% possesses a higher number of sorption sites than La-0.5%, which was observed in a marked increase in its adsorption capacity without polarizing. Nevertheless, this carbon barely increased its removal capacity when polarized. For this, most interactions towards fluoride must be related to its chemisorption by the La(III) clusters [36].

The materials were further characterized using electrochemical impedance spectroscopy. Figure 4.2a and 4.2b present the Nyquist and Bode plots, respectively, of the modified carbons (La-0.5% and La-1.5%) in 0.1 M NaF, which are similar to others reported for comparable systems [49,222,223]. The pristine activated carbon without lanthanum (GAC) was added to the graphs for further comparison. Regardless the content of lanthanum, the Nyquist spectra showed a well-defined flat capacitive loop at high frequencies. Then, as the frequency decreased, the impedance responses describe the beginning of a second inconclusive loop, alluding the presence of an additional time constant. From a qualitatively analysis of Figure 1a, it is possible to observe that the Nyquist diagrams for GAC and La-

0.5% had a similar behavior, i.e., the electrical nature of the substrate was not significantly modified at a low La(III) content.

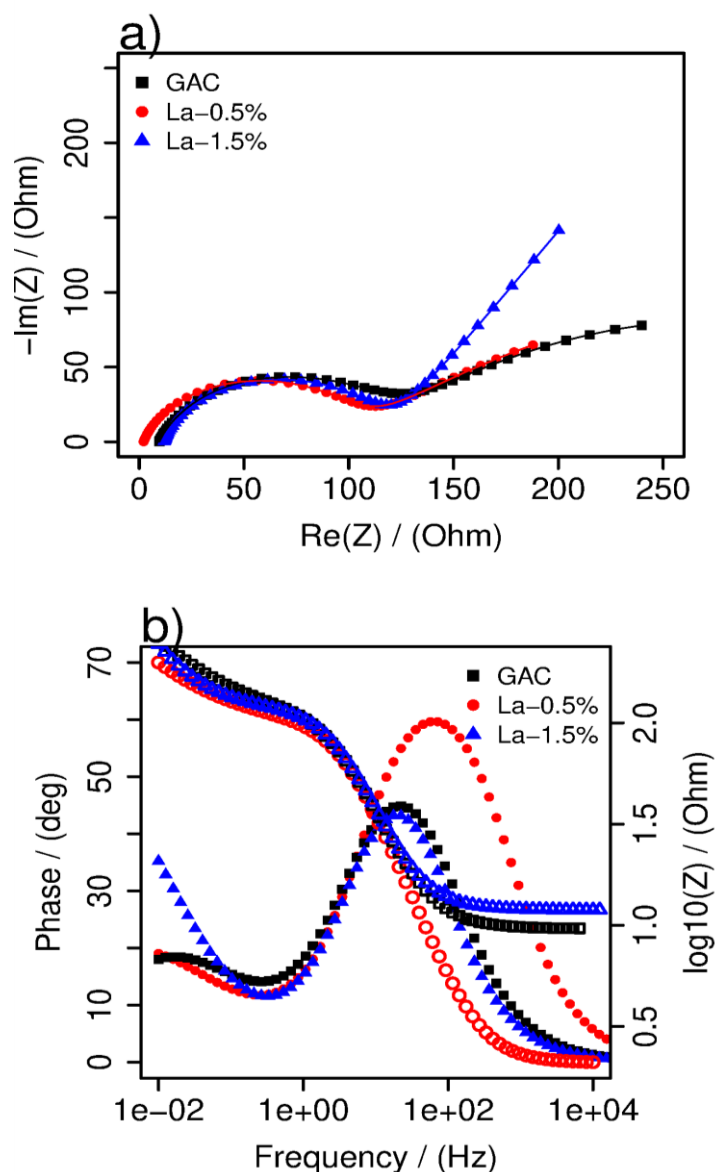


Figure 4.2. Electrochemical impedance spectroscopy at the open circuit potential of the studied activated carbons: a) Nyquist plots and b) Bode plots in 0.1 M NaF ( $f_0 = 10$  kHz,  $f_f = 10$  mHz,  $M = 50$  mg,  $V = 50$  mL,  $E_{amp} = 10$  mV, Ag/AgCl/3M NaCl as reference electrode, SSM as counter electrode). For the Nyquist plots, the fitting model is represented by the continuous lines over the experimental data points.

Accordingly, an equivalent circuit (Figure 4.3) was proposed to develop a quantitative analysis of each measured spectra. The equivalent circuit presents the  $R_s$  in series coupled with two non-ideal capacitances of the double layer (CPE1 and CPE2 associated with the

exponents  $n_1$  and  $n_2$ , respectively) and one or two charge-transfer resistances ( $R_{ct1}$  and  $R_{ct2}$ ), depending on the electrode. The obtained results are shown in Table 4.1.

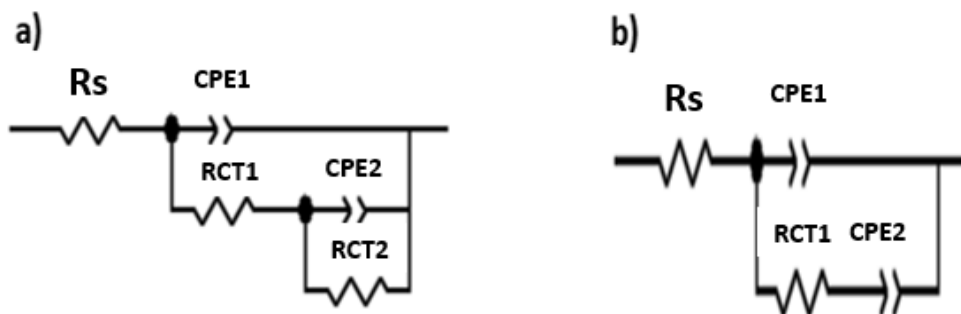


Figure 4.3. Equivalent circuits used to fit the electrodes in a 0.1 M NaF solution for a) the pristine carbon and La-0.5% and b) La-1.5%.  $R_s$ : resistance of the electrolyte, CPE are capacitances of the electrical double-layer and  $R_{ct}$  correspond to charge-transfer resistances.

Table 4.1. Electrical parameters obtained from the fitting of the equivalent circuits for each electrode in 0.1 M NaF.

Electrode	$R_s$ ( $\Omega$ )	$R_{ct1}$ ( $\Omega$ )	$R_{ct2}$ ( $\Omega$ )	CPE1 ( $\Omega s^{-(1-n)}$ )	$n_1$	CPE2 ( $\Omega s^{-(1-n)}$ )	$n_2$
GAC	9.62	113.6	319	$6 \times 10^{-4}$	0.80	$2.41 \times 10^{-2}$	0.59
La-0.5%	2.89	103.2	455.5	$4.76 \times 10^{-4}$	0.83	$3.31 \times 10^{-2}$	0.52
La-1.5%	11.91	107.5	---	$5.42 \times 10^{-4}$	0.83	$3.77 \times 10^{-2}$	0.66

First-of-all, the lowest value of the real component obtained at the highest frequency measured (10 kHz) is associated with a serial resistance,  $R_s$ , that involves the resistances either of the electrode or the electrolyte. Since in all cases, the concentration of the electrolyte remains constant, the observed changes in this value must be inversely related to the conductivity of each electrode. As can be observed, La-0.5% presented the lowest value (2.89  $\Omega$ ), followed by GAC (9.62  $\Omega$ ) and La-1.5% (11.91  $\Omega$ ), for which La-0.5% presented higher electrical conductivity among the electrodes, as was observed in the previous chapter and resumed above [178]. This is also in good agreement with the signals from the Bode diagrams at high frequencies (Figure 1b), in which the phase angle shift and the lowest impedance magnitude signal was observed for La-0.5%, followed by GAC and La-1.5%.

The impedance data showed the presence of one charge-transfer resistance for La-1.5% ( $R_{ct1} = 107.5 \Omega$ ), while GAC and La-0.5% presented two,  $R_{ct1}$  (113.6 and 103.2  $\Omega$ , respectively) and  $R_{ct2}$  (319  $\Omega$  and 455.5  $\Omega$ , respectively). These charge-transfer resistances must be related to spontaneous reactions on the carbon surface. The most conventional reactions in these systems are the spontaneous oxidation of the carbon surface [104], which comprise the formation of oxygenated functionalities and even the formation of  $CO_2$  from carbon atoms [131]; another common and highly reported reaction is that of oxygen reduction [131]. From current knowledge, it seems impossible to assign a specific faradaic reaction to each  $R_{ct}$  value determined by electrochemical impedance spectroscopy.

The values of CPE1 (0.6, 0.48 and 0.54 mF, for GAC, La-0.5% and La-1.5%, respectively) were associated to the capacitance of the most external area, probably to the macropores and the stainless-steel mesh, as the values were in the same order of magnitude to those previously measured for the stainless-steel mesh alone (0.313 mF [49]). In contrast, the values of CPE2 were two orders of magnitude higher (24.1, 33.1 and 37.7 mF, for GAC, La-0.5% and La-1.5%, respectively) and were associated to the capacitance of narrower pores, as they present higher conductivity [209]. It is also worth to highlight the difference in the exponents, in which CPE1 reached typical values for non-ideal surfaces, such as porous substrates [224]. This could be attributed, first, to an heterogeneous adsorption taking place [49], which is also in good agreement with proposing that the adsorption took place in different pore-size distributions (the macropores *versus* the meso and micropores).

At the medium range of frequencies ( $\sim 1$ -100 Hz), the time for ions to enter into the narrower pores of the carbon was higher, thus increasing the values of CPE2. This signal is usually attributed to diffuse-layer resistances due to the formation of the electrical double-layer (large slope) or to limitations in the diffusion of ions in the electrolyte (small slope) [223], which is in good agreement with the  $n_2$  values of  $\sim 0.5$ . As can be observed, La-1.5% presented a more positive and shorter slope segment, while it also presented the highest value of  $n_2$  and it could translate as a less resistive (restrictive) mass-transport for this carbon. In contrast, the pristine carbon and La-0.5% presented a very similar slope and behavior and, consequently, similar values of  $n_2$ . As the transport through the micropores is more restrictive. This is also in good agreement with the similarities observed in the micropore content for GAC and La-0.5%.

The electrodes were also further characterized by electrochemical impedance spectroscopy (Figure 4.2c and 4.2d) in a 5 ppm  $F^-$  solution (the working solution). The equivalent circuit (Figure 4.5) and the fitting parameters (Table 4.2) of all electrodes showed marked increases in the values of the impedances. This was due to a decrease in the ionic strength of the electrolyte for this set of impedance spectra, from 0.1 M to 0.263 mM NaF, which increases the resistance of the solution. The circuit presented the same components: an  $R_s$  in series with non-ideal capacitances of the double-layer (CPE1 and CPE2 associated with

the exponents  $n_1$  and  $n_2$ , respectively), with a couple of charge-transfer resistances ( $R_{ct1}$  and  $R_{ct2}$ ).

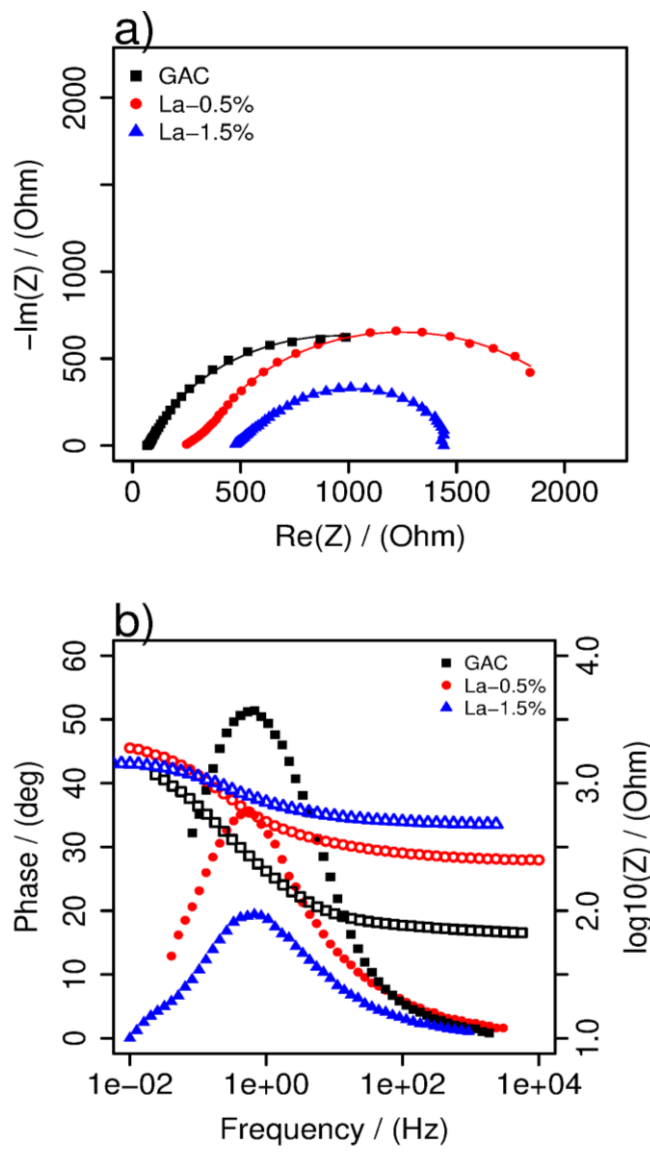


Figure 4.4. Electrochemical impedance spectroscopy at the open circuit potential of the studied activated carbons: a) Nyquist plots and b) Bode plots in 5 ppm  $F^-$  or 0.263 mM NaF ( $f_0 = 10$  kHz,  $f_f = 10$  mHz,  $M = 50$  mg,  $V = 50$  mL,  $E_{amp} = 10$  mV, Ag/AgCl/3M NaCl as reference electrode, SSM as counter electrode). For the Nyquist plots, the fitting model is represented by the continuous lines over the experimental data points.

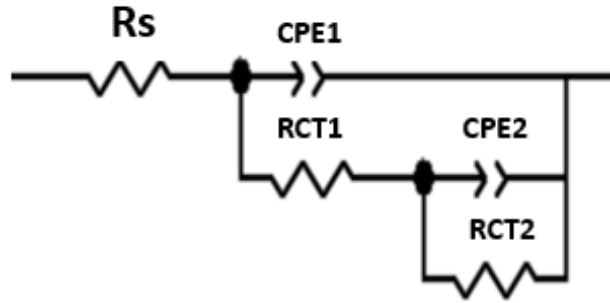


Figure 4.5. Equivalent circuits used to fit the electrodes in a 5 ppm  $F^-$  solution.  $R_s$ : resistance of the electrolyte, CPE are capacitances of the electrical double-layer and  $R_{ct}$  correspond to charge-transfer resistances.

Table 4.2. Values of resistance and capacitances obtained from the equivalent circuits for each electrode in a 5 ppm  $F^-$  solution.

Electrode	$R_s$ ( $\Omega$ )	$R_{ct1}$ ( $\Omega$ )	$R_{ct2}$ ( $\Omega$ )	CPE1 ( $\Omega s^{-(1-n)}$ )	$n_1$	CPE2 ( $\Omega s^{-(1-n)}$ )	$n_2$
GAC	67	15.07	1769	$2.72 \times 10^{-4}$	0.78	$6.55 \times 10^{-4}$	0.79
La-0.5%	250	180.5	1767	$2.56 \times 10^{-4}$	0.69	$3.15 \times 10^{-4}$	0.84
La-1.5%	476	222.4	794.1	$2.77 \times 10^{-4}$	0.73	$3.92 \times 10^{-4}$	0.80

Regarding the component  $R_s$ , the lowest value was obtained by the pristine carbon (67  $\Omega$ ), followed by La-0.5% (250  $\Omega$ ) and La-1.5% (476  $\Omega$ ), for which La-1.5% presents the lowest electrical conductivity, compared to the information obtained from the concentrated electrolyte. This was also observed in the Bode modulus diagram at high frequencies (Figure 1d). The elements CPE1 and CPE2 are related to non-ideal capacitances of the electrical double-layer and again showed a higher value for CPE2, although the values of CPE1 and CPE2 were in the same order of magnitude. This could be related to the overlapping of the micro and mesopores in this experimental conditions [113] (EDL thickness = 18.67 nm in  $C_0 = 0.263$  mM for a 1:1 electrolyte,  $T = 25$   $^{\circ}C$  and  $\epsilon_{water} = 78.54$  [84]), which reduced the available pore space and the value of the capacitance.

For the charge transfer resistances, the values of  $R_{ct1}$  increased as a function of increasing the La(III) content (GAC = 15.1  $\Omega$ , La-0.5% = 180.5  $\Omega$  and La-1.5% = 222.4  $\Omega$ ), while  $R_{ct2}$  was only substantially smaller for La-1.5% (794.1  $\Omega$ ), but very similar between GAC

(1769  $\Omega$ ) and La-0.5% (1767  $\Omega$ ). Then,  $R_{ct1}$  increased as a function of decreasing the electrical conductivity of the electrodes in this diluted media. The similarities in the  $R_{ct2}$  values between GAC and La-0.5% could be directly related to their higher pore volume, i.e., to a higher and probably more available surface of these electrode. In this same sense, La-1.5% presented a lower available polarizable surface to induce the charge-transfer reaction due to its occluded pore space, which explains its much lower value.

Figure 4.6 shows the capacitance of both modified carbons at different applied potentials obtained from the second set of impedance in a 5 ppm  $F^-$  solution to identify the potentials of zero charge ( $E_{PZC}$ ), which is marked with asterisks in the respective Figure. The modified carbons La-0.5% and La-1.5% presented a  $E_{PZC}$  of 0.2 and 0.55 V vs. Ag/AgCl/3M NaCl (or  $\sim 0.5$  and  $\sim 0.85$  V<sub>cell</sub>), respectively, which was more positive than that of the pristine activated carbon, of 0 V vs. Ag/AgCl/3M NaCl [178]. The  $E_{PZC}$  is highly correlated with the surface chemistry of the electrodes [49,50,111,178], for which the  $E_{PZC}$  values differ as a function of increasing the La(III) content. The La(III) clusters provided terminal hydroxyls that deprotonated at the working solution, increasing the input of negative charges and thus, changed the net charge of the modified carbons to negative values, as was previously corroborated by determining the points of zero charge of all electrodes [178]. According to the classical double-layer theory, the adsorption of anions is highly favorable at more positive potentials than both identified  $E_{PZC}$  values [84], for which, 1.2 V<sub>cell</sub> was selected as the polarization potential for the electrosorption kinetics.

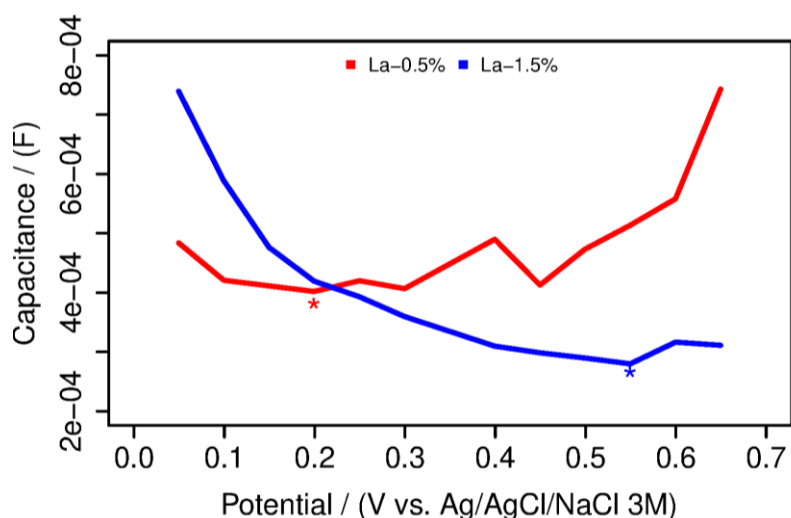


Figure 4.6. Potentials of zero charge in 5 ppm or 0.263 mM  $F^-$  ( $f = 100$  mHz,  $M = 50$  mg,  $V = 50$  mL,  $E_{amp} = 10$  mV, Ag/AgCl/3M NaCl as reference electrode, SSM as counter electrode). The asterisks denote the potential of zero charge for each electrode.

To close this section, the information from the diluted electrolyte adjusted better to the results of the electrosorption kinetics and most characterization data obtained in the previous chapter. It is more useful to obtain information in the working solution. Then,

characterization techniques in diluted media could be more relevant to predict the electrosorption performance of electrodes, as has been already implemented for the potentials of zero charge [104]. Finally, there are other implications, such as those related to personal safety (if working with more toxic pollutants, such as arsenic or chromium) and to waste management and disposal.

### ***4.3.2 Electrosorption kinetics***

#### ***4.3.2.1 Binary solutions***

The black lines in Figure 4.7a and 4.7b show the electrosorption kinetics in the presence of fluoride alone at 1.2 V<sub>cell</sub> in a 0.263 mM (~5 ppm) F<sup>-</sup> solution for the modified carbons La-0.5% and La-1.5%, respectively. The response is a function of the La(III) content in the matrices, in which higher content promoted a higher and faster fluoride removal. The initial fluoride concentration decreased 15% ( $q = 19.25 \mu\text{mol g}^{-1}$ ) and 33% ( $q = 32.85 \mu\text{mol g}^{-1}$ ) for La-0.5% and La-1.5%, for which La-1.5% removed 2.2 times more fluoride than La-0.5% at the equilibrium. Table 4.3 shows the removal velocities of fluoride and of fluoride in the presence of each competing anion. Again, the velocity of La-1.5% towards fluoride alone ( $1.82 \mu\text{mol g}^{-1} \text{min}^{-1}$ ) was higher compared to that of La-0.5% ( $1.223 \mu\text{mol g}^{-1} \text{min}^{-1}$ ), although it is only 1.5 times higher, compared to the ratio of capacities computed above. This is a direct evidence of the contribution of the electrical stimulus and subsequent enhancement of the mass-transport by migration effects to increase the removal velocity of the more conductive carbon La-0.5%.



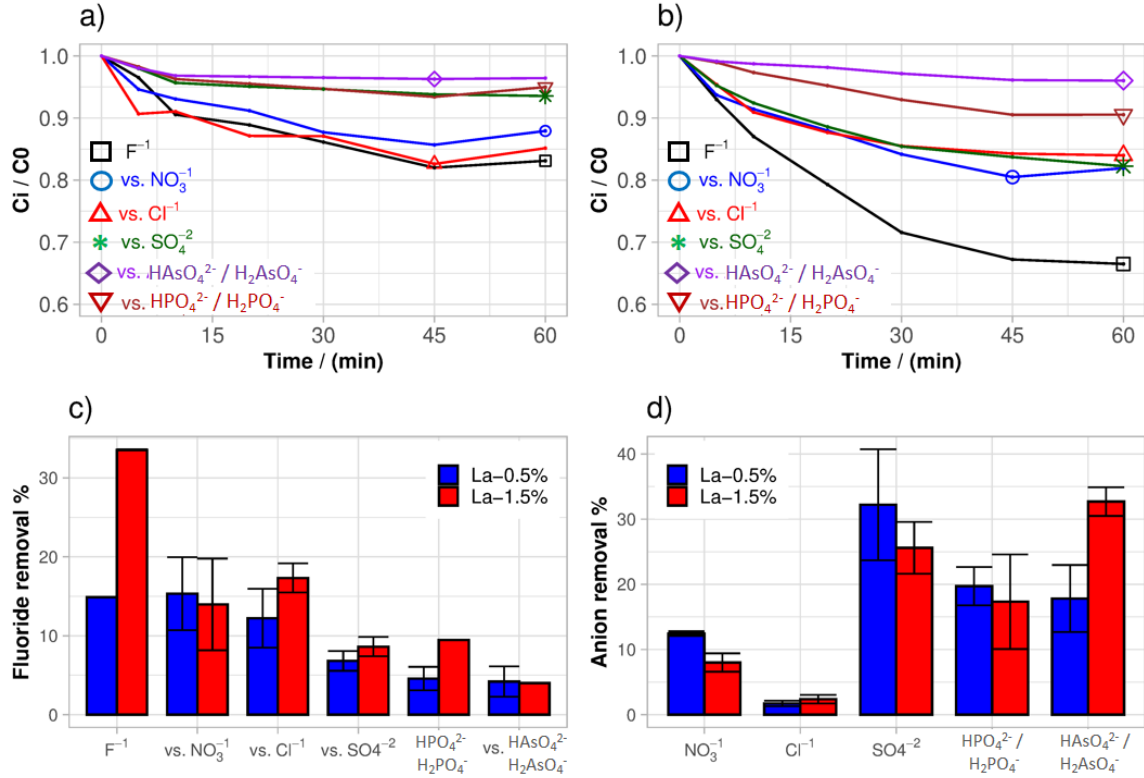


Figure 4.7. Electrosorption kinetics of fluoride and of binary solutions comprising fluoride in the presence of several competing anions of environmental relevance (fluoride vs. anion) for a) La-0.5% and b) La-1.5%. c) Obtained capacities of fluoride electrosorption kinetics for each competing anion and for each carbon at  $t = 60$  min. d) Obtained capacities for each competing anion for each carbon at  $t = 60$  min ( $C_0 = 0.263$  mM of each anion,  $M = 50$  mg,  $V = 50$  mL,  $E_{cell} = 1.2$  V,  $pH_0 = \sim 7$ ,  $T = 25$  °C and 120-130 rpm, SSM as counter electrode).

Table 3. Electrosorption velocities of fluoride and of fluoride in the presence of competing anions of environmental relevance (binary solutions) for both carbons (at  $t = 10$  min, in  $\mu\text{mol g}^{-1} \text{min}^{-1}$ ).

Kinetics	La-0.5%	La-1.5%
$F^-$	1.223	1.820
$F^-$ vs. $Cl^-$	1.277	1.240
$F^-$ vs. $NO_3^-$	0.940	1.203
$F^-$ vs. $SO_4^{2-}$	0.525	0.953
$F^-$ vs. $HAsO_4^{2-}/H_2AsO_4^-$	0.410	0.158
$F^-$ vs. $HPO_4^{2-}/H_2PO_4^-$	0.492	0.385

Regarding the anion competition and continuing with the analysis of the fluoride removal velocities (Table 4.3), the presence of chloride did not affect the removal velocity of fluoride of the electrode La-0.5% ( $1.277 \mu\text{mol g}^{-1} \text{min}^{-1}$ ), while La-1.5% decreased 32% its velocity ( $1.24 \mu\text{mol g}^{-1} \text{min}^{-1}$ ), compared to evaluating fluoride alone. Nitrate promoted a similar behavior than chloride for La-1.5%, although the velocity of La-0.5% decreased 25% ( $0.94 \mu\text{mol g}^{-1} \text{min}^{-1}$ ). Finally, the divalent species, sulfate, phosphate and arsenate, decreased more than half the removal velocity, compared to that when evaluating fluoride alone. From these anions, arsenate produced the lowest decreases in velocities of 66% ( $0.41 \mu\text{mol g}^{-1} \text{min}^{-1}$ ) and 91% ( $0.158 \mu\text{mol g}^{-1} \text{min}^{-1}$ ) for La-0.5% and La-1.5%, respectively.

Figure 4.7c states the global comparison of the removal percentages for each competing anion and for each carbon. As can be observed, nitrate and chloride practically did not compete with fluoride for the modified carbon La-0.5% as its fluoride removal was not significantly affected by the presence of these anions. Nevertheless, the other anions decreased the fluoride removal for this same modified carbon to only 6.8, 4.6 and 4.2% in the presence of sulfate, phosphate, and arsenate, respectively. On the other hand, the modified carbon La-1.5% presented a significant decrease in its fluoride removal by all competing anions in these binary solutions, even in the presence of chloride and nitrate. These particular anions (chloride and nitrate) decreased its removal to 13.9% and 17.3%, compared to its 33% performance in the presence of fluoride alone. As with La-0.5%, the species with higher charge promoted higher competition and decreased its removal to 13.6%, 9.5% and 4% in the presence of sulfate, phosphate and arsenate, respectively.

As can be observed, there are no significant differences in the fluoride removal between both electrodes when competing with most anions, except for nitrate and phosphate. All these results show that La-1.5% was less selective towards fluoride. As La-0.5% presented both mechanisms (chemisorption by the La(III) clusters and electrosorption by its good electrical conductivity), it was less affected by the presence of competing anions, compared to La-1.5%, which removes fluoride mostly by chemisorption.

Figure 4.7d shows the removal of each of the competing anions during the kinetics. Here it is reiterated that the species with higher electrostatic charge were removed more, compared to monovalent species. As can be observed, the anion with the lowest removal was chloride, attaining only 3% at most, for which chloride can be considered an indifferent anion to both chemisorption and physisorption processes and for both modified carbons. On the other hand, even when chloride was indifferent, its presence decreased the electrosorption performance for fluoride. The removal of nitrate was much higher than that of chloride and with significant differences between both carbons. The removal of the divalent species was higher for both carbons, which correlated adequately with Figure 4.7c, i.e., the removal of these species was far more favorable. Charge seems to be the most important parameter to explain the results, which is in good agreement with other reports

[141,225–227]. A more complete discussion on several parameters that are associated to selectivity will be addressed upon next.

Table 4.4 presents different thermodynamic values associated to the selective removal of anions. Fluoride presents the higher size and stronger solvation energy of the monovalent anions. Then, as the dynamics of an ion in solution depends on the number of waters clinging to it, fluoride presents the lowest diffusion coefficient, ion mobility and ionic conductivity, compared to nitrate and chloride (Table 4). Slight differences in these same parameters can be appreciated between chloride and nitrate due to differences in their hydration energy, even when their hydrated radii are very similar.

*Table 4.4. Thermodynamic values of interest of the studied anions and of sodium cation.*

Ion	Hydrated radius (nm)	Hydration energy (KJ mol <sup>-1</sup> )	Ionic conductivity (S cm <sup>2</sup> mol <sup>-1</sup> )	Ion Mobility (10 <sup>-4</sup> cm <sup>2</sup> V <sup>-1</sup> S <sup>-1</sup> )	Diffusion coefficient (10 <sup>-5</sup> cm <sup>2</sup> s <sup>-1</sup> )
Na <sup>+</sup>	0.358	-409	50.11	5.19	1.334
F <sup>-</sup>	0.352	-515	55.4	5.7	1.475
Cl <sup>-</sup>	0.332	-381	76.31	7.91	3.032
NO <sub>3</sub> <sup>-</sup>	0.335	-314	71.42	7.14	1.902
SO <sub>4</sub> <sup>-2</sup>	0.379	-1059	160	16.5	2.13
HAsO <sub>4</sub> <sup>-2</sup>	0.22	---	34	---	0.905
HPO <sub>4</sub> <sup>-2</sup>	0.327	---	114	---	1.518
OH <sup>-</sup>	0.30	-460	198	20.5	5.273

For the specific case of porous electrodes, ion transport (and the removal capacity) mostly correlates to the hydration energy, as less energetically hydrated species may detach from their hydration waters, drift faster and penetrate easier into a pore [98,228,229]. This information cannot be directly abstracted from the hydrated radii. Hydration also promotes the electrosorption (retention) of these monovalent anions at different distances from an electrically polarized surface. Nitrate and chloride can be allocated at closer distances and can even specifically adsorb to the electrode surface [46]. On the other hand, the specific

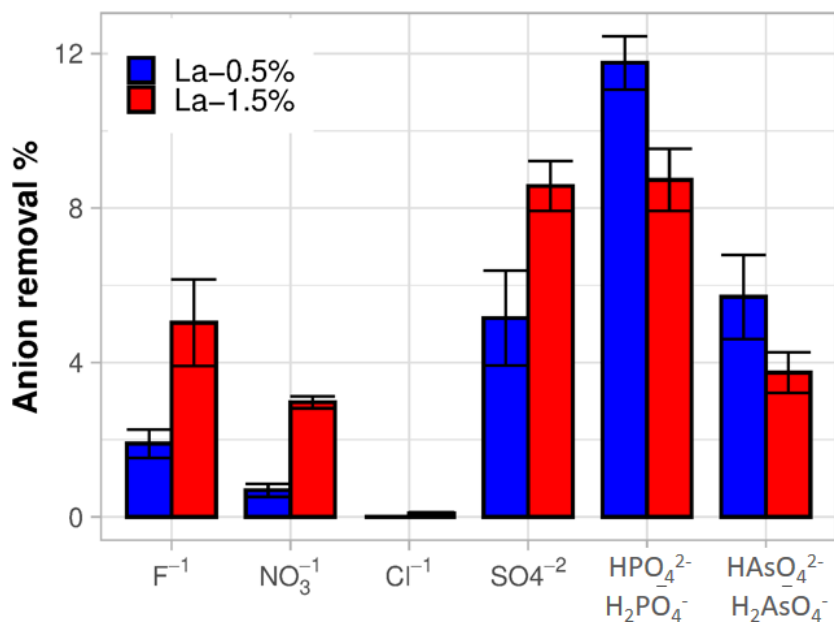
adsorption of fluoride is much less viable [95] as it is retained at longer distances. This could explain the lack of competition between the monovalent anions and fluoride. For La-1.5%, this carbon presented a lower polarizable surface, for which the main mechanism to retain ions was reduced to their chemisorption to La(III), increasing the competition and decreasing the removal of fluoride.

In this regard, the competition between the studied monovalent anions ( $F^-$ ,  $NO_3^-$  and  $Cl^-$ ) has been widely reported with different outcomes and explanations in porous electrodes for capacitive processes. Some studies have observed a clear and marked competition between the monovalent anions [47,143–145], while other works found that were indifferent [176,220]. The authors of this work consider that both situations are plausible, as all evaluated electrodes and conditions are different among these studies. As a matter of fact, both results were obtained in this study: the monovalent anions were indifferent and did not affect the fluoride removal for La-0.5%, while decreased the fluoride removal by half for La-1.5%.

More competition by the divalent anions was expected, not only due to their higher electrostatic interaction towards the polarized surface, but also due to their higher transport (diffusion coefficients, ionic conductivities and ionic mobilities) compared to that of fluoride. This correlates adequately with other studies in which the charge was the most predominant factor [141,225–227].

#### ***4.3.2.2 Complex mixture involving all anions***

Figure 4.8 shows the kinetics involving all the evaluated anions in one experimental set, all present also in equimolar initial concentrations ( $C_0 = 0.263$  mM  $F^-$ ,  $0.263$  mM of  $Cl^-$ ,  $0.263$  mM  $NO_3^-$ ,  $0.263$  mM  $SO_4^{2-}$ ,  $0.263$  mM  $PO_4^{x-}$  and  $0.263$  mM  $AsO_4^{x-}$ ). Here, the electrosorption removal of fluoride decreased to only ~2% and ~5% by La-0.5% and La-1.5%, respectively. This is the lowest obtained removal for the electrode La-0.5%, while the removal of La-1.5% was insignificantly different from the removal observed when competing with arsenate.



\*Figure 4.8. Electrosorption removal of each anion in the complex mixture (at  $t = 60$  min) in equimolar initial concentrations by La-0.5% and La-1.5% ( $C_0 = 0.263$  mM of each anion,  $M = 50$  mg,  $V = 50$  mL,  $E_{cell} = 1.2$  V,  $pH_0 = \sim 7$ ,  $T = 25$  °C and 120-130 rpm, SSM as counter electrode).

The highest removal achieved by the electrode La-0.5% was towards phosphate (11.7%), which has a high charge and the smallest hydrated radius (Table 4.4). Sulfate (5.1%) and arsenate (5.7%) presented a similar removal, while the monovalent anions presented a much lower removal, being that of fluoride the highest. For La-1.5%, sulfate (8.5%) and phosphate (8.7%) presented the highest removal, i.e., the anions with the highest ionic conductivity (Table 4.4). This could imply that these fastest anions reached sooner to the carbon surface. The removal of arsenate (3.8%) was somewhat similar to that of fluoride and nitrate for this same carbon. In this experimental set-up, charge again seems more relevant compared to other parameters (Table 4.4).

It is worth mentioning to close this section of the electrosorption kinetics with some data related to the stability of the electrosorption cell. First, iron was not detected by ICP, for which the current collector (the stainless-steel mesh) was not oxidized during the polarization process. On the other hand, Lanthanum, was only detected in significant amounts in the samples containing phosphate, but only for La-1.5%, for which lanthanum is not being expelled at most of the studied conditions.

#### 4.3.2.3 pH and conductivity

Figure 4.9a and 4.9b show measurements of pH during the electrosorption kinetics for the evaluated carbons. As can be observed, both carbons showed an increase in the pH of the solution during the electrosorption process. This was attributed to the chemisorption

mechanism occurring during both the adsorption [36] and electrosorption [50] processes, in which some of the exposed hydroxyls from the La(III) clusters are exchanged by anionic adsorbates in the solution.

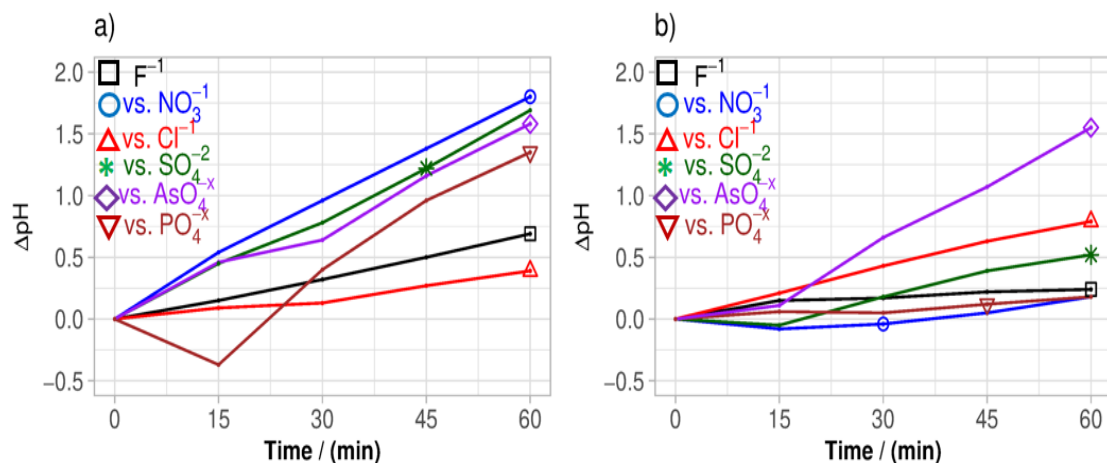


Figure 4.9. Measured changes in the pH (y-axis in different scale) during the electrosorption kinetics of binary solutions for a) La-0.5% and b) La-1.5%. ( $C_0 = 0.263$  mM of each anion,  $M = 50$  mg,  $V = 50$  mL,  $E_{cell} = 1.2$  V,  $pH_0 = \sim 7$ ,  $T = 25$  °C and 120-130 rpm, SSM as counter electrode). Due to space, phosphate and arsenate species are represented as  $PO_4^{x-}$  and  $AsO_4^{x-}$ .

On the other hand, the conductivity measurements (Figure 4.10a and 4.10b) did not vary for most samples, probably due to the low molar concentrations evaluated. As an example,  $100 \mu\text{S cm}^{-1}$  corresponds to the lowest calibration standard of the conductimeter ( $\sim 0.8$  mM NaCl), which is higher than the concentration of the binary mixtures (0.526 mM). The electrosorption kinetics for fluoride alone presented the lowest conductivity. The addition of competing anions increased at least two-fold the conductivity of the solution, which is in good agreement with the two-fold increase in molar concentration of ionic species and the solution with sulfate presented the highest conductivity among all binary solutions.

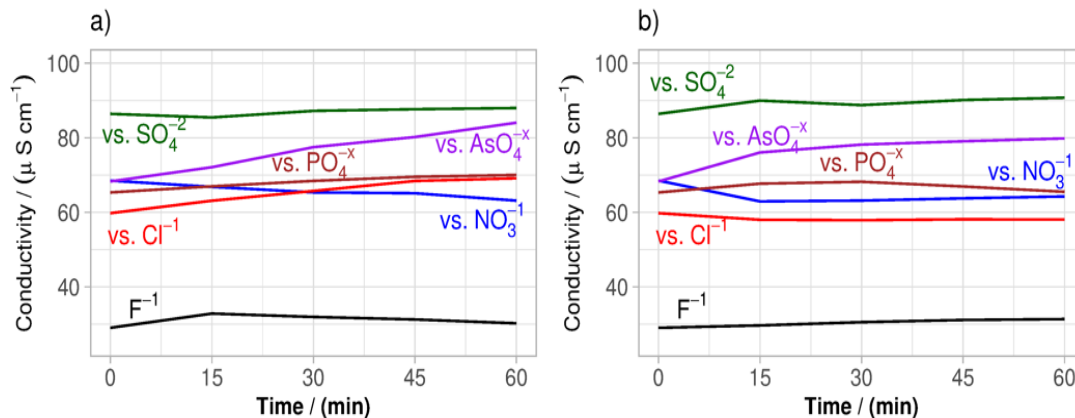


Figure 4.10. Measured changes in the conductivity during the electroadsorption kinetics of binary solutions for a) La-0.5% and b) La-1.5% ( $C_0 = 0.263$  mM of each anion,  $M = 50$  mg,  $V = 50$  mL,  $E_{cell} = 1.2$  V,  $pH_0 = \sim 7$ ,  $T = 25$  °C and 120-130 rpm, SSM as counter electrode). Due to space, phosphate and arsenate species are represented as  $PO_4^{x-}$  and  $AsO_4^{x-}$

#### 4.4 Conclusions

Electrochemical impedance spectroscopy is mostly performed in concentrated electrolytes and several aspects of the spectra have been widely reported and identified to date. Here it is worth to highlight the information that derived from contrasting the same electrolyte in different concentrations (0.1 M and 0.263 mM NaF), in which the information obtained from the diluted electrolyte correlated at a major degree with the electroadsorption performance of the evaluated electrodes.

Fluoride removal when not competing with other anions reached 15% and 33% in the studied conditions, which is relevant considering the low initial concentration of adsorbate. The presence of chloride and nitrate in equimolar initial concentrations did not significantly affect the removal of fluoride for La-0.5%, but was decreased by half for La-1.5%. This was explained considering that La-0.5% presented a mixture of adsorption (well-dispersed La(III) clusters) and electroadsorption (electrically polarizable surface) sites for allocating the monovalent anions at different distances and sites. The divalent anions presented higher competition towards fluoride, by both electrostatic interactions and chemisorption to the La(III) cluster.

Here it was observed that charge was one predominant parameter to understand and explain the obtained results of selectivity between the evaluated anions. Hydrated radii also provided very useful information and has been extensively used for these purposes, although it presents some limitations. For this, there have been several efforts to correlate

the results with the hydration energies of ions instead. Finally, evaluating selectivity using equimolar initial concentrations in binary solutions allowed us to discern the anions that competed the most during fluoride electrosorption by the two modified carbon electrodes, which was different from the results obtained by the complex mixture.



## Chapter five: Global discussion

Electrosorption is a process for water treatment and it has been widely applied specifically for desalination processes. The most recurrent electrode used for capacitive processes are those that comprise carbon-based materials, especially those of activated carbon. Activated carbons are characterized for their porous and highly complex matrix, which contrasts to other more simple electrode materials (planar, non-porous and/or surfaces with an ordered porosity). As several research groups have addressed electrosorption in a conventional and monodisciplinary form, this has led not only to several dubious findings and conclusions, but also to a lack of proper discussion and understanding of the electrosorption cell, in general.

As was observed in this work, the electrical polarization of the commercial activated carbons enhanced both the removal capacity and rate of fluoride, obtaining increases of ~6 times, compared to the capacity obtained by conventional adsorption. In addition, the electrodes presented a desorption step by polarizing at negative potentials that was efficient (the regeneration ranged from ~60% to >90%, depending on the studied carbon), easy to implement (desorption was performed *in situ*), economic (without using concentrated solutions nor any other reagent) and fast (less than ~60 minutes).

This thesis dedicated some experiments to understand the effect of the polarization potential in the performance of electrodes. , mostly limited to  $1.23 V_{\text{cell}}$ . As was discussed, even when water electrolysis is thermodynamically viable, it could still present some kinetic limitations. There are indeed electrosorption systems that polarized beyond this potential and did not observe a significant increase in the removal capacity and rate of their system, while other systems did increase their performance at even much higher potentials, of up to  $2 V_{\text{cell}}$ .

The surface modification of activated carbon matrices with metals has also proven to increase the performance of the pristine adsorbent, especially towards highly polar species, such as fluoride. For the specific case of the studied electrodes, La(III) is an excellent modifying agent due to its (Lewis) acid hardness, which provides excellent affinity towards fluoride, a hard Lewis base. In addition, the oxyhydroxides of this metal increased the polarity of the surface, which accelerated the wettability of the surface, among other benefits. An specific effort was made to correlate most of the characterization data (textural, physicochemical and electrochemical), as the impregnation of La(III) had a pronounce effect in all this properties.

Few electrosorption approaches have truly understood the correlation between the surface chemistry and the electrical properties of activated carbons. Regarding the surface chemistry and surface charges, the addition of La(III) promoted the acidification of the

point of zero charge and the anodization of the potential of zero charge. This work is also a pioneer in understanding and explaining the effect of the surface charges in the surface potential and thus, in the outer potential. The outer potential should also be in correct agreement with the applied polarization or the inner potential, which should be a more formal and correct understanding of the amphoteric Donnan model.

Regarding the electrosorption performance, the main hypothesis of this thesis was corroborated and accepted, as the La(III) addition and the electric polarization were demonstrated to be synergistic in the global fluoride removal of the matrices, although some conditions arose. In this aspect, the hybrid electrodes presented several effects in fluoride electrosorption as a function of the La(III) loading on the carbon, the polarization profile and the applied potential value. As was observed, La-0.5% could be polarized from the beginning or after fluoride conventional adsorption and reach the same concentration, although its polarization from the beginning increased its removal rate. This is in excellent agreement with the results of most published works, in which there has not been observed marked differences between both profiles. La-1.5% presented a faster and higher fluoride removal by conventional adsorption (without polarizing), but its polarization from the beginning did not present a significant effect in both fluoride removal capacity and rate. Nevertheless, its performance could be further increased by its electrical polarization after fluoride adsorption.

Previous discussion is of interest as, first-of-all, there are practically no reports on contrasting both polarization profiles, for which it has not been previously reported and thus, evaluated. For this, an extensive discussion and evidences were displayed to provide evidence of the existence of the electrical blockage of the pores. The electrical blockage of the narrower pores can also be diminished by understanding the mechanisms taking place at the electrode-electrolyte interface, as was addressed when studying the polarization profile. This was tackled by conventional *in situ* techniques, the point and potential of zero charge. After this finding, it was concluded that the electrosorption performance could be enhanced by selecting the most adequate polarization profile, specifically for electrodes that undergo significant changes in their surface charges after the adsorption equilibrium.

This study also centered in evaluating the current profiles obtained during the electrosorption kinetics. The current profiles provide interesting information about the electrodes, such as the available polarizable surface, its electrical conductivity and its charging process in the studied electrolyte. Valuable information was also abstracted from linear sweep voltammetry about the polarization window of each electrode. Future works should make an effort to correlate this data with other, for example, the current and charge profile during electrosorption, as current increases not always correlate by both methods (potentiodynamic and potentiostatic polarization). All the mentioned techniques and analysis are also valuable as they are performed in the working electrolyte, compared to other techniques performed in concentrated solutions.

The last part to discuss in this section is related to the study of selectivity. The approach used based in equimolar initial concentrations has been oddly observed in other reports. Nevertheless, this approach could be easier to compare to different systems (electrodes, adsorbates and concentrations) and more useful information could be abstracted from this experimental set-up.

## Final conclusions

The hypothesis of the thesis was confirmed, as the electric polarization of the activated carbons increased the fluoride removal capacity and rate of the adsorbents (with and without lanthanum). For the specific case of the unmodified activated carbons, the effect of the pore-size distribution was isolated from other variables. The presence of mesopores increased the mass-transport of fluoride and aided to allocate the electrical double-layers, for which the bituminous carbon performed better as an electrode. On the other hand, the polarization limit of the cells was not limited to that of water electrolysis reaction. Here, a thermodynamic explanation was included to justify the assumption that water electrolysis is probably not occurring in the system.

The successful impregnation of the bituminous carbon with La(III) promoted the formation of clusters of different sizes, which blocked the pores, decreased the surface area and pore volume and thus, the electrical conductivity of the modified matrices. The modified carbon with the lowest La(III) content, La-0.5%, achieved the same removal capacity independently of the polarization profile, but its polarization from the beginning increased its removal rate. La-1.5% presented a similar removal by conventional adsorption and electrosorption (polarized from the beginning), but its polarization after the adsorption equilibrium increased its removal by 50% compared to both processes individually (conventional adsorption and electrosorption polarized from the beginning). Finally, La-2.0% was unsuitable for electrosorption, due to its unstable behavior when electrically polarized.

Previous phenomenon was explained by following interfacial information related to the surface charges of the surface by *in situ* techniques and information. This was attributed to an electrical blockage of the narrower pores by the excess of negative charges from the exposed hydroxyls from the La(III) clusters. The polarization profile should become a default parameter to improve the electrosorption process in which the net surface charges of the electrodes change during the adsorption step.

The modified carbon chemisorbed fluoride by a ligand-exchange mechanism, even during its electrical polarization. Because of this chemisorption process, fluoride did not desorb after the depolarization of the electrode. The pristine carbon did release fluoride when depolarized but its performance decreased significantly after each cycle. When reversing the polarization of the electrodes at -0.5 V, fluoride desorption was attained for the modified carbon and at a much faster rate. Finally, the polarization process promoted the oxidation of the surface of both carbons.

The studies of selectivity showed a high competition mainly against the species with higher charge, although La-1.5% decreased its fluoride electrosorption performance also in the

presence of chloride and nitrate, while La-0.5% was not affected by such anions. This was explained considering that La-0.5% presents a mixture of adsorption (well-dispersed La(III) clusters) and electrosorption (electrically polarizable surface) sites for allocating the studied anions at the studied conditions.

## Perspectives

\* The optimization of La(III) addition could have been easily achieved using another impregnation technique, in which the La(III) content increases without negatively reducing the micropore:mesopore ratio. Other better modifications can include the impregnation of La(III) nanostructures by a microwave-assisted synthesis or even a cathodic protection of the micropores while impregnating.

\* Impregnate with more specific La(III) compounds or phases. The lanthanum oxide would provide much lower hydroxyls than the lanthanum hydroxide, for which the surface charges will tend to remain positive. Certain metallic oxide phases can protonate and thus increase the positive input of charges.

\* Then, the addition or a better allocation and size of the clusters that do not significantly decrease the micropores (less physical blockage) and favoring the formation of the lanthanum oxide that protonates and increases the positive surface charges (less electrical blockage) would present a highly synergistic effect in fluoride removal.

\* Regarding the effect of textures: i) an activated carbon comprising mainly mesopores; ii) activated carbons with ordered porosity and; iii) activated carbons from synthetic precursors, which present less tortuosity and higher electrical conductivity, iv) increasing the positive charges of the surface by thermal treatments in inert atmospheres, or by impregnating the surface with nitrogen-containing functional groups.

\* It has been widely addressed that hybrid membrane-capacitive electrodes present much higher and faster adsorbate removal, but also with much a higher charge-efficiency. In this cell configuration, the electrodes are spaced by anion and cathode-selective membranes at their respective electrodes. Of course, in the asymmetric cell here studied, both electrodes could be spaced by a fluoride-selective membrane. Regarding the cathode, this electrode could also comprise an alkaline activated carbon, thus increasing fluoride removal also by electrostatics.

## References

- [1] R.P. Schwarzenbach, T. Egli, T.B. Hofstetter, U. von Gunten, B. Wehrli, Global Water Pollution and Human Health, Annual Review of Environment and Resources. 35 (2010) 109–136. <https://doi.org/10.1146/annurev-environ-100809-125342>.
- [2] S.E. Manahan, Environmental Chemistry, 7th Editio, CRC Press LLC, NY, 2000.
- [3] World Health Organization, Guidelines for Drinking-Water Quality: fourth edition incorporating the first addendum, Geneva., 2017.
- [4] M.B. Cruz-Ayala, S.B. Megdal, An Overview of Managed Aquifer Recharge in Mexico and Its Legal Framework, Water. 12 (2020) 474. <https://doi.org/10.3390/w12020474>.
- [5] M. Kummu, P.J. Ward, H. De Moel, O. Varis, Is physical water scarcity a new phenomenon? Global assessment of water shortage over the last two millennia, Environmental Research Letters. 5 (2010). <https://doi.org/10.1088/1748-9326/5/3/034006>.
- [6] R.I. McDonald, P. Green, D. Balk, B.M. Fekete, C. Revenga, M. Todd, M. Montgomery, Urban growth, climate change, and freshwater availability, Proceedings of the National Academy of Sciences of the United States of America. 108 (2011) 6312–6317. <https://doi.org/10.1073/pnas.1011615108>.
- [7] A. Mashhadi, M.E. Shafiee, E.Z. Berglund, Agent-based modeling to simulate the dynamics of urban water supply: Climate, population growth, and water shortages, Sustainable Cities and Society. 28 (2017) 420–434. <https://doi.org/10.1016/j.scs.2016.10.001>.
- [8] W. Stumm, J.J. Morgan, Aquatic Chemistry: Chemical Equilibria and Rates in Natural Waters., 3rd Edition, Wiley, NY, 1970.
- [9] A.B. Cardona, J.J.R. Carrillo, M.A.H. Armienta, Elementos traza: contaminación y valores de fondo en aguas subterráneas de San Luis Potosí, SLP, México, 32 (1993) 277–286.
- [10] C. Contreras-Servín, M.G. Galindo-Mendoza, Abasto futuro de agua potable, análisis espacial y vulnerabilidad de la ciudad de San Luis Potosí, México, Revista Colombiana de Geografía. (2008) 127–137.
- [11] J.J. Carrillo-Rivera, A. Cardona, W.M. Edmunds, Use of abstraction regime and knowledge of hydrogeological conditions to control high-fluoride concentration in

abstracted groundwater: San Luis Potosí Basin, Mexico, *Journal of Hydrology*. 261 (2002) 24–47. [https://doi.org/10.1016/S0022-1694\(01\)00566-2](https://doi.org/10.1016/S0022-1694(01)00566-2).

[12] M. Tsubo, S. Walker, M. Hensley, Quantifying risk for water harvesting under semi-arid conditions: Part I. Rainfall intensity generation, *Agricultural Water Management*. 76 (2005) 77–93. <https://doi.org/10.1016/j.agwat.2005.01.008>.

[13] F. Ziadat, A. Bruggeman, T. Oweis, N. Haddad, S. Mazahreh, W. Sartawi, M. Syuof, A Participatory GIS Approach for Assessing Land Suitability for Rainwater Harvesting in an Arid Rangeland Environment, *Arid Land Research and Management*. 26 (2012) 297–311. <https://doi.org/10.1080/15324982.2012.709214>.

[14] E. Huber-Sannwald, M.R. Palacios, J.T.A. Moreno, M. Braasch, R.M.M. Peña, J.G. de A. Verduzco, K.M. Santos, Navigating challenges and opportunities of land degradation and sustainable livelihood development in dryland social-ecological systems: A case study from Mexico, *Philosophical Transactions of the Royal Society B: Biological Sciences*. 367 (2012) 3158–3177. <https://doi.org/10.1098/rstb.2011.0349>.

[15] E. Huber-Sannwald, F.T. Maestre, J.E. Herrick, J.F. Reynolds, Ecohydrological feedbacks and linkages associated with land degradation: A case study from Mexico, *Hydrological Processes*. 20 (2006) 3395–3411. <https://doi.org/10.1002/hyp.6337>.

[16] V.P. Tewari, R. Arya, Degradation of arid rangelands in Thar Desert, India: A review, 19 (2005) 1–12. <https://doi.org/10.1080/15324980590887056>.

[17] J.J. Carrillo R., M.A. Armienta, Diferenciación de la contaminación inorgánica en las aguas subterráneas del Valle de la Ciudad de San Luis Potosí, SLP, México, *Geofísica Internacional*. 28 (1989) 763–783.

[18] B. López-Álvarez, J.A. Ramos-Leal, J. Moran-Ramírez, A.C. Benavides, G.H. García, Origin of water quality of a hanging aquifer and its relation with changes in land use in the San Luis Potosí valley | Origen de la calidad del agua del acuífero colgado y su relación con los cambios de uso de suelo en el valle de San Luis Potosí, *Boletín de La Sociedad Geológica Mexicana*. 65 (2013).

[19] J.J. Carrillo-Rivera, A. Cardona, D. Moss, Importance of the vertical component of groundwater flow: A hydrogeochemical approach in the valley of San Luis Potosí, Mexico, *Journal of Hydrology*. 185 (1996) 23–44. [https://doi.org/10.1016/S0022-1694\(96\)03014-4](https://doi.org/10.1016/S0022-1694(96)03014-4).

[20] J. Ramos-Leal, H. López-Loera, V. Ruiz, J. Aranda-Gómez, Sucesión de eventos y geometría de la parte central del acuífero del graben de Villa de Reyes (San Luis Potosí, México) inferida a partir de datos geoelectrónicos, *Revista Mexicana de Ciencias Geológicas*, ISSN 1026-8774, Vol. 24, Nº. 1, 2007, Pags. 31-46. (2007).



- [21] M. Grimaldo, F. Turrubiarres, J. Milan, A. Pozos, C. Alfaro, F. Díaz-Barriga, Endemic fluorosis in San Luis Potosi, Mexico. III. Screening for fluoride exposure with a geographic information system, *Fluoride*. 30 (1997) 33–40.
- [22] A.M. Ortega-Guerrero, Presencia, distribución, hidrogeoquímica y origen de arsénico, fluoruro y otros elementos traza disueltos en agua subterránea, a escala de cuenca hidrológica tributaria de Lerma-Chapala, México, *Revista Mexicana de Ciencias Geológicas*. 26 (2009) 143–161. <https://doi.org/10.1016/j.scitotenv.2015.09.085>.
- [23] M.T. Orozco-Esquivel, A.F. Nieto-Samaniego, S.A. Alaniz-Alvarez, Origin of rhyolitic lavas in the mesa central, Mexico, by crustal melting related to extension, *Journal of Volcanology and Geothermal Research*. 118 (2002) 37–56. [https://doi.org/10.1016/S0377-0273\(02\)00249-4](https://doi.org/10.1016/S0377-0273(02)00249-4).
- [24] M. Grimaldo, V.H. Borja-Aburto, A.L. Ramirez, M. Ponce, M. Rosas, F. Diaz-Barriga, Endemic fluorosis in San Luis Potosi, Mexico. I. Identification of risk factors associated with human exposure to fluoride., *Environmental Research*. 68 (1995) 25–30.
- [25] F. Díaz-Barriga, R. Layva, J. Quistián, J.P. Loyola-Rodríguez, A. Pozos, M. Grimaldo, Endemic Fluorosis in San Luis Potosi, Mexico IV. Sources of fluoride exposure, *Environmental Research*. 30 (1997) 219–222.
- [26] L. Brunton, B. Chabner, B. Knollmann, Goodman y Gilman. Las bases farmacológicas de la terapéutica., in: Goodman y Gilman. Las Bases Farmacológicas de La Terapéutica., McGraw-Hill/ Interamericana de España, S.A.U., Ciudad de México, México, 2011.
- [27] A. Guyton, J. Hall, Tratado de fisiología médica, in: Tratado de Fisiología médica, McGraw-Hill/Interamericana de España, S.A.U., Ciudad de México, México, 2001.
- [28] W.M. Edmunds, P.L. Smedley, Fluoride in Natural Waters - Springer, *Essentials of Medical Geology*. (1992) 1–44. [https://doi.org/10.1007/978-94-007-4375-5\\_13](https://doi.org/10.1007/978-94-007-4375-5_13).
- [29] D.L. Ozsvath, Fluoride and environmental health: A review, *Reviews in Environmental Science and Biotechnology*. 8 (2009) 59–79. <https://doi.org/10.1007/s11157-008-9136-9>.
- [30] World Health Organization, Guidelines for Drinking-Water Quality, in: Geneva. World Health Organization (Ed.), Fourth edi, 2011.
- [31] J.K. Fawell, World Health Organization., Fluoride in drinking-water, 2006. <https://doi.org/10.1007/BF01783490>.

- [32] J. Doull, K. Boekelheide, B. Farishian, R. Isaacson, J. Klotz, J. Kumar, H. Limeback, C. Poole, J. Puzas, N. Reed, others, Fluoride in drinking water: A scientific review of EPA's standards, National Academies, Washington. (2006) 205–223.
- [33] J.A. Novelo Baeza, Proyecto de Norma Oficial Mexicana PROY-NOM-127-SSA1-2017, Agua para uso y consumo humano. Límites permisibles de la calidad del agua, (2019).
- [34] N. Mobeen, P. Kumar, Defluoridation techniques - a critical review, Asian Journal of Pharmaceutical and Clinical Research. 10 (2017) 64–71. <https://doi.org/10.22159/ajpcr.2017.v10i6.13942>.
- [35] Meenakshi, R.C. Maheshwari, Fluoride in drinking water and its removal, Journal of Hazardous Materials. 137 (2006) 456–463. <https://doi.org/10.1016/j.jhazmat.2006.02.024>.
- [36] E. Vences-Alvarez, L.H. Velazquez-Jimenez, L.F. Chazaro-Ruiz, P.E. Diaz-Flores, J.R. Rangel-Mendez, Fluoride removal in water by a hybrid adsorbent lanthanum-carbon, Journal of Colloid and Interface Science. 455 (2015) 194–202. <https://doi.org/10.1016/j.jcis.2015.05.048>.
- [37] S. Dubey, M. Agrawal, A.B. Gupta, Advances in coagulation technique for treatment of fluoride-contaminated water: A critical review, Reviews in Chemical Engineering. (2018). <https://doi.org/10.1515/revce-2017-0043>.
- [38] A. Jeihanipour, J. Shen, G. Abbt-Braun, S.A. Huber, G. Mkongo, A.I. Schäfer, Seasonal variation of organic matter characteristics and fluoride concentration in the Maji ya Chai River (Tanzania): Impact on treatability by nanofiltration/reverse osmosis, Science of the Total Environment. 637-638 (2018) 1209–1220. <https://doi.org/10.1016/j.scitotenv.2018.05.113>.
- [39] D. Feng, C. Aldrich, H. Tan, Treatment of acid mine water by use of heavy metal precipitation and ion exchange, Minerals Engineering. 13 (2000) 623–642. [https://doi.org/10.1016/S0892-6875\(00\)00045-5](https://doi.org/10.1016/S0892-6875(00)00045-5).
- [40] H. Wang, H. Zhong, L. Liu, B. Quan, Defluoridation Effect for High Fluorine Geothermal Water Using Electric Flocculation Method, Nature Environmenta and Pollution Technology 16. 16 (2017) 923–927.
- [41] J. Lu, Q. Tang, Z.R. Wang, C. Xu, S.L. Lin, A study on continuous and batch electrocoagulation process for fluoride removal, Desalination and Water Treatment. 57 (2016) 28417–28425. <https://doi.org/10.1080/19443994.2016.1186567>.
- [42] R. Mondal, S. Pal, D.V. Bhalani, V. Bhadja, U. Chatterjee, S.K. Jewrajka, Preparation of polyvinylidene fluoride blend anion exchange membranes via non-solvent

induced phase inversion for desalination and fluoride removal, *Desalination*. 445 (2018) 85–94. <https://doi.org/10.1016/j.desal.2018.07.032>.

[43] M.E. Suss, S. Porada, X. Sun, P.M. Biesheuvel, J. Yoon, V. Presser, Water desalination via capacitive deionization: What is it and what can we expect from it?, 8 (2015) 2296–2319. <https://doi.org/10.1039/c5ee00519a>.

[44] J.G. Gamaethiralalage, K. Singh, S. Sahin, J. Yoon, M. Elimelech, M.E. Suss, P. Liang, P.M. Biesheuvel, R.L. Zornitta, L.C.P.M. de Smet, Recent advances in ion selectivity with capacitive deionization, *Energy & Environmental Science*. (2021). <https://doi.org/10.1039/d0ee03145c>.

[45] J. Choi, P. Dorji, H.K. Shon, S. Hong, Applications of capacitive deionization: Desalination, softening, selective removal, and energy efficiency, 449 (2019) 118–130. <https://doi.org/10.1016/j.desal.2018.10.013>.

[46] X. Zhang, K. Zuo, X. Zhang, C. Zhang, P. Liang, Selective ion separation by capacitive deionization (CDI) based technologies: A state-of-the-art review, *Environmental Science: Water Research and Technology*. 6 (2020) 243–257. <https://doi.org/10.1039/c9ew00835g>.

[47] Z. Chen, H. Zhang, C. Wu, Y. Wang, W. Li, A study of electrosorption selectivity of anions by activated carbon electrodes in capacitive deionization, *Desalination*. 369 (2015) 46–50. <https://doi.org/10.1016/j.desal.2015.04.022>.

[48] Y. Wu, G. Jiang, G. Liu, G. Lui, Z.P. Cano, Q. Li, Z. Zhang, A. Yu, Z. Zhang, Z. Chen, A 3D ordered hierarchically porous non-carbon electrode for highly effective and efficient capacitive deionization, *Journal of Materials Chemistry A*. 7 (2019) 15633–15639. <https://doi.org/10.1039/c9ta04025k>.

[49] R. Santoyo-Cisneros, J.R. Rangel-Mendez, J.L. Nava, E.R. Larios-Durán, L.F. Chazaro-Ruiz, Influence of surface chemistry of activated carbon electrodes on electro-assisted adsorption of arsenate, *Journal of Hazardous Materials*. 392 (2020) 122349. <https://doi.org/10.1016/j.jhazmat.2020.122349>.

[50] D.R. Martinez-Vargas, E.R. Larios-Durán, L.F. Chazaro-Ruiz, J.R. Rangel-mendez, Correlation between physicochemical and electrochemical properties of an activated carbon doped with lanthanum for fluoride electrosorption, *Separation and Purification Technology*. 268 (2021). <https://doi.org/10.1016/j.seppur.2021.118702>.

[51] M.I. López-Cázares, E.D. Isaacs-Páez, J. Ascacio-Valdés, C.N. Aguilar-González, J.R. Rangel-Mendez, L.F. Chazaro-Ruiz, Electro-assisted naproxen adsorption followed by its electrodegradation and simultaneous electroreactivation of the activated carbon

electrode, Separation and Purification Technology. 258 (2021). <https://doi.org/10.1016/j.seppur.2020.118030>.

[52] A. Bán, A. Schäfer, H. Wendt, Fundamentals of electrosorption on activated carbon for wastewater treatment of industrial effluents, Journal of Applied Electrochemistry. 28 (1998) 227–236. <https://doi.org/10.1023/A:1003247229049>.

[53] K.Y. Foo, B.H. Hameed, A short review of activated carbon assisted electrosorption process: An overview, current stage and future prospects, Journal of Hazardous Materials. 170 (2009) 552–559. <https://doi.org/10.1016/j.jhazmat.2009.05.057>.

[54] L.M. Chang, X.Y. Duan, W. Liu, Preparation and electrosorption desalination performance of activated carbon electrode with titania, Desalination. 270 (2011) 285–290. <https://doi.org/10.1016/j.desal.2011.01.008>.

[55] Y. Li, C. Zhang, Y. Jiang, T.J. Wang, Electrically enhanced adsorption and green regeneration for fluoride removal using Ti(OH)<sub>4</sub>-loaded activated carbon electrodes, Chemosphere. 200 (2018) 554–560. <https://doi.org/10.1016/j.chemosphere.2018.02.112>.

[56] M.W. Ryoo, G. Seo, Improvement in capacitive deionization function of activated carbon cloth by titania modification, Water Research. 37 (2003) 1527–1534. [https://doi.org/10.1016/S0043-1354\(02\)00531-6](https://doi.org/10.1016/S0043-1354(02)00531-6).

[57] P. Wu, L. Xia, M. Dai, L. Lin, S. Song, Electrosorption of fluoride on TiO<sub>2</sub>-loaded activated carbon in water, Colloids and Surfaces A: Physicochemical and Engineering Aspects. 502 (2016) 66–73. <https://doi.org/10.1016/j.colsurfa.2016.05.020>.

[58] A.S. Yasin, I.M.A. Mohamed, H.M. Mousa, C.H. Park, C.S. Kim, Facile synthesis of TiO<sub>2</sub>/ZrO<sub>2</sub> nanofibers/nitrogen co-doped activated carbon to enhance the desalination and bacterial inactivation via capacitive deionization, Scientific Reports. 8 (2018). <https://doi.org/10.1038/s41598-017-19027-w>.

[59] L. Zou, G. Morris, D. Qi, Using activated carbon electrode in electrosorptive deionisation of brackish water, Desalination. 225 (2008) 329–340. <https://doi.org/10.1016/j.desal.2007.07.014>.

[60] D. Ma, Y. Wang, X. Han, S. Xu, J. Wang, Electrode configuration optimization of capacitive deionization cells based on zero charge potential of the electrodes, Separation and Purification Technology. 189 (2017) 467–474. <https://doi.org/10.1016/j.seppur.2017.08.025>.

[61] R.L. Zornitta, L.A.M. Ruotolo, Simultaneous analysis of electrosorption capacity and kinetics for CDI desalination using different electrode configurations, Chemical Engineering Journal. 332 (2018) 33–41. <https://doi.org/10.1016/j.cej.2017.09.067>.

- [62] X. Gao, S. Porada, A. Omosebi, K.L. Liu, P.M. Biesheuvel, J. Landon, Complementary surface charge for enhanced capacitive deionization, *Water Research*. 92 (2016) 275–282. <https://doi.org/10.1016/j.watres.2016.01.048>.
- [63] B.M. Asquith, J. Meier-Haack, B.P. Ladewig, Cation exchange copolymer enhanced electrosorption, *Desalination*. 345 (2014) 94–100. <https://doi.org/10.1016/j.desal.2014.04.027>.
- [64] P. Liang, L. Yuan, X. Yang, S. Zhou, X. Huang, Coupling ion-exchangers with inexpensive activated carbon fiber electrodes to enhance the performance of capacitive deionization cells for domestic wastewater desalination, *Water Research*. 47 (2013) 2523–2530. <https://doi.org/10.1016/j.watres.2013.02.037>.
- [65] H. Marsh, F. Rodriguez-Reinoso, *Activated carbon*, Elsevier Science & Technology Books, 2006.
- [66] T.J. Bandoz, C.O. Ania, Surface chemistry of activated carbons and its characterization, in: *Activated Carbon Surface in Environmental Remediation*, 2006: pp. 159–229.
- [67] M.A. Montes-Morán, D. Suárez, J.A. Menéndez, E. Fuente, On the nature of basic sites on carbon surfaces: An overview, *Carbon*. 42 (2004) 1219–1225. <https://doi.org/10.1016/j.carbon.2004.01.023>.
- [68] C.A. Leon y Leon, J.M. Solar, V. Calemma, L.R. Radovic, Evidence for the protonation of basal plane sites on carbon, *Carbon*. 30 (1992) 797–811. [https://doi.org/10.1016/0008-6223\(92\)90164-R](https://doi.org/10.1016/0008-6223(92)90164-R).
- [69] C.A. Leon, D. Leon, L.R. Radovic, Interfacial chemistry and electrochemistry of carbon surfaces, in: P.A. Throver (Ed.), *Chemistry and Physics of Carbon Vol 24*, Marcel Dekker, Inc., New York, 1991: p. 50.
- [70] IUPAC, *Compendium of Chemical Terminology (The "Gold Book")*, 2nd ed., Blackwell Scientific Publications, Oxford, 2019.
- [71] W. Ryoo, J.L. Dickson, V.V. Dhanuka, S.E. Webber, R.T. Bonnecaze, K.P. Johnston, Electrostatic stabilization of colloids in carbon dioxide: Electrophoresis and dielectrophoresis, *Langmuir*. 21 (2005) 5914–5923. <https://doi.org/10.1021/la046770w>.
- [72] B. Timmer, M. Sluyters-Rehbach, J.H. Sluyters, Electrode Kinetics and Double Layer Structure, *Surface Science*. 18 (1969) 44–61. [https://doi.org/10.1016/0039-6028\(69\)90266-0](https://doi.org/10.1016/0039-6028(69)90266-0).
- [73] B.B. Damaskin, A.N. Frumkin, Potentials of zero charge, interaction of metals with water and adsorption of organic substances-III. The role of the water dipoles in the

structure of the dense part of the electric double layer, *Electrochimica Acta*. 19 (1974) 173–176. [https://doi.org/10.1016/0013-4686\(74\)85013-9](https://doi.org/10.1016/0013-4686(74)85013-9).

[74] J.A. Menéndez, M.J. Illán-Gómez, C.A.L. y León, L.R. Radovic, On the difference between the isoelectric point and the point of zero charge of carbons, *Carbon*. 33 (1995) 1655–1657. [https://doi.org/10.1016/0008-6223\(95\)96817-R](https://doi.org/10.1016/0008-6223(95)96817-R).

[75] M.S. Shafeeyan, W. Mohd, A. Wan, A. Houshmand, A. Shamiri, A review on surface modification of activated carbon for carbon dioxide adsorption, *Journal of Analytical and Applied Pyrolysis*. 89 (2010) 143–151. <https://doi.org/10.1016/j.jaap.2010.07.006>.

[76] H.P. Boehm, Some aspects of the surface chemistry of carbon blacks and other carbons, *Carbon*. 32 (1994) 759–769. [https://doi.org/10.1016/0008-6223\(94\)90031-0](https://doi.org/10.1016/0008-6223(94)90031-0).

[77] J.L. Figueiredo, M.F.R. Pereira, M.M.A. Freitas, J.J.M. Órfão, Modification of the surface chemistry of activated carbons, *Carbon*. 37 (1999) 1379–1389. [https://doi.org/10.1016/S0008-6223\(98\)00333-9](https://doi.org/10.1016/S0008-6223(98)00333-9).

[78] I.I. Salame, T.J. Bandoz, Surface chemistry of activated carbons: Combining the results of temperature-programmed desorption, Boehm, and potentiometric titrations, *Journal of Colloid and Interface Science*. 240 (2001) 252–258. <https://doi.org/10.1006/jcis.2001.7596>.

[79] J.A. Menéndez, J. Phillips, B. Xia, L.R. Radovic, On the modification and characterization of chemical surface properties of activated carbon: In the search of carbons with stable basic properties, *Langmuir*. 12 (1996) 4404–4410. <https://doi.org/10.1021/la9602022>.

[80] C.A. León y León, L.R. Radovic, Interfacial Chemistry and Electrochemistry of Carbon Surfaces, in: *Chemistry & Physics of Carbon*, Vol. 24, 1993: pp. 213–285.

[81] S. Biniak, A. Swiatkowski, M. Pakula, Electrochemical Studies of Phenomena at Active Carbon-Electrolyte Solution Interfaces, in: L.R. Radovic (Ed.), *Chemistry and Physics of Carbon Vol 27*, Marcel Dekker, Inc., New York, 2001: pp. 125–226.

[82] J.C. Charlier, J.P. Issi, Electrical conductivity of novel forms of carbon, *Journal of Physics and Chemistry of Solids*. 57 (1996) 957–965. [https://doi.org/10.1016/0022-3697\(95\)00382-7](https://doi.org/10.1016/0022-3697(95)00382-7).

[83] H. Shi, Activated carbons and double layer capacitance, *Electrochimica Acta*. 41 (1996) 1633–1639. [https://doi.org/10.1016/0013-4686\(95\)00416-5](https://doi.org/10.1016/0013-4686(95)00416-5).

[84] A.J. Bard, L.R. Faulkner, *Electrochemical Methods. Fundamentals and Applications*, 2nd editio, John Wiley & Sons, Inc., NY, 2001.

- [85] F. Silva, Trends in Interfacial Electrochemistry, Springer Netherlands, Dordrecht, 1986.
- [86] J.O'M. Bockris, K.N. Reddy, M. Gamboa-Aldeco, Modern Electrochemistry 2A, 2nd editio, Kluwer Academic Publishers, NY, 2002.
- [87] R.K. Parveen, Theory for staircase voltammetry and linear scan voltammetry on fractal electrodes: Emergence of anomalous Randles-Sevcik behavior, *Electrochimica Acta*. 111 (2013) 223–233. <https://doi.org/10.1016/j.electacta.2013.07.163>.
- [88] J.W. Schultze, K.J. Vetter, EXPERIMENTAL DETERMINATION AND INTERPRETATION OF THE ELECTROSORPTION VALENCY GAMMA, *Electroanalytical Chemistry and Interfacial Electrochemistry*. 44 (1973) 63–81.
- [89] J.J. Sheng, EOR mechanisms of wettability alteration and its comparison with IFT, 2020. <https://doi.org/10.1016/b978-0-12-815905-7.00009-8>.
- [90] S. Trasatti, Work function, electronegativity, and electrochemical behaviour of metals. II. Potentials of zero charge and "electrochemical" work functions, *Journal of Electroanalytical Chemistry*. 33 (1971) 351–378. [https://doi.org/10.1016/S0022-0728\(71\)80123-7](https://doi.org/10.1016/S0022-0728(71)80123-7).
- [91] B.S. Bagotsky, Fundamentals of Electrochemistry, 2nd editio, John Wiley & Sons, Inc, NJ, 2006.
- [92] J.O.M. Bockris, M.A. Habib, Contributions of water dipoles to double layer properties: A three-state water model, *Electrochimica Acta*. 22 (1977) 41–46. [https://doi.org/10.1016/0013-4686\(77\)85051-2](https://doi.org/10.1016/0013-4686(77)85051-2).
- [93] J. Lyklema, Ionic components of charge in the electrical double layer in reversible systems, *Transactions of the Faraday Society*. 59 (1963) 418–427. <https://doi.org/10.1039/tf9635900418>.
- [94] N.F. Uvarov, A.S. Ulihin, Y.G. Mateyshina, Nanocomposite Alkali-Ion Solid Electrolytes, Elsevier Inc., 2018. <https://doi.org/10.1016/B978-0-12-814807-5.00011-5>.
- [95] D.C. Grahame, The electrical double layer and the theory of electrocapillarity, *Chemical Reviews*. 41 (1947) 441–501. <https://doi.org/10.1021/cr60130a002>.
- [96] E.R. Nightingale, Phenomenological theory of ion solvation. Effective radii of hydrated ions, *Journal of Physical Chemistry*. 63 (1959) 1381–1387. <https://doi.org/10.1021/j150579a011>.



- [97] J. Marañón Di Leo, J. Marañón, Hydration and diffusion of cations in nanopores, in: *Journal of Molecular Structure: THEOCHEM*, 2005: pp. 53–57. <https://doi.org/10.1016/j.theochem.2005.02.070>.
- [98] L.A. Richards, A.I. Schäfer, B.S. Richards, B. Corry, The importance of dehydration in determining ion transport in narrow pores, *Small*. 8 (2012) 1701–1709. <https://doi.org/10.1002/sml.201102056>.
- [99] J.C. Crittenden, M.W. Harza, *Water treatment principles and design.*, 2nd editio, Wiley, New Jersey, 2005.
- [100] A. Omosibi, X. Gao, J. Rentschler, J. Landon, K. Liu, Continuous operation of membrane capacitive deionization cells assembled with dissimilar potential of zero charge electrode pairs, *Journal of Colloid and Interface Science*. 446 (2015) 345–351. <https://doi.org/10.1016/j.jcis.2014.11.013>.
- [101] T. Wu, G. Wang, F. Zhan, Q. Dong, Q. Ren, J. Wang, J. Qiu, Surface-treated carbon electrodes with modified potential of zero charge for capacitive deionization, *Water Research*. 93 (2016) 30–37. <https://doi.org/10.1016/j.watres.2016.02.004>.
- [102] C.M.A. Brett, A.M.O. Brett, *Applications, Electrochemistry. Principles Methods and Applications*, 2nd editio, Oxford University Press, Great Britain, 1994.
- [103] X. Gao, A. Omosibi, J. Landon, K. Liu, Enhanced Salt Removal in an Inverted Capacitive Deionization Cell Using Amine Modified Microporous Carbon Cathodes, *Environmental Science and Technology*. 49 (2015) 10920–10926. <https://doi.org/10.1021/acs.est.5b02320>.
- [104] A. Omosibi, X. Gao, J. Landon, K. Liu, Asymmetric Electrode Configuration for Enhanced Membrane Capacitive Deionization, *ACS Applied Material & Interfaces*. 6 (2014) 12640–12649. <https://doi.org/10.1021/am5026209>.
- [105] E. Avraham, M. Noked, I. Cohen, A. Soffer, D. Aurbach, The Dependence of the Desalination Performance in Capacitive Deionization Processes on the Electrodes PZC, *Journal of The Electrochemical Society*. 158 (2011) P168. <https://doi.org/10.1149/2.078112jes>.
- [106] J.O'M. Bockris, K.N. Reddy, *Modern Electrochemistry 1*, 2nd editio, Kluwer Academic Publishers, NY, 2002.
- [107] A. López Valdivieso, J.L. Reyes Bahena, S. Song, R. Herrera Urbina, Temperature effect on the zeta potential and fluoride adsorption at the  $\alpha$ -Al<sub>2</sub>O<sub>3</sub>/aqueous solution interface, *Journal of Colloid and Interface Science*. 298 (2006) 1–5. <https://doi.org/10.1016/j.jcis.2005.11.060>.



- [108] E. Deliyanni, T.J. Bandosz, Importance of carbon surface chemistry in development of iron-carbon composite adsorbents for arsenate removal, *Journal of Hazardous Materials*. 186 (2011) 667–674. <https://doi.org/10.1016/j.jhazmat.2010.11.055>.
- [109] J.A. Arcibar-Orozco, D.B. Josue, J.C. Rios-Hurtado, J.R. Rangel-Mendez, Influence of iron content, surface area and charge distribution in the arsenic removal by activated carbons, *Chemical Engineering Journal*. 249 (2014) 201–209. <https://doi.org/10.1016/j.cej.2014.03.096>.
- [110] E. Bayram, E. Ayranci, A systematic study on the changes in properties of an activated carbon cloth upon polarization, *Electrochimica Acta*. 56 (2011) 2184–2189. <https://doi.org/10.1016/j.electacta.2010.12.018>.
- [111] X. Gao, A. Omosebi, J. Landon, K. Liu, Surface charge enhanced carbon electrodes for stable and efficient capacitive deionization using inverted adsorption-desorption behavior, *Energy and Environmental Science*. 8 (2015) 897–909. <https://doi.org/10.1039/c4ee03172e>.
- [112] P.M. Biesheuvel, Activated carbon is an electron-conducting amphoteric ion adsorbent, (2015) 1–9. <http://arxiv.org/abs/1509.06354>.
- [113] K.L. Yang, T.Y. Ying, S. Yiacoumi, C. Tsouris, E.S. Vittoratos, Electrosorption of ions from aqueous solutions by carbon aerogel: An electrical double-layer model, *Langmuir*. 17 (2001) 1961–1969. <https://doi.org/10.1021/la001527s>.
- [114] T.Y. Ying, K.L. Yang, S. Yiacoumi, C. Tsouris, Electrosorption of ions from aqueous solutions by nanostructured carbon aerogel, *Journal of Colloid and Interface Science*. 250 (2002) 18–27. <https://doi.org/10.1006/jcis.2002.8314>.
- [115] A. Tanimura, A. Kovalenko, F. Hirata, Molecular theory of an electrochemical double layer in a nanoporous carbon supercapacitor, *Chemical Physics Letters*. 378 (2003) 638–646. [https://doi.org/10.1016/S0009-2614\(03\)01336-8](https://doi.org/10.1016/S0009-2614(03)01336-8).
- [116] B. Jia, W. Zhang, Preparation and Application of Electrodes in Capacitive Deionization (CDI): a State-of-Art Review, *Nanoscale Research Letters*. 11 (2016) 1–25. <https://doi.org/10.1186/s11671-016-1284-1>.
- [117] E.N. Gueyes, A.N. Shocron, A. Simanovski, P.M. Biesheuvel, M.E. Suss, A one-dimensional model for water desalination by flow-through electrode capacitive deionization, *Desalination*. 415 (2017) 8–13. <https://doi.org/10.1016/j.desal.2017.03.013>.
- [118] P.M. Biesheuvel, H.V.M. Hamelers, M.E. Suss, Theory of Water Desalination by Porous Electrodes with Immobile Chemical Charge, *Colloids and Interface Science Communications*. 9 (2015) 1–5. <https://doi.org/10.1016/j.colcom.2015.12.001>.

- [119] P.M. Biesheuvel, Thermodynamic cycle analysis for capacitive deionization, *Journal of Colloid and Interface Science*. 332 (2009) 258–264. <https://doi.org/10.1016/j.jcis.2008.12.018>.
- [120] P.M. Biesheuvel, S. Porada, M. Levi, M.Z. Bazant, Attractive forces in microporous carbon electrodes for capacitive deionization, *Journal of Solid State Electrochemistry*. 18 (2014) 1365–1376. <https://doi.org/10.1007/s10008-014-2383-5>.
- [121] A.H. Galama, J.W. Post, M.A. Cohen Stuart, P.M. Biesheuvel, Validity of the Boltzmann equation to describe Donnan equilibrium at the membrane-solution interface, *Journal of Membrane Science*. 442 (2013) 131–139. <https://doi.org/10.1016/j.memsci.2013.04.022>.
- [122] R. Zhao, P.M. Biesheuvel, H. Miedema, H. Bruning, A. van der Wal, Charge efficiency: A functional tool to probe the double-layer structure inside of porous electrodes and application in the modeling of capacitive deionization, *Journal of Physical Chemistry Letters*. 1 (2010) 205–210. <https://doi.org/10.1021/jz900154h>.
- [123] T. Kim, J.E. Dykstra, S. Porada, A. van der Wal, J. Yoon, P.M. Biesheuvel, Enhanced charge efficiency and reduced energy use in capacitive deionization by increasing the discharge voltage, *Journal of Colloid and Interface Science*. 446 (2015) 317–326. <https://doi.org/10.1016/j.jcis.2014.08.041>.
- [124] Z.H. Huang, M. Wang, L. Wang, F. Kang, Relation between the charge efficiency of activated carbon fiber and its desalination performance, *Langmuir*. 28 (2012) 5079–5084. <https://doi.org/10.1021/la204690s>.
- [125] D. He, C.E. Wong, W. Tang, P. Kovalsky, T. David Waite, Faradaic Reactions in Water Desalination by Batch-Mode Capacitive Deionization, *Environmental Science and Technology Letters*. 3 (2016) 222–226. <https://doi.org/10.1021/acs.estlett.6b00124>.
- [126] Y. Bouhadana, M. Ben-Tzion, A. Soffer, D. Aurbach, A control system for operating and investigating reactors: The demonstration of parasitic reactions in the water desalination by capacitive de-ionization, *Desalination*. 268 (2011) 253–261. <https://doi.org/10.1016/j.desal.2010.10.037>.
- [127] S. Porada, R. Zhao, A. Van Der Wal, V. Presser, P.M. Biesheuvel, Review on the science and technology of water desalination by capacitive deionization, *Progress in Materials Science*. 58 (2013) 1388–1442. <https://doi.org/10.1016/j.pmatsci.2013.03.005>.
- [128] T. Kim, J. Yu, C. Kim, J. Yoon, Hydrogen peroxide generation in flow-mode capacitive deionization, *Journal of Electroanalytical Chemistry*. 776 (2016) 101–104. <https://doi.org/10.1016/j.jelechem.2016.07.001>.

- [129] F. Duan, X. Du, Y. Li, H. Cao, Y. Zhang, Desalination stability of capacitive deionization using ordered mesoporous carbon: Effect of oxygen-containing surface groups and pore properties, *Desalination*. 376 (2015) 17–24. <https://doi.org/10.1016/j.desal.2015.08.009>.
- [130] I. Cohen, E. Avraham, Y. Bouhadana, A. Soffer, D. Aurbach, The effect of the flow-regime, reversal of polarization, and oxygen on the long term stability in capacitive de-ionization processes, *Electrochimica Acta*. 153 (2015) 106–114. <https://doi.org/10.1016/j.electacta.2014.12.007>.
- [131] C. Zhang, D. He, J. Ma, W. Tang, T.D. Waite, Faradaic reactions in capacitive deionization (CDI) - problems and possibilities: A review, 128 (2018) 314–330. <https://doi.org/10.1016/j.watres.2017.10.024>.
- [132] M. Haro, G. Rasines, C. MacÍas, C.O. Ania, Stability of a carbon gel electrode when used for the electro-assisted removal of ions from brackish water, *Carbon*. 49 (2011) 3723–3730. <https://doi.org/10.1016/j.carbon.2011.05.001>.
- [133] I. Cohen, E. Avraham, Y. Bouhadana, A. Soffer, D. Aurbach, Long term stability of capacitive de-ionization processes for water desalination: The challenge of positive electrodes corrosion, *Electrochimica Acta*. 106 (2013) 91–100. <https://doi.org/10.1016/j.electacta.2013.05.029>.
- [134] T.J. Bandoz, C.O. Ania, Surface chemistry of activated carbons and its characterization, in: *Activated Carbon Surface in Environmental Remediation*, 2006: pp. 159–229. [https://doi.org/10.1016/S1573-4285\(06\)80013-X](https://doi.org/10.1016/S1573-4285(06)80013-X).
- [135] J.E. Dykstra, K.J. Keesman, P.M. Biesheuvel, A. van der Wal, Theory of pH changes in water desalination by capacitive deionization, *Water Research*. 119 (2017) 178–186. <https://doi.org/10.1016/j.watres.2017.04.039>.
- [136] R. Berenguer, J.P. Marco-Lozar, C. Quijada, D. Cazorla-Amorós, E. Morallón, Effect of electrochemical treatments on the surface chemistry of activated carbon, *Carbon*. 47 (2009) 1018–1027. <https://doi.org/10.1016/j.carbon.2008.12.022>.
- [137] D. Lu, W. Cai, Y. Wang, Optimization of the voltage window for long-term capacitive deionization stability, *Desalination*. 424 (2017) 53–61. <https://doi.org/10.1016/j.desal.2017.09.026>.
- [138] X. Gao, A. Omosebi, J. Landon, K. Liu, Dependence of the Capacitive Deionization Performance on Potential of Zero Charge Shifting of Carbon Xerogel Electrodes during Long-Term Operation, *Journal of The Electrochemical Society*. 161 (2014) E159–E166. <https://doi.org/10.1149/2.0561412jes>.

- [139] Q. Dong, D. Yang, L. Luo, Q. He, F. Cai, S. Cheng, Y. Chen, Engineering porous biochar for capacitive fluorine removal, *Separation and Purification Technology*. 257 (2021) 117932. <https://doi.org/10.1016/j.seppur.2020.117932>.
- [140] Y. Li, Y. Jiang, T.J. Wang, C. Zhang, H. Wang, Performance of fluoride electrosorption using micropore-dominant activated carbon as an electrode, *Separation and Purification Technology*. 172 (2017) 415–421. <https://doi.org/10.1016/j.seppur.2016.08.043>.
- [141] M.S. Gaikwad, C. Balomajumder, Simultaneous electrosorptive removal of chromium(VI) and fluoride ions by capacitive deionization (CDI): Multicomponent isotherm modeling and kinetic study, *Separation and Purification Technology*. 186 (2017) 272–281. <https://doi.org/10.1016/j.seppur.2017.06.017>.
- [142] M.S. Gaikwad, C. Balomajumder, Removal of Cr(VI) and fluoride by membrane capacitive deionization with nanoporous and microporous *Limonia acidissima* (wood apple) shell activated carbon electrode, *Separation and Purification Technology*. 195 (2018) 305–313. <https://doi.org/10.1016/j.seppur.2017.12.006>.
- [143] W. Tang, P. Kovalsky, B. Cao, T.D. Waite, Investigation of fluoride removal from low-salinity groundwater by single-pass constant-voltage capacitive deionization, *Water Research*. 99 (2016) 112–121. <https://doi.org/10.1016/j.watres.2016.04.047>.
- [144] W. Tang, P. Kovalsky, D. He, T.D. Waite, Fluoride and nitrate removal from brackish groundwaters by batch-mode capacitive deionization, *Water Research*. 84 (2015) 342–349. <https://doi.org/10.1016/j.watres.2015.08.012>.
- [145] W. Tang, P. Kovalsky, B. Cao, D. He, T.D. Waite, Fluoride Removal from Brackish Groundwaters by Constant Current Capacitive Deionization (CDI), *Environmental Science and Technology*. 50 (2016) 10570–10579. <https://doi.org/10.1021/acs.est.6b03307>.
- [146] S. Jagtap, M.K. Yenkie, S. Das, S. Rayalu, Synthesis and characterization of lanthanum impregnated chitosan flakes for fluoride removal in water, *Desalination*. 273 (2011) 267–275. <https://doi.org/10.1016/j.desal.2010.12.032>.
- [147] T. Robshaw, S. Tukra, D.B. Hammond, G.J. Leggett, M.D. Ogden, Highly efficient fluoride extraction from simulant leachate of spent potlining via La-loaded chelating resin. An equilibrium study, *Journal of Hazardous Materials*. 361 (2019) 200–209. <https://doi.org/10.1016/j.jhazmat.2018.07.036>.
- [148] S.a. Wasay, M.J. Haran, S. Tokunaga, Adsorption of fluoride, phosphate, and arsenate ions on lanthanum-impregnated silica gel, *Water Environment Research*. 68 (1996) 295–300. <https://doi.org/10.2175/106143096X127730>.

- [149] C.R.N. Rao, J. Karthikeyan, Removal of fluoride from water by adsorption onto lanthanum oxide, *Water, Air, and Soil Pollution*. 223 (2012) 1101–1114. <https://doi.org/10.1007/s11270-011-0928-0>.
- [150] S. Sahu, L. Mallik, S. Pahi, B. Barik, U.K. Sahu, M. Sillanpää, R.K. Patel, Facile synthesis of poly o-toluidine modified lanthanum phosphate nanocomposite as a superior adsorbent for selective fluoride removal: A mechanistic and kinetic study, *Chemosphere*. 252 (2020). <https://doi.org/10.1016/j.chemosphere.2020.126551>.
- [151] Y. Yu, C. Wang, X. Guo, J. Paul Chen, Modification of carbon derived from *Sargassum* sp. by lanthanum for enhanced adsorption of fluoride, *Journal of Colloid and Interface Science*. 441 (2015) 113–120. <https://doi.org/10.1016/j.jcis.2014.10.039>.
- [152] H. Paudyal, B. Pangeni, K. Nath Ghimire, K. Inoue, K. Ohto, H. Kawakita, S. Alam, Adsorption behavior of orange waste gel for some rare earth ions and its application to the removal of fluoride from water, *Chemical Engineering Journal*. 195-196 (2012) 289–296. <https://doi.org/10.1016/j.cej.2012.04.061>.
- [153] H. Deng, X. Yu, Adsorption of fluoride, arsenate and phosphate in aqueous solution by cerium impregnated fibrous protein, *Chemical Engineering Journal*. 184 (2012) 205–212. <https://doi.org/10.1016/j.cej.2012.01.031>.
- [154] R. Yao, F. Meng, L. Zhang, D. Ma, M. Wang, Defluoridation of water using neodymium-modified chitosan, *Journal of Hazardous Materials*. 165 (2009) 454–460. <https://doi.org/10.1016/j.jhazmat.2008.10.052>.
- [155] V. Sivasankar, S. Muruges, S. Rajkumar, A. Darchen, Cerium dispersed in carbon (CeDC) and its adsorption behavior: A first example of tailored adsorbent for fluoride removal from drinking water, *Chemical Engineering Journal*. 214 (2013) 45–54. <https://doi.org/10.1016/j.cej.2012.10.023>.
- [156] A.M. Raichur, M. Jyoti Basu, Adsorption of fluoride onto mixed rare earth oxides, *Separation and Purification Technology*. 24 (2001) 121–127. [https://doi.org/10.1016/S1383-5866\(00\)00219-7](https://doi.org/10.1016/S1383-5866(00)00219-7).
- [157] V.P. Persy, G.J. Behets, A.R. Bervoets, M.E. De Broe, P.C. D’Haese, Lanthanum: A safe phosphate binder, *Seminars in Dialysis*. 19 (2006) 195–199. <https://doi.org/10.1111/j.1525-139X.2006.00169.x>.
- [158] G.J. Behets, K.V. Mubiana, L. Lamberts, K. Finsterle, N. Traill, R. Blust, P.C. D’Haese, Use of lanthanum for water treatment A matter of concern?, *Chemosphere*. 239 (2020) 124780. <https://doi.org/10.1016/j.chemosphere.2019.124780>.

- [159] H. Herrmann, J. Nolde, S. Berger, S. Heise, Aquatic ecotoxicity of lanthanum - A review and an attempt to derive water and sediment quality criteria, *Ecotoxicology and Environmental Safety*. 124 (2016) 213–238. <https://doi.org/10.1016/j.ecoenv.2015.09.033>.
- [160] A.M. Malvandi, S. Shahba, A. Mohammadipour, S.H. Rastegar-Moghaddam, M. Abudayyak, Cell and molecular toxicity of lanthanum nanoparticles: are there possible risks to humans?, *Nanotoxicology*. 15 (2021) 951–972. <https://doi.org/10.1080/17435390.2021.1940340>.
- [161] C.H. Lim, Toxicity of two different sized lanthanum oxides in cultured cells and sprague-dawley rats, *Toxicological Research*. 31 (2015) 181–189. <https://doi.org/10.5487/TR.2015.31.2.181>.
- [162] M.W. Raza, S. Kiran, A. Razaq, M.F. Iqbal, A. Hassan, S. Hussain, M.N. Ashiq, Z. Meng, Strategy to enhance the electrochemical characteristics of lanthanum sulfide nanorods for supercapacitor applications, *Journal of Nanoparticle Research*. 23 (2021) 207. <https://doi.org/10.1007/s11051-021-05307-0>.
- [163] X. Zhang, L. Zhang, Z. Li, Z. Jiang, Q. Zheng, B. Lin, B. Pan, Rational Design of Antifouling Polymeric Nanocomposite for Sustainable Fluoride Removal from NOM-Rich Water, *Environmental Science and Technology*. 51 (2017) 13363–13371. <https://doi.org/10.1021/acs.est.7b04164>.
- [164] H. Xu, J. Xu, Electrical properties of Ge metal–oxide–semiconductor capacitors with high-k La<sub>2</sub>O<sub>3</sub> gate dielectric incorporated by N or/and Ti, *Journal of Semiconductors*. 37 (2016) 1–5. <https://doi.org/10.1088/1674-4926/37/6/064006>.
- [165] A.A. Yadav, A.C. Lokhande, J.H. Kim, C.D. Lokhande, Supercapacitive activities of porous La<sub>2</sub>O<sub>3</sub> symmetric flexible solid-state device by hydrothermal method, *International Journal of Hydrogen Energy*. 41 (2016) 18311–18319. <https://doi.org/10.1016/j.ijhydene.2016.08.028>.
- [166] Y. Wang, R. Jia, Y. Zhao, C. Li, Y. Zhang, Investigation of Leakage Current Mechanisms in La<sub>2</sub>O<sub>3</sub>/SiO<sub>2</sub>/4H-SiC MOS Capacitors with Varied SiO<sub>2</sub> Thickness, *Journal of the Electronic Materials*. 45 (2016) 5600–5605. <https://doi.org/10.1007/s11664-016-4760-6>.
- [167] A.A. Yadav, V.S. Kumbhar, S.J. Patil, N.R. Chodankar, C.D. Lokhande, Supercapacitive properties of chemically deposited La<sub>2</sub>O<sub>3</sub> thin film, *Ceramics International*. 42 (2016) 2079–2084. <https://doi.org/10.1016/j.ceramint.2015.09.098>.
- [168] R. Rajagopal, K.S. Ryu, Facile hydrothermal synthesis of lanthanum oxide/hydroxide nanoparticles anchored reduced graphene oxide for supercapacitor

applications, *Journal of Industrial and Engineering Chemistry*. 60 (2018) 441–450. <https://doi.org/10.1016/j.jiec.2017.11.031>.

[169] Q. Li, J. Ni, Y. Wu, Y. Du, W. Ding, S. Geng, Synthesis and characterization of La(OH)<sub>3</sub> nanopowders from hydrolysis of lanthanum carbide, *Journal of Rare Earths*. 29 (2011) 416–419. [https://doi.org/10.1016/S1002-0721\(10\)60471-1](https://doi.org/10.1016/S1002-0721(10)60471-1).

[170] M. Lu, Y. Cao, Y. Xue, W. Qiu, Preparation of Graphene Oxide/La<sub>2</sub>Ti<sub>2</sub>O<sub>7</sub> Composites with Enhanced Electrochemical Performances for Supercapacitors, *ACS Omega*. 6 (2021) 27994–28003. <https://doi.org/10.1021/acsomega.1c03863>.

[171] J.E. Dykstra, S. Porada, A. van der Wal, P.M. Biesheuvel, Energy consumption in capacitive deionization – Constant current versus constant voltage operation, *Water Research*. 143 (2018) 367–375. <https://doi.org/10.1016/j.watres.2018.06.034>.

[172] C.L. Yeh, H.C. Hsi, K.C. Li, C.H. Hou, Improved performance in capacitive deionization of activated carbon electrodes with a tunable mesopore and micropore ratio, *Desalination*. 367 (2015) 60–68. <https://doi.org/10.1016/j.desal.2015.03.035>.

[173] M. Noked, E. Avraham, A. Soffer, D. Aurbach, The rate-determining step of electroadsorption processes into nanoporous carbon electrodes related to water desalination, *Journal of Physical Chemistry C*. 113 (2009) 21319–21327. <https://doi.org/10.1021/jp905987j>.

[174] Y. Li, J. Shen, J. Li, X. Sun, J. Shen, W. Han, L. Wang, A protic salt-derived porous carbon for efficient capacitive deionization: Balance between porous structure and chemical composition, *Carbon*. 116 (2017) 21–32. <https://doi.org/10.1016/j.carbon.2017.01.084>.

[175] L. Han, K.G. Karthikeyan, M.A. Anderson, K.B. Gregory, Exploring the impact of pore size distribution on the performance of carbon electrodes for capacitive deionization, *Journal of Colloid and Interface Science*. 430 (2014) 93–99. <https://doi.org/10.1016/j.jcis.2014.05.015>.

[176] G. Park, S.P. Hong, C. Lee, J. Lee, J. Yoon, Selective fluoride removal in capacitive deionization by reduced graphene oxide/hydroxyapatite composite electrode, *Journal of Colloid and Interface Science*. 581 (2021) 396–402. <https://doi.org/10.1016/j.jcis.2020.07.108>.

[177] G. Wang, D. Li, S. Wang, Z. Zhao, S. Lv, J. Qiu, Ternary NiFeMn layered metal oxide (LDO) compounds for capacitive deionization defluoridation: The unique role of Mn, *Separation and Purification Technology*. 254 (2021) 117667. <https://doi.org/10.1016/j.seppur.2020.117667>.



- [178] D.R. Martinez-Vargas, J.R. Rangel-Mendez, L.F. Chazaro-Ruiz, Fluoride electrosorption by hybrid La(III)-activated carbon electrodes under the influence of the La(III) content and the polarization profile, *Journal of Environmental Chemical Engineering*. 10 (2021) 106926. <https://doi.org/10.1016/j.jece.2021.106926>.
- [179] C.2018. Consejo Potosino de Ciencia y Tecnológica, Identificación, propuesta de manejo y evaluación de la sostenibilidad en el abastecimiento de aguas a las comunidades urbanas y rurales del Estado de San Luis Potosí, en el contexto de la agenda 2030, PhD thesis, n.d.
- [180] R.C. Bansal, M. Goyal, *Activated carbon adsorption*, Taylor & Francis, New York, 2005.
- [181] J. Jagiellot, Stable Numerical Solution of the Adsorption Integral Equation Using Splines, *Langmuir*. 10 (1994) 2778–2785.
- [182] T.J. Bandoz, J. Jagiello, C. Contescu, J.A. Schwarz, Characterization of the surfaces of activated carbons in terms of their acidity constant distributions, *Carbon*. 31 (1993) 1193–1202. [https://doi.org/10.1016/0008-6223\(93\)90072-I](https://doi.org/10.1016/0008-6223(93)90072-I).
- [183] D.W. Smith, Ionic hydration enthalpies, *Journal of Chemical Education*. 54 (1977) 540–542.
- [184] R. Lin, P.L. Taberna, J. Chmiola, D. Guay, Y. Gogotsi, P. Simon, Microelectrode Study of Pore Size, Ion Size, and Solvent Effects on the Charge/Discharge Behavior of Microporous Carbons for Electrical Double-Layer Capacitors, *Journal of The Electrochemical Society*. 156 (2009) A7. <https://doi.org/10.1149/1.3002376>.
- [185] S. yun ZHOU, X. hai LI, Z. xing WANG, H. jun GUO, W. jie PENG, Effect of activated carbon and electrolyte on properties of supercapacitor, *Transactions of Nonferrous Metals Society of China (English Edition)*. 17 (2007) 1328–1333. [https://doi.org/10.1016/S1003-6326\(07\)60271-4](https://doi.org/10.1016/S1003-6326(07)60271-4).
- [186] J. Chmiola, G. Yushin, Y. Gogotsi, C. Portet, P. Simon, P.L. Taberna, Anomalous increase in carbon at pore sizes less than 1 nanometer, *Science*. 313 (2006) 1760–1763. <https://doi.org/10.1126/science.1132195>.
- [187] S. Das, S. Chakraborty, S.K. Mitra, Redefining electrical double layer thickness in narrow confinements: Effect of solvent polarization, *Physical Review E - Statistical, Nonlinear, and Soft Matter Physics*. 85 (2012) 1–6. <https://doi.org/10.1103/PhysRevE.85.051508>.



- [188] J.E. Zuliani, S. Tong, D.W. Kirk, C.Q. Jia, Isolating the effect of pore size distribution on electrochemical double-layer capacitance using activated fluid coke, *Journal of Power Sources*. 300 (2015) 190–198. <https://doi.org/10.1016/j.jpowsour.2015.09.030>.
- [189] K.L. Yang, S. Yiacoumi, C. Tsouris, Electrosorption capacitance of nanostructured carbon aerogel obtained by cyclic voltammetry, *Journal of Electroanalytical Chemistry*. 540 (2003) 159–167. [https://doi.org/10.1016/S0022-0728\(02\)01308-6](https://doi.org/10.1016/S0022-0728(02)01308-6).
- [190] C.H. Hou, C. Liang, S. Yiacoumi, S. Dai, C. Tsouris, Electrosorption capacitance of nanostructured carbon-based materials, *Journal of Colloid and Interface Science*. 302 (2006) 54–61. <https://doi.org/10.1016/j.jcis.2006.06.009>.
- [191] M.S. Kilic, M.Z. Bazant, A. Ajdari, Steric effects in the dynamics of electrolytes at large applied voltages. I. Double-layer charging, *Physical Review E - Statistical, Nonlinear, and Soft Matter Physics*. 75 (2007) 1–16. <https://doi.org/10.1103/PhysRevE.75.021502>.
- [192] M.S. Kilic, M.Z. Bazant, A. Ajdari, Steric effects in the dynamics of electrolytes at large applied voltages. II. Modified Poisson-Nernst-Planck equations, *Physical Review E - Statistical, Nonlinear, and Soft Matter Physics*. 75 (2007) 1–11. <https://doi.org/10.1103/PhysRevE.75.021503>.
- [193] R.B. Schoch, J. Han, P. Renaud, Transport phenomena in nanofluidics, *Reviews of Modern Physics*. 80 (2008) 839–883. <https://doi.org/10.1103/RevModPhys.80.839>.
- [194] H.S. Kwak, E.F. Hasselbrink, Timescales for relaxation to Boltzmann equilibrium in nanopores, *Journal of Colloid and Interface Science*. 284 (2005) 753–758. <https://doi.org/10.1016/j.jcis.2004.10.074>.
- [195] J.K. Fawell, World Health Organization., Fluoride in drinking-water, 2006. <https://doi.org/10.1007/BF01783490>.
- [196] World Health Organization, Guidelines for Drinking-Water Quality, in: Geneva. World Health Organization (Ed.), Fourth edi, 2011.
- [197] W.M. Edmunds, P.L. Smedley, Fluoride in Natural Waters - Springer, Essentials of Medical Geology. (1992) 1–44. [https://doi.org/10.1007/978-94-007-4375-5\\_13](https://doi.org/10.1007/978-94-007-4375-5_13).
- [198] M. Aslan, M. Zeiger, N. Jäckel, I. Grobelsek, D. Weingarh, V. Presser, Improved capacitive deionization performance of mixed hydrophobic/hydrophilic activated carbon electrodes, *Journal of Physics Condensed Matter*. 28 (2016). <https://doi.org/10.1088/0953-8984/28/11/114003>.
- [199] J. Lee, S. Kim, C. Kim, J. Yoon, Hybrid capacitive deionization to enhance the desalination performance of capacitive techniques, *Energy Environ. Sci*. 7 (2014) 3683–3689. <https://doi.org/10.1039/C4EE02378A>.

- [200] A. Ramachandran, A. Hemmatifar, S.A. Hawks, M. Stadermann, J.G. Santiago, Self similarities in desalination dynamics and performance using capacitive deionization, *Water Research*. 140 (2018) 323–334. <https://doi.org/10.1016/j.watres.2018.04.042>.
- [201] R. Zhao, O. Satpradit, H.H.M. Rijnaarts, P.M. Biesheuvel, A. van der Wal, Optimization of salt adsorption rate in membrane capacitive deionization, *Water Research*. 47 (2013) 1941–1952. <https://doi.org/10.1016/j.watres.2013.01.025>.
- [202] Y.H. Liu, H.C. Hsi, K.C. Li, C.H. Hou, Electrodeposited manganese dioxide/activated carbon composite as a high-performance electrode material for capacitive deionization, *ACS Sustainable Chemistry and Engineering*. 4 (2016) 4762–4770. <https://doi.org/10.1021/acssuschemeng.6b00974>.
- [203] J.W. Palko, D.I. Oyarzun, B. Ha, M. Stadermann, J.G. Santiago, Nitrate removal from water using electrostatic regeneration of functionalized adsorbent, *Chemical Engineering Journal*. 334 (2018) 1289–1296. <https://doi.org/10.1016/j.cej.2017.10.161>.
- [204] E. Auer, A. Freund, J. Pietsch, T. Tacke, Carbons as supports for industrial precious metal catalysts, *Applied Catalysis A: General*. 173 (1998) 259–271. [https://doi.org/10.1016/S0926-860X\(98\)00184-7](https://doi.org/10.1016/S0926-860X(98)00184-7).
- [205] F. Rodríguez-Reinoso, The Role of Carbon Materials in Heterogeneous Catalysis, 2013 International Conference on Localization and GNSS, ICL-GNSS 2013. 36 (1998) 159–175. <https://doi.org/10.1109/ICL-GNSS.2013.6577279>.
- [206] M. Endo, Y.A. Kim, M. Ezaka, K. Osada, T. Yanagisawa, T. Hayashi, M. Terrones, M.S. Dresselhaus, Selective and efficient impregnation of metal nanoparticles on cup-stacked-type carbon nanofibers, *Nano Letters*. 3 (2003) 723–726. <https://doi.org/10.1021/nl034136h>.
- [207] J. Chmiola, C. Largeot, P.L. Taberna, P. Simon, Y. Gogotsi, Desolvation of ions in subnanometer pores and its effect on capacitance and double-layer theory, *Angewandte Chemie - International Edition*. 47 (2008) 3392–3395. <https://doi.org/10.1002/anie.200704894>.
- [208] J. Chmiola, G. Yushin, R. Dash, Y. Gogotsi, Effect of pore size and surface area of carbide derived carbons on specific capacitance, *Journal of Power Sources*. 158 (2006) 765–772. <https://doi.org/10.1016/j.jpowsour.2005.09.008>.
- [209] J. Chmiola, G. Yushin, R. Dash, Y. Gogotsi, Effect of pore size and surface area of carbide derived carbons on specific capacitance, *Journal of Power Sources*. 158 (2006) 765–772. <https://doi.org/10.1016/j.jpowsour.2005.09.008>.

- [210] T.M. Mubita, J.E. Dykstra, P.M. Biesheuvel, A. van der Wal, S. Porada, Selective adsorption of nitrate over chloride in microporous carbons, *Water Research*. 164 (2019) 114885. <https://doi.org/10.1016/j.watres.2019.114885>.
- [211] T.M. Mubita, S. Porada, P.M. Biesheuvel, A. van der Wal, J.E. Dykstra, Capacitive deionization with wire-shaped electrodes, *Electrochimica Acta*. 270 (2018) 165–173. <https://doi.org/10.1016/j.electacta.2018.03.082>.
- [212] C. Largeot, C. Portet, J. Chmiola, P. Taberna, Y. Gogotsi, P. Simon, Relation between the Ion Size and Pore Size for an Electric Double-Layer Capacitor, *Journal of the American Chemical Society*. 130 (2008) 2730–2731. <https://doi.org/10.1016/j.carbon.2007.10.023>(15).
- [213] C.J. Gabelich, T.D. Tran, I.H. “Mel”. Suffet, Electrosorption of Inorganic Salts from Aqueous Solution Using Carbon Aerogels, *Environmental Science & Technology*. 36 (2002) 3010–3019. <https://doi.org/10.1021/es0112745>.
- [214] A.G. Pandolfo, A.F. Hollenkamp, Carbon properties and their role in supercapacitors, *Journal of Power Sources*. 157 (2006) 11–27. <https://doi.org/10.1016/J.JPOWSOUR.2006.02.065>.
- [215] H. Tobias, A. Soffer, The immersion potential of high surface electrodes, *Journal of Electroanalytical Chemistry*. 148 (1983) 221–232. [https://doi.org/10.1016/0368-1874\(83\)80210-x](https://doi.org/10.1016/0368-1874(83)80210-x).
- [216] M.R. Awual, S.A. El-Safty, A. Jyo, Removal of trace arsenic(V) and phosphate from water by a highly selective ligand exchange adsorbent, *Journal of Environmental Sciences*. 23 (2011) 1947–1954. [https://doi.org/10.1016/S1001-0742\(10\)60645-6](https://doi.org/10.1016/S1001-0742(10)60645-6).
- [217] H. Paudyal, B. Pangeni, K. Inoue, H. Kawakita, K. Ohto, H. Harada, S. Alam, Adsorptive removal of fluoride from aqueous solution using orange waste loaded with multi-valent metal ions, *Journal of Hazardous Materials*. 192 (2011) 676–682. <https://doi.org/10.1016/j.jhazmat.2011.05.070>.
- [218] B.L. Phillips, J.A. Tossell, W.H. Casey, Experimental and theoretical treatment of elementary ligand exchange reactions in aluminum complexes, *Environmental Science and Technology*. 32 (1998) 2865–2870. <https://doi.org/10.1021/es9802246>.
- [219] Y. Zhao, X. Li, L. Liu, F. Chen, Fluoride removal by Fe(III)-loaded ligand exchange cotton cellulose adsorbent from drinking water, *Carbohydrate Polymers*. 72 (2008) 144–150. <https://doi.org/10.1016/j.carbpol.2007.07.038>.
- [220] M. Grzegorzec, K. Majewska-Nowak, A.E. Ahmed, Removal of fluoride from multicomponent water solutions with the use of monovalent selective ion-exchange

membranes, *Science of the Total Environment*. 722 (2020) 137681. <https://doi.org/10.1016/j.scitotenv.2020.137681>.

[221] Q. Zhang, S. Bolisetty, Y. Cao, S. Handschin, J. Adamcik, Q. Peng, R. Mezzenga, Selective and Efficient Removal of Fluoride from Water: In Situ Engineered Amyloid Fibril/ZrO<sub>2</sub> Hybrid Membranes, *Angewandte Chemie - International Edition*. 58 (2019) 6012–6016. <https://doi.org/10.1002/anie.201901596>.

[222] C. Portet, P.L. Taberna, P. Simon, C. Laberty-Robert, Modification of Al current collector surface by sol-gel deposit for carbon-carbon supercapacitor applications, *Electrochimica Acta*. 49 (2004) 905–912. <https://doi.org/10.1016/j.electacta.2003.09.043>.

[223] B.A. Mei, O. Munteshari, J. Lau, B. Dunn, L. Pilon, Physical Interpretations of Nyquist Plots for EDLC Electrodes and Devices, *Journal of Physical Chemistry C*. 122 (2018) 194–206. <https://doi.org/10.1021/acs.jpcc.7b10582>.

[224] M. Orazem, B. Tribollet, Tribollet, b.: *Electrochemical impedance spectroscopy*. Wiley-interscience, new york, 2008. <https://doi.org/10.1002/9780470381588>.

[225] S.J. Seo, H. Jeon, J.K. Lee, G.Y. Kim, D. Park, H. Nojima, J. Lee, S.H. Moon, Investigation on removal of hardness ions by capacitive deionization (CDI) for water softening applications, *Water Research*. 44 (2010) 2267–2275. <https://doi.org/10.1016/j.watres.2009.10.020>.

[226] R. Zhao, M. van Soestbergen, H.H.M. Rijnaarts, A. van der Wal, M.Z. Bazant, P.M. Biesheuvel, Time-dependent ion selectivity in capacitive charging of porous electrodes, *Journal of Colloid and Interface Science*. 384 (2012) 38–44. <https://doi.org/10.1016/j.jcis.2012.06.022>.

[227] M. Mossad, L. Zou, A study of the capacitive deionisation performance under various operational conditions, *Journal of Hazardous Materials*. 213-214 (2012) 491–497. <https://doi.org/10.1016/j.jhazmat.2012.02.036>.

[228] J. Dzubiella, J.P. Hansen, Electric-field-controlled water and ion permeation of a hydrophobic nanopore, *Journal of Chemical Physics*. 122 (2005) 1–14. <https://doi.org/10.1063/1.1927514>.

[229] Y. Yu, J. Fan, J. Xia, Y. Zhu, H. Wu, F. Wang, Dehydration impeding ionic conductance through two-dimensional angstrom-scale slits, *Nanoscale*. 11 (2019) 8449–8457. <https://doi.org/10.1039/c9nr00317g>.